

Sea Grant College Program

MIT-Y-85-001 C2

RECEIVED
1985 OCT 27 10:27 AM



NATIONAL SEA GRANT DEPOSITORY
PELL LIBRARY BUILDING
URI, NARRAGANSETT BAY CAMPUS
NARRAGANSETT, RI 02882

Massachusetts Institute
of Technology
Cambridge, Massachusetts
02139

CIRCULATING COPY
Sea Grant Depository

**A ROBUST DESIGN METHOD FOR
IMPEDANCE CONTROL OF
CONSTRAINED DYNAMIC SYSTEMS**

Homayoon Kazerooni

**MITSG 85-35TN
February 1985**

**MIT Sea Grant College Program
Massachusetts Institute of Technology
Cambridge, MA 02139**

**Grant No.: NA84AA-D-00046
Project No.: R/V-7**

date published: December 1985

**NATIONAL SEA GRANT DEPOSITORY
PELL LIBRARY BUILDING
URI, NARRAGANSETT BAY CAMPUS
NARRAGANSETT, RI 02882**

This Sea Grant report is being published as part of the MIT Program's Technical Note series. The research was conducted by Homayoon Kazerooni in fulfillment of a Master of Science degree in MIT's Department of Ocean Engineering. The thesis supervisor was Thomas B. Sheridan, Professor of Mechanical Engineering and Applied Psychology.

Copies of this report may be ordered from

Sea Grant Information Center
MIT Sea Grant College Program
Room E38-320
Massachusetts Institute of Technology
77 Massachusetts Ave.
Cambridge, MA 02139

cost: \$14.00

Abstract

A ROBUST DESIGN METHOD FOR IMPEDANCE CONTROL OF CONSTRAINED DYNAMIC SYSTEMS

by

Homayoon Kazerooni

Submitted to the Department of Mechanical
Engineering on February 13, 1985, in partial
fulfillment of the requirements for the degree of
DOCTOR OF SCIENCE in Mechanical Engineering

The goal is to develop a method for design of controllers of constrained dynamic systems in the presence of model uncertainties. The controller must carry out fine maneuvers when the dynamic system is not constrained, and compliant motions, with or without interaction-force measurement when the system is constrained. At the same time stability must be preserved if bounded uncertainties are allowed in modelling the system.

Dynamic systems such as manipulators are subject to interaction loads (forces and torques) when they maneuver in a constrained work-space. If we define *compliance* as a measure of the ability of a dynamic system to react to interaction loads, we can state our object as assuring compliant motion in the global cartesian coordinate frame for the class of dynamic systems that must maneuver in constrained environments. Examples of these systems are manipulators interacting with the environment or underwater vehicles maneuvering while they are tied to structures by cables.

Stability of the system and environment as a whole and the preservation of stability in the face of changes are two fundamental issues that have been considered in the design method. We start with conventional controller-design specifications concerning the treatment of external loads when the system is not constrained. Generalizing this concept to include cases when the system is constrained, we state a set of design specifications to assure the desired compliant motion in the cartesian coordinate frame and stability in the presence of bounded uncertainties. This will lead us to select a time-invariant stable target impedance that both assures the global stability of the system and its environment and fulfils the design specifications. The target impedance is specified in terms of certain second order matrix polynomials.

In general, the closed-loop behavior of a system cannot be shaped arbitrarily over an arbitrarily wide frequency range. We prove, however, that a special class of impedances that represent our set of performance specifications are mathematically achievable asymptotically through state-feedback and interaction-force feedforward as actuator bandwidths become large, and we offer a geometrical design method for achieving them in the presence of model uncertainties. Simple closed-form expressions for the required feedforward and feedback gains are obtained as the solution to an eigenstructure assignment. This design method reveals a classical trade-off between a system's performance and its stability relative to model uncertainties. We deal with two classes of such uncertainties. While the first class of model uncertainties is formed from the uncertainties in the parameters of the modelled dynamics, the high frequency unmodelled dynamics form the second class of model uncertainties. The multivariable Nyquist criterion is used to examine trade-offs in stability robustness against approximation of desired target impedances over bounded frequency ranges. When only output feedback is available, an observer is derived. By exploiting the eigenstructure of the observer, when loop transfer recovery takes place, direct eigenstructure assignment (dual to the impedance control synthesis) can be used to compute the desired "observer" gains. Finally, the theoretical results and methodology are illustrated by applications to problems in planar manipulators and underwater vehicles.

Professor D. Hardt	(Committee Member)
Professor N. Hogan	(Committee Member)
Professor P. Houpt	(Thesis Co-supervisor)
Professor T. Sheridan	(Thesis Co-supervisor & Committee Chairman)



Acknowledgements

I would like to thank Professor Thomas Sheridan, whose supervision, patience, and support made this thesis possible. He gave me the opportunity to work and learn in the Man-Machine Systems Laboratory.

I wish to express my appreciation to Professor Neville Hogan and Professor Paul Houpt for their advice and guidance.

I would also like to thank Professor David Hardt and George Goodman for their constructive suggestions.

Many thanks to Professor Bruce Kramer who trusted me and allowed me to use his laboratory facilities to test some of my theoretical results.

I thank all my friends, in whose company life has been more pleasant.

This research was conducted at the MIT Man-Machine Systems Laboratory with financial support from MIT Sea Grant under NOAA grant number NA81AA-D-00069. I appreciate this generosity.

Table of Contents

Abstract	1
Acknowledgements	4
Table of Contents	5
Lists of Symbols	7
1. Introduction	9
2. Fundamentals	13
2.1 Background	13
2.2 Performance Specifications	17
2.3 Stability Robustness Specifications	21
2.4 Examples	22
2.4.1 Underwater Vehicle with Cables	22
2.4.2 Grinding	24
2.4.3 Turning a Crank	26
2.4.4 Peg-in-Hole	27
2.5 Representations of Target Dynamics	27
3. Eigenstructure Analysis of the Target Dynamics	29
3.1 Geometric Properties	29
3.2 <i>Simplicity</i> of the Target Dynamics	33
3.3 <i>Stability</i> of the Target Dynamics	34
4. Dynamic Behavior of the Manipulators	35
4.1 Mathematical Modelling	35
4.2 Model Uncertainties	42
5. Compensator Design	46
5.1 Background	46
5.2 State-Feedback Design	48
5.2.1 Manipulator Eigenstructure	50
5.2.2 Actuator Eigenstructure	52
5.2.3 Computation of G	54
5.3 Force-Feedforward Design	55
5.3.1 Theorem	55
5.3.2 Computation of G_d	56
5.3.3 Summary of the Design Method	57
5.3.4 Selection of the J-Matrix	58
5.4 Stability Robustness and the Eigenstructure of the Actuators	59
6. Examples	63

6.1 Example 1	63
6.2 Example 2	74
6.3 Simulation	80
6.4 Experiment	85
7. An Approach to Loop Transfer Recovery Using Eigenstructure Assignment	88
7.1 Introduction	88
7.2 Background	89
7.3 Asymptotic Eigenstructure Properties of the LTR Method	94
7.4 Comments	101
7.5 Design Method	102
7.6 Example	103
7.7 Conclusion	106
8. Conclusion	108
Appendix A. Stability	111
Appendix B. Simple Impedances	117
Appendix C.	123
Appendix D.	125
Appendix E. Stability Robustness	131

Lists of Symbols

The following symbols are used throughout this thesis, except in Chapter 7. Their definitions will be found on the pages indicated. The list of symbols used in Chapter 7 is given on page 89.

	page number		page number
A	40	J	17
A_a	39	J_e	112
A_t	27	J_c	31
B	40	j_s	119
B_a	39	K	14
B_t	27	k_e	112
C	17	k_s	119
C_e	112	L	40
C_t	27	L_p	56
c_s	119	m_i	51
$D(\lambda)$	31	$M(\Theta)$	35
$E'(s)$	114	$M(\Theta_0)$	37
$E(j\omega)$	42	N_i	51
$e(\omega)$	42	$P(\Theta)$	36
$F(\Theta)$	36	p_i	30
$F^f(t)$	37	$Q(\Theta, \Theta)$	36
F_o	37	q_i	30
$F^s(\Theta_0)$	37	q_s	119
$F^s(\Theta)$	36	r_i^T	31
$f_i^f(t)$	36	r_i^i	120
$G_t(s)$	28	R	120
G	46	S	48
$G_o(j\omega)$	59	s_i	48
G_1, G_2, G_3	56	t_i	128
$G_p^i(s)$	42	$T(\Theta, \Theta)$	35
G_d	46	T_s	38
$G_{c_i}(s)$	48	$T_e \text{ \& } T_y$	113
$G_p^o(s)$	40		
$G_p(s)$	40		
$G_1(j\omega) \text{ \& } G_2(j\omega)$	125		
$G_e(s)$	116		
g_i	53		
$GR(\Theta_0)$	37		

page number	page number		
u_j	48	γ_1 & γ_2	19
U_{11}	49	γ	58
U_{12}	49	Λ	32
U_{21}	49	λ_i	30
U_{22}	49	λ_s	119
U	48	λ_{si}	39
U_1	49	$\Theta(t)$	35
U_2	49	$\theta_i(t)$	35
U_{12}^T	129	ρ	55
v_j	32	ω_b	55
V	32	ω_o	14
W^T	126	ω_x	44
w_i^T	125	ω_{i^2}	120
z_i	30	Ω^2	120
α	60	$\Delta\Theta(t)$	31
β	18	Ξ	57
β_{ij}	19	ξ	121
$\Delta D(t)$	38		
$\Delta_e(t)$ & ΔD_e^o	112		
$\Delta D(j\omega)$	14		
$\delta d_j(t)$	38		
$\Delta F(t)$	37		
$\Delta N(t)$	38		
$\delta n_j(t)$	38		
$\Delta T(t)$	38		
$\delta t_j(t)$	38		
$\Delta\Theta(t)$	37		
$\Delta\Theta(j\omega)$	48		
$\Delta U(t)$	39		
$\delta u_j(t)$	39		
$\Delta Y(t)$	27		
ΔY_e	112		
$\Delta Y(j\omega)$	14		
$\Delta W(t)$	113		
$\Delta X(t)$	40		

Chapter 1

Introduction

For a broad class of mechanical systems under closed-loop control, fundamental differences in behavior and controller design complexity can be attributed to two types of maneuvers: unconstrained and constrained. In the first case, the dynamic system (e.g., a manipulator or an underwater vehicle) is driven in its work-space without contact with the environment. Note that the environment might exist in the system work-space without imposing any constraint on the system motion. In the constrained maneuvers, the system is driven in its work-space so the environment continuously exerts a dynamic or kinematic constraint on the system's motion. A dynamic maneuver such as leading a manipulator in a free environment toward a metal surface and then grinding the surface may consist of both types of maneuvers.

Spray painting by a manipulator is an example of the first class of maneuver. The end-point of the manipulator travels through certain points in its work-space without any restriction. Other examples of systems with unconstrained maneuvers are space or underwater vehicles that can be driven to various points without coming in contact with the environment. On the other hand, inserting a computer board in a slot (i.e., the peg-in-hole problem) or turning a crank by means of a manipulator are examples of constrained maneuvers; the end-point of the manipulator is in contact with the environment and cannot move in all directions. An underwater vehicle that is connected to a structure via cables (or flexible connectors or mechanical arms) is an example of a constrained system. Although such a system will remain unconstrained as long as the cables are not tensioned, its motion will become constrained if the vehicle is driven in its work-space such that the cables are tensioned. (See Section 2.4.1 for further details.) Our classification of maneuvers as unconstrained and constrained is similar to the classification introduced by Whitney [55], who categorized manipulations into "rearrangement" tasks and "force" tasks. Another slightly different classification is given by Hogan [22], who classified the manipulations into "non-energetic" and "energetic" interactions. This thesis deals with constrained maneuvering.

The rejection of external loads is an important design specification when the dynamic system is not constrained. Once the system crosses the boundary of the unconstrained environment (i.e., the dynamic system interacts with the environment), the dynamics of the

system will change and stability will no longer be guaranteed with the same controller. The compensator tries to reject the interaction loads, causing more interaction forces and torques. Saturation, large and undesirable contact forces, limit cycles in the motion of the system, and possible instability are the result of this type of maneuvering. Figure 6-14 in Chapter 6 is the result of a simulation of such behavior. Plot b in Figure 6-14 in Chapter 6 shows the position of an underwater vehicle in a constrained maneuver using a position controller designed for maneuvering in an unconstrained environment. Plot a is the reference input position to the controlled system. Region 1 in plot b shows the successful maneuver of the system when the vehicle is not constrained, while region 2 exhibits the position of the vehicle when the system encounters the environment. The limit cycle evident in this region shows that controllers that guarantee positioning capabilities in unconstrained maneuvering do not, in general, permit desirable behavior in constrained maneuvering.

In constrained maneuvering, the interaction loads must be accommodated rather than resisted. If we define "compliance" as a measure of the ability of a dynamic system to react to interaction forces and torques, we can state our object as assuring compliant motion in the global cartesian coordinate frame for dynamic systems that must maneuver in constrained environments. Previous researchers have suggested two approaches for assuring compliant motion for dynamic systems. The first approach is aimed at controlling force (torque) and position (orientation) in a non-conflicting way. In this method, force (torque) is commanded along (about) those directions constrained by the environment, while position (orientation) is commanded along (about) those directions in which the system is unconstrained and free to move. The second approach is aimed at developing a relationship between interaction loads (forces and torques) and system motion (position and orientation). By controlling the position and orientation of the dynamic system and specifying this relationship, a designer can ensure that a system will be able to maneuver in a constrained environment while maintaining appropriate contact forces and torques.

The first approach was motivated by several studies. Paul and Shimano [43] partitioned the motion of a system into position- and force-control in a global cartesian coordinate frame. Then, with the help of a decision-making "logic" hidden in a supervisory computer program, they arrived at the two sets of actuators that could best contribute to the position control loop and the force control loop. Railbert and Craig [46] also partitioned the motion of the system in a global cartesian coordinate frame. They used a position controller to move the system in unconstrained directions and a force controller to push the system against the environment with the desired contact force. They then arrived at input values for the

actuators (without assuring stability) such that all actuators would contribute to both partitions. Whitney [55] arrived at a single-loop velocity-control scheme with the net effect of controlling the contact force. Similar work in the generation of compliant motion has been done by Mason [38] and Wu and Paul [61]. Common to all such methods for ensuring compliant motion is the dependence of the controller's structure on both the kinematics and dynamics of the system and of its environment. For example, if the end-point of a manipulator travels from one constrained point to another such that the environment at the new point exerts constraints that differ from the constraints at the first point, then a new controller with a different structure must be designed to accommodate the new constraints.

In the second approach toward generating compliant motion, a relationship is defined between the motion (position and orientation) of the system and the interaction loads. Salisbury [50] started by defining a linear static function that relates interaction forces and torques to end-point position and orientation via a stiffness matrix in a cartesian coordinate frame. Monitoring this relationship by means of a computer program ensures that the system will be able to maneuver successfully in a constrained environment. In his seminal work, Salisbury justified the stiffness matrix as the representative of a behavior that manipulators must exhibit while they are used as positioning systems. The method of stiffness control offers neither assurance of global dynamic stability nor a guarantee of a specified frequency range of operation.

This thesis addresses the problem of closed-loop control of dynamic systems such as manipulators that operate in constrained environments, with or without interaction force measurement, in the presence of bounded model uncertainties. Central to the approach is the notion of mechanical impedance as a parametrization of a rational set of performance specifications to generate the compliant motion while preserving stability in the presence of bounded model uncertainties. Preservation of the stability of the dynamic system and the environment taken together as a whole is also a fundamental issue in constrained maneuvering. The proposed impedance guarantees this global stability also.

In Chapter 2 of this thesis, we explain (without getting involved in mathematics and design methodologies) points of practical importance in generating the compliant motion of a dynamic system. We start with conventional controller design specifications concerning the accommodation of interaction loads when the system is not constrained. Then we generalize this concept to apply to situations in which the system is constrained. Next, we parametrize the necessary performance specifications in a simple mathematical form. This will take us to an "impedance control" strategy for generating compliant motion. The concept of impedance

control is defined by Hogan [17, 18, 19, 20, 21, 22] independent of any specific design methodology. Impedance control is an in-depth approach of Salisbury's stiffness control; therefore, it is considered to be part of the second approach toward developing compliant motion. After defining and justifying impedance control in Chapter 2, we derive the eigenstructure properties of the proposed impedance in Chapter 3. We also address the stability of the target dynamics and their global stability with the environment in Chapter 3 and Appendix A. In Chapter 4, we present a dynamic model for a manipulator with actuators suitable for impedance control. We consider two classes of uncertainties in the modelling of the dynamic system. While the first class of model uncertainties involves the uncertainties in the parameters of the modelled dynamics, the high frequency unmodelled dynamics form the second class of model uncertainties. We deal with both uncertainties in the design method.

Chapter 5 explains the design methodology for impedance control. The design method is simply a computation of state-feedback and force-feedforward gain based on the eigenstructure assignment of the closed-loop system. The achievement of the target dynamics and preservation of the stability robustness in presence of bounded model uncertainties are the key issues in the design method. State-feedback and force-feedforward gains are chosen to guarantee the achievement of the target dynamics while preserving stability in the presence of model uncertainties. In Chapter 6 we give examples, simulations and some experimental results of the design methodology. Chapter 7 stands by itself as a technical paper; this chapter is not necessarily a part of the design technique for impedance control, but provides a new geometrical method for designing an observer for estimating the unmeasurable states of a system. Using the material of Chapter 7, an output feedback controller can be designed to achieve the target dynamics. The work presented in this document makes extensive use of the concepts and methods of control theory. While every effort has been made to explain the application of this material to impedance control, this document (except Chapter 7) is not an exposition of control theory generally.

Throughout this thesis, we take our dynamic system to be a serial-link manipulator. The theory of impedance control can equally be applied to constrained underwater or space vehicles. A vehicle can dynamically be assumed to be a one-link manipulator with 6 degrees of freedom.

Chapter 2

Fundamentals

2.1 Background

For the classes of dynamic systems that are used as positioning systems, control compensators traditionally have been designed so that the system's outputs (position and orientation) follow the commands, while rejecting the external loads (forces and torques). The two specifications (command-following and external-load rejection) typically require large open-loop gains for the frequency range in which the command inputs and the external loads contain the most power. Since commands and external loads usually contain low-frequency signals, command-following and external-load rejection properties taken together establish a design specification at low frequencies. To achieve the above properties over a large frequency range is not trivial; loop gains cannot be made arbitrarily large over an arbitrarily wide frequency range. A designer is always faced with certain performance trade-offs; these involve command-following and external-load rejection versus stability robustness to high-frequency unmodelled dynamics. The conflict between these two sets of objectives is evident in most positioning systems.

If the above controller design procedure were successful for constrained dynamic systems, such as manipulators that must cope with the environment or underwater vehicles connected to structures by cables, there would be little to complain about. In general, manipulation may fall into one of two categories. In the first category, the manipulator end-point is free to move in all directions, as in spray painting. In the second, the manipulator end-point interacts mechanically with the environment. Most assembly operations and underwater manipulations require mechanical interactions with the environment or with the object being manipulated. Such interactions imply constraints on the system's states. At this stage, the nature of the environmental constraint (which is the result of the interaction between the dynamic system and the environment) does not matter. The environment could exert a kinematic or a dynamic constraint on the system.

If one designs a model-based compensator for an unconstrained dynamic system, bearing in mind the objectives of disturbance rejection and robustness to model uncertainties, then

the closed-loop system will operate according to the specified criteria as long as the system travels inside the unconstrained environment. The system will try to reject all external loads and reach the assigned reference inputs. However, once the system crosses the boundary of the unconstrained environment (i.e., the dynamic system interacts with the environment), the dynamics of the system will change and stability will no longer be guaranteed. In fact, the system is now likely to become unstable. Even if stability is preserved, large contact forces may result. (See Reference [55] for a design method in which stability depends on the characteristics of the environment.)

In traditional controller-design methodology, external-load rejection is an important consequence of the design specifications. This property is useful as long as the system is unconstrained. Once the system is constrained, the compensator treats the interaction loads as disturbances and tries to reject them, thus causing more interaction forces and torques. Saturation, instability, and physical failure are the consequences of this type of interaction. But, in many applications such external loads should be accommodated rather than resisted.

An alternative to external-load rejection arises if it is possible to specify the interaction loads generated in response to imposed motion. The design objective is to provide a stabilizing dynamic compensator for the system such that the ratio of the motion of the closed-loop system to an interaction load is constant within a given operating frequency range. The above statement can be mathematically expressed by equation (2.1).

$$\Delta D(j\omega) = K \Delta Y(j\omega) \quad \text{for all } 0 < \omega < \omega_0 \quad (2.1)$$

where:

$\Delta D(j\omega)$ = $n \times 1$ vector of deviation of the interaction load (forces and torques) from equilibrium value in the global coordinate frame

$\Delta Y(j\omega)$ = $n \times 1$ vector of deviation of the interaction-port position and orientation from an equilibrium point in the global coordinate frame

K = $n \times n$ real-valued non-singular stiffness matrix with constant members

ω_0 = frequency range of operation

j = complex number notation, $\sqrt{-1}$

The stiffness matrix [50] is the designer's choice that, depending on the application, contains different values for each direction. By specifying K , the designer governs the behavior of the system in constrained maneuvers. Large members of the K -matrix imply large interaction

forces and torques. Small members of the K-matrix allow a considerable motion of the system to interaction forces and torques. Stiffness values, in one sense, represent the type of behavior a designer may wish a stable positioning system to exhibit. For example, if the system is expected to encounter some physical constraint in a particular direction, a stiffness value must be selected such that the desired contact force is ensured in that direction; in directions in which the system is not likely to meet any physical constraints, a stiffness value with a proper position set-point must be selected such that the system follows the desired reference inputs. Therefore, a K-matrix can be formed to contain stiffness values appropriate for different directions. Even though a diagonal stiffness matrix is appealing for the purpose of static uncoupling, the K-matrix is not restricted to any structure at this stage. Selection of the K-matrix is considered as the first item of the set of *performance specifications*.

The system must also reject the disturbances (if there are any). If disturbances (e.g., force measurement noise) and interaction loads both contain the same frequency range (or even if the frequency spectra of both signals overlap), then the system in general cannot differentiate between the disturbances and the interaction loads. Here we assume that the disturbances and force measurement noise act on the system at frequencies greater than ω_0 (see Section 2.4.2 for an example). An analogy can be observed in tracking systems; if measurement noise and reference inputs share some frequency spectrum, the system will follow the noise as well as the reference inputs. The reference inputs must contain components with frequency spectra much smaller than the spectrum of the measurement noise.

Mechanical systems are not generally responsive to external loads at high frequencies; as the frequency increases, the effect of the feedback disappears gradually, depending on the type of controller used, until the inertia of the system dominates its overall motion. Therefore, depending on the dynamics of the system, equation (2.1) may not hold for a wide frequency range. It is necessary to consider the specification of ω_0 as the second item of the set of performance specifications. In other words, two independent issues are addressed by equation (2.1): first, a simple relationship between $\Delta D(j\omega)$ and $\Delta Y(j\omega)$; second, the frequency range of operation, ω_0 , such that equation (2.1) holds true.

Besides choosing an appropriate stiffness matrix, K, and a viable ω_0 , a designer must also guarantee the stability of the closed-loop system. Therefore, stability is considered to be the third item of the performance specifications.

The stiffness matrix, K, the frequency range of operation, ω_0 , and the stability of the closed-loop system form the set of performance specifications. Note that this set of

performance specifications (stiffness, frequency range of operation, and stability) is just a contemporary and practical way of formulating the properties that will enable the closed-loop system to handle constrained maneuvers.

The achievement of the set of performance specifications is not trivial; the stiffness of the system cannot be shaped arbitrarily over an arbitrary frequency range. A designer must accept a certain trade-off between performance specifications and stability robustness to model uncertainties. The conflict between the performance specifications and *stability robustness specifications* is evident in most closed-loop control systems. The sets of performance specifications and stability robustness specifications taken together establish a complete set of *controller design specifications*. Figure 2-1 shows how this set is categorized.

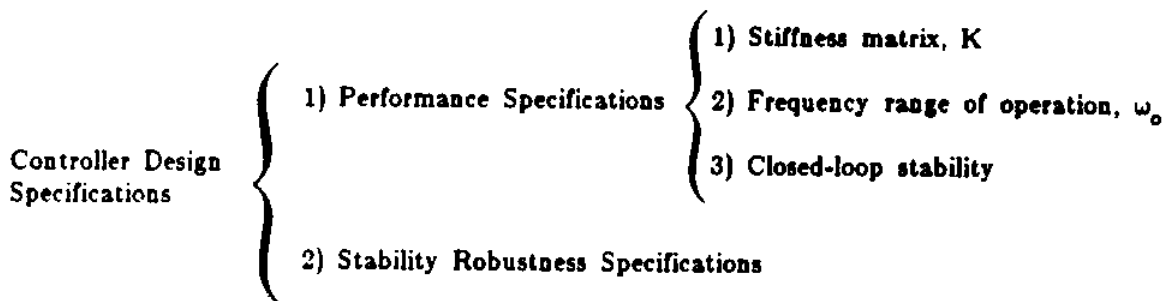


Figure 2-1: Controller Design Specifications

Establishing the set of performance specifications (K, ω_0 and stability) gives designers a chance to express (at least to themselves) what they wish to have happen during a constrained manipulation via a manipulator. Note that the set of performance specifications does not imply any choice of control techniques. We have not even said how one might achieve the set of performance specifications. Such a set only allows designers to translate their objectives (after understanding the mechanics of the problem) into a form that is meaningful from the standpoint of control theory.

2.2 Performance Specifications

We are looking for a mathematical model that will enable us to parametrize the three items of the set of performance specifications (K , ω_0 and stability). The parametrization must allow the designer to specify the stiffness matrix, K , and the frequency range of operation, ω_0 , independently, while guaranteeing stability. All such performance specifications can be mathematically expressed by equation (2.2).

$$\Delta D(s) = [K + C s + J s^2] \Delta Y(s), \quad s=j\omega \quad \text{for all } 0 < \omega < \omega_0 \quad (2.2)$$

$$[K + C s + J s^2] = \text{impedance}$$

K , C and J are $n \times n$ real-valued non-singular matrices. Note that it is still necessary to achieve equation (2.2) for all $0 < \omega < \omega_0$. Since equation (2.2) can give a stable eigenstructure for the closed-loop behavior, it is preferable to equation (2.1). We use the Laplace operators in equation (2.2), to emphasize that the entire set of performance specifications can be shown by a linear dynamic equation in the time domain. (See Section 2.5.) Proper selection of the K -matrix allows the designer to express the desired stiffness, while judicious choice of the inertia matrix, J , and the damping matrix, C , assures the achievement of ω_0 and stability of the system. To clarify the contribution of J , C and K , consider Figure 2-2, the plot of $\Delta Y(j\omega)/\Delta D(j\omega)$ from equation (2.2) when $n=1$ and the system is slightly underdamped.

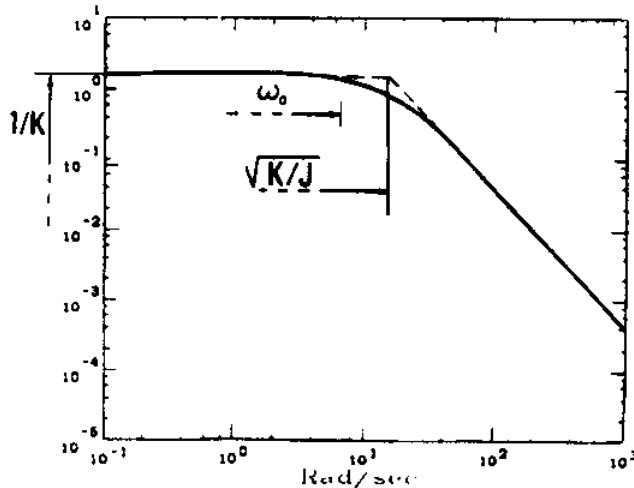


Figure 2-2: Plot of $\Delta Y(j\omega)/\Delta D(j\omega)$ when $n=1$

$\Delta Y(j\omega)/\Delta D(j\omega)$ remains very close to $1/K$ for some bounded frequency range. In other words, the plot of $\Delta Y(j\omega)/\Delta D(j\omega)$ approximately exhibits the relationship in equation (2.1) for

some bounded frequency range. Therefore, K in equation (2.2) parametrizes the first item of the set of performance specifications. Let the frequency range for which inequality (2.3) is true be ω_0 .

$$| Js^2 + Cs | < \beta | K | \quad s = j\omega \quad (2.3)$$

where β is a positive number less than one which measures how close the proposed impedance is to K . Note that our only purpose for introducing β is to say that for the bounded frequency range $(0, \omega_0)$, the impedance in equation (2.2) behaves approximately like the K -matrix. β represents this approximation and is not a design parameter. If K is given, then ω_0 and the stability of the system (the second and third items of the set of performance specifications, as given by equation (2.2)) depend on J and C . In other words, a designer can change either J or C to affect ω_0 and the stability of the system. For example, for a given K and C , decreasing J causes the corner frequency, $\sqrt{K/J}$, and consequently ω_0 , to increase. Changing J also moves the eigenvalues of the system. For a given positive set of K and C , a negative J locates one eigenvalue in the right half complex plane, while a positive J guarantees that both eigenvalues always stay in the left half complex plane. The dependence of ω_0 and the stability of the system on C can be investigated in a similar way. Because of the dependence of ω_0 and the stability of equation (2.2) on J and C , it can be shown that for a given K , there exist many J and C such that two eigenvalues of the system are always in the left half complex plane and $\Delta Y(j\omega)/\Delta D(j\omega)$ remains arbitrarily close to $1/K$ for all $0 < \omega < \omega_0$. We consider J and C as two factors that parametrize the second and third items of the performance specifications. If we consider C as a parameter that only guarantees a stable and slightly over-damped (or slightly under-damped) system, then we can claim that J is the only effective parameter in increasing or decreasing the frequency range of operation, ω_0 , for a given K . Since a heavy system is always slower than a light system, a large target inertia, J , implies a slow system (narrow ω_0), while a small target inertia implies a fast system (wide ω_0).

The parametrization of the set of performance specifications in the case of more than one dimension is similar to the case when $n=1$. Matrix K in equation (2.2) models the first item of the set of performance specifications because the behavior of $[Js^2 + Cs + K]$ approximates that of K for some bounded frequency range. In other words, for some bounded frequency range, inequality

$$| j_i js^2 + c_i js | < \beta_{ij} | k_{ij} | \quad s = j\omega \quad (2.4)$$

is true, where $\beta_{i j}$ is a positive number less than one which measures how close $[J s^2 + C s + K]$ is to K . Here again, the only purpose of introducing $\beta_{i j}$ is to say that for the bounded frequency range of $(0, \omega_0)$, the impedance in equation (2.2) behaves approximately like the K -matrix. We call this frequency range ω_0 . $j_{i j}$, $c_{i j}$ and $k_{i j}$ are members of J , C and K . ω_0 and the stability of the system depend on matrices J and C . It can be shown that for a given matrix K , there exist many J and C matrices such that the $2n$ eigenvalues of equation (2.2) are in the left half complex plane and $[J s^2 + C s + K]$ is close to K for all $0 < \omega < \omega_0$. For example, if J and C are selected to be $\gamma_1 K$ and $\gamma_2 K$ (where γ_1 and γ_2 are scalars), then the characteristic equation of equation (2.2) yields n uncoupled second-order equations for the eigenvalues of the system. γ_1 and γ_2 can be selected such that all eigenvalues are in the left half complex plane. The smaller γ_1 is selected to be, the wider ω_0 will be. Of course, this may not be the best way of choosing J and C , but it does show that there exist many J and C matrices such that with a proper K , equation (2.2) models all three items of the set of performance specifications. Again, if we consider matrix C as a parameter that only guarantees a stable and slightly over-damped (or slightly under-damped) system, then we can claim that matrix J is the only effective parameter in increasing or decreasing the frequency range of operation, ω_0 , for a given K -matrix. The following is a summary of the parametrization of the set of performance specifications:

stiffness matrix $> K$;
 ω_0 $> J$;
 stability $> C$.

At this stage, we do not restrain matrices J , C and K to any structure. The only restriction is that J , C and K be non-singular matrices.

Equation (2.2) is not the only possible parametrization of the performance specifications. Similarity of the natural behavior of manipulators to the form introduced by equation (2.2) is one reason for the choice of the second-order impedance. Within some bounded frequency range, manipulator dynamics are governed by Newton's equations, which are of second order for each degree of freedom. Practitioners tend to observe an attenuation in frequency response tests on manipulators for some bounded frequency range which can be approximated 40db per decade. At high frequencies, other dynamics contribute to the dynamic behavior of manipulators. We chose a second-order impedance because of this dynamic similarity. Chapter 3 and Appendices A and B explain some properties of the second-order impedances. Throughout this thesis, equation (2.2) is referred to as the *target dynamics*. Other forms of this equation are presented in Section 2.5.

Without any justification at this stage, we claim that $\Delta Y(j\omega)$ and $\Delta D(j\omega)$ must be small in magnitude. This restriction does not mean that this theory cannot be applied when large contact forces are involved. A large contact force (torque) can be produced by many incremental forces, $\Delta D(j\omega)$, where $\Delta D(j\omega)$ is very small at each stage. This restriction on the size of these variables is clarified in Chapter 4.

Here, we use an example to illustrate a potential difficulty with matrix J . Consider a diagonal K -matrix. If K is chosen so that $K = \text{diag}(k_1, k_2, \dots, k_n)$, then $J = \text{diag}(j_1, j_2, \dots, j_n)$ and $C = \text{diag}(c_1, c_2, \dots, c_n)$ can be selected to guarantee that each channel has the desired frequency range of operation. J need not, however, be a diagonal matrix to guarantee the uncoupling of motion in the desired operating frequency range. Even though K is selected to be a diagonal matrix to ensure uncoupling, there exist an infinite number of J -matrices (not necessarily diagonal) that can guarantee this uncoupling for the desired frequency range of operation. This is true because Js^2 is effective only at high frequencies ($\omega > \omega_0$); for all $0 < \omega < \omega_0$, K plays the most important role in determining the response of the system. The size of J is important, not its structure. Of course, the diagonal structure for J makes its selection much easier. As stated earlier, $[Js^2 + Cs + K]$ remains very close to K for some bounded frequency range, $0 < \omega < \omega_0$. For all $0 < \omega < \omega_0$, $[Js^2 + Cs + K]$ behaves approximately like K , and the contact loads that are generated in response to those components of the imposed motion $\Delta Y(j\omega)$ that live in the operating region $0 < \omega < \omega_0$ is approximately equal to $K \Delta Y(j\omega)$, which is nearly independent of J . (Of course, the response of the system outside the frequency range of operation ($\omega_0 < \omega < \infty$) depends on J .) On the other hand, ω_0 establishes the frequency range in which the size of K is much larger than $J\omega^2$. Dependence of ω_0 on the size of J and the independence of the system's response from J , show that the size of J is important and not its structure. (One can consider the size of the J -matrix in terms of its singular values.) A diagonal or a non-diagonal J is equally suitable for an impedance as long as the size of the matrix guarantees that $\Delta D(j\omega) \approx K \Delta Y(j\omega)$ for all $0 < \omega < \omega_0$. In Chapter 5 we will arrive at a non-diagonal J , which can guarantee an uncoupled stiffness for $0 < \omega < \omega_0$ without any force measurements. See Section 5.3.4 for a discussion of the selection of the J -matrix.

By specifying the matrices J , C and K , a designer can modulate the *impedance* of the system. If a dynamic system is in contact with its environment and a new reference point is commanded (e.g., by a supervisor program), then, since the parameters of the impedance in equation (2.2) are under control, the resulting interaction load on the system will also be under control. This means that the controlled dynamic system will behave like a system that

accepts a set of position and orientation commands and reflects a set of forces and torques as output. This is the fundamental characteristic of *impedance control* that cannot be attributed to *admittance control*. In other words, impedance control always allows for closed-loop positioning capabilities. Stiffness control [50] also offers this characteristic. By assigning different position and orientation commands and by maintaining complete control in equation (2.2), a designer can achieve the desired contact forces and torques.

Impedance control can be contrasted with the two conventional modes of controlling a dynamic system: position control and force control. Position control works well for unconstrained space, but causes difficulty when environmental constraints exist. In contrast, force control is desirable for manipulations in constrained space. Position control and force control are two extreme cases of impedance control. The former implies very high impedance, while the latter implies very low impedance.

2.3 Stability Robustness Specifications

The stability robustness specifications arise from the existence of model uncertainties [49, 33]. The model uncertainties fall into two classes. Lack of exact knowledge about the parameters of the modelled dynamics (e.g., the inertia matrix) constitutes the first class of model uncertainties. High-frequency unmodelled dynamics (such as bending or torsion dynamics of the members) form the second class of unmodelled dynamics. Note that the model uncertainties of the second class generally give rise to modelling error only at high frequencies, while the model uncertainties of the first class can contribute to modelling error at all frequencies. If the compensated system does not satisfy the stability robustness specifications, the system may not become unstable. This is true because our robustness test is a sufficient condition for stability. Satisfaction of the robustness test guarantees stability, while the failure of the robustness test does not necessarily imply instability. If one cannot meet the stability robustness specifications at high frequencies, it is necessary to consider the higher-order dynamics (if at all possible) when modelling the system. Adding the higher-order dynamics to the system allows for weaker stability robustness specifications at high frequencies. If higher-order dynamics cannot be determined, it is necessary to compromise on the set of performance specifications. A small ω_0 will allow designers to meet strong sets of stability robustness specifications at high frequencies. On the other hand, with a very small ω_0 , stability robustness to parameter uncertainties may not be satisfied. This is true because

stability robustness to parameter uncertainties assigns a lower bound on ω_o . To achieve a wide ω_o , a designer should have a good model of the system at high frequencies (and consequently, a weak set of stability robustness specifications at high frequencies). Because of the conflict between desired ω_o and stability robustness to high frequency dynamics, it is a struggle to meet both sets of specifications for a given model uncertainty. The frequency range of operation, ω_o , cannot be selected to be arbitrarily wide if a good model of the system does not exist at high frequencies, while a good model of the system at high frequencies makes it possible to retain the target dynamics for a wide ω_o . The relation between ω_o and stability robustness will be presented in Chapter 5. Even though ω_o is the major candidate that can be used to compromise against stability robustness specifications, there are other freedoms in design technique that sometimes can be used for the same purpose. This will be clarified in Chapter 5.

2.4 Examples

The following examples illustrate some applications of impedance control. For the purpose of understanding the application of this theory, the problems in these examples are simplified.

2.4.1 Underwater Vehicle with Cables

Most deep underwater operations are done by underwater vehicles equipped with manipulators. Because of the large inertia of these vehicles (relative to the manipulator inertia) and their uncontrollability in some directions, it is not trivial to maneuver these vehicles during a manipulative task. In performing a task (e.g., opening a valve), it is preferable to keep the vehicle as a stable platform and maneuver the manipulator. An underwater vehicle is always subject to external forces resulting from water motion, manipulator reactions and power/communications tethers. These external forces on the vehicle act over a wide frequency range. Rejection of all external loads on the vehicle and maintenance of the position and orientation of the vehicle over a wide frequency range of operation by feedback is not trivial. This is true because uncertainties in the model (e.g., hydraulic actuator system) will assign an upper bound for the bandwidth of the compensated loop transfer function. Low-frequency external loads on the vehicle can be rejected by

feedback, and high-frequency loads do not affect the vehicle motion. On the other hand, there exist external loads with a frequency range of operation too large to be compensated by feedback, but small enough to affect the vehicle's motion. This frequency range is near the cross-over frequency of the compensated open-loop transfer function. In other words, when most of a vehicle's external loads that are deep inside the bandwidth of the compensated open-loop can be rejected by feedback, external loads that are far outside the bandwidth cannot affect the vehicle motion. But external loads that lie between these two frequency ranges can affect the vehicle motion. (The analogy can be observed in airplanes. Passengers always feel some disturbances. These disturbances act over a frequency range that cannot be compensated completely by feedback.) To overcome this problem, the vehicle can be connected to the structure by cables. This can be done by the manipulator on the vehicle. The cables' end-points can be equipped with magnets, suckers or hooks, and the cables can be tensioned by using the vehicle's thrusters in the necessary directions. Figure 2-3-a shows this arrangement.

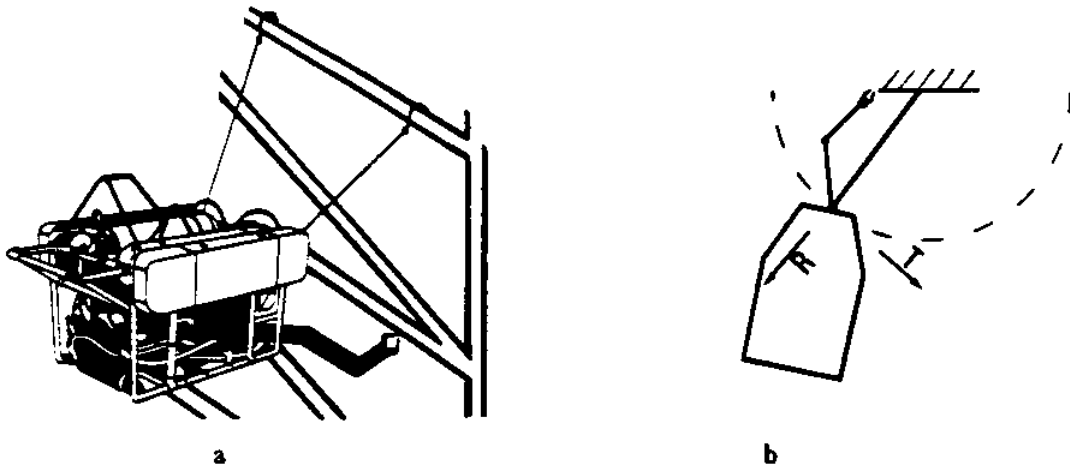


Figure 2-3: Constrained Ocean Vehicle

Maintaining the tension of the cables between the structure and the vehicle will give the vehicle a more definite position and orientation. If the cables are stiff, their dynamics may overcome the vehicle's inertia for some bounded frequency range. The stiffnesses of the cables will dominate the dynamics of the system of vehicle and cables over a wide frequency range. This frequency range can be approximated by $\sqrt{\text{cables stiffness/vehicle inertia}}$. Throughout this frequency range, the system of the vehicle and its cables behaves like a very stiff spring, and external loads in this frequency range do not affect the vehicle.

The above procedure for positioning the vehicle implies the existence of significant interaction forces between the vehicle and its environment via the cables. The cables impose

dynamic constraints on the vehicle's motion. In any mission, it is desirable to control the position and orientation of the vehicle and the tension of the cables, even though the number of cables and the locations of their attachments to the structure may not be known in advance. Here we can see the application of impedance control to this type of constrained maneuvering in which the existence and general character of the constraint is certain, but the exact nature of the dynamics and geometry of the constraint is not known in advance.

Consider the case in which there is just one cable between the vehicle and the structure in Figure 2-3-b. There is no constraint on the vehicle's motion in direction T; therefore, it is necessary to consider a closed-loop positioning system with a large stiffness for the vehicle along direction T. A large stiffness in direction T guarantees a good closed-loop positioning system in that direction. There is a constraint on the vehicle's motion in direction R because of the cable. It is necessary to consider a small stiffness for the vehicle in direction R guaranteeing only a slight tension in the cable when the vehicle is commanded to move from unconstrained space to constrained space. Of course, once the vehicle is moving on the circle, one can increase the stiffness in direction R to produce more cable tension. The frequency content of the command input implies a proper value for ω_0 . Stiffness values in various directions, a suitable value for ω_0 and the requirement of stability imply proper values for K, J and C.

2.4.2 Grinding*

Consider the grinding of a surface by a manipulator, as shown in Figure 2-4. The object is to use the manipulator to smooth the surface down to the dashed line [30]. Here we give an approach in which this task is performed by a manipulator. It is intuitive to design a closed-loop positioning system for the manipulator with a large stiffness value in direction R and a low stiffness value in direction T. In many tasks, it is beneficial to produce the compliant motion in an active end-effector with a few degrees of freedom instead of producing the compliant motion for the entire arm. A large stiffness value in direction R causes the end point of the manipulator to reject the external loads and stay very close to the commanded trajectory (dashed line). The larger the stiffness of the manipulator in direction R, the smoother the surface will be. Given the volume of the metal to be removed,

*Section 2.4.2 was shaped from discussions with Bruce Kramer, Reginald Gott and John Bausch.

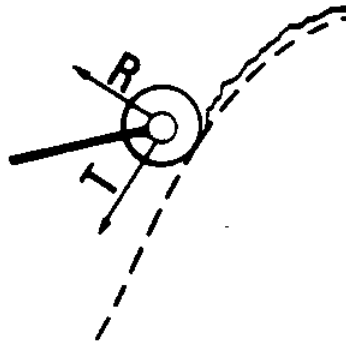


Figure 2-4: Grinding a Surface via a Manipulator

the desired tolerance in direction R prescribes an approximate value for stiffness in direction R.

The force necessary to cut in direction T at a constant traverse speed is approximately proportional to the volume of the metal to be removed [3]. Therefore, the larger the "bumps" on the surface, the slower the manipulator's end-point must move in direction T. This is necessary because a slower speed of the end-point along the surface implies less volume of the metal to be removed per unit of time, and consequently, less force in direction T. To remove the metal from the surface, the manipulator should slow down in response to external loads resulting from large "bumps." The above explanation means that it is necessary for the manipulator to accommodate the external loads along direction T, which directly implies a small stiffness value in direction T. If a designer does not accommodate the external loads by specifying a small stiffness value in direction T, then large "bumps" on the surface will produce large contact forces in direction T. Two problems are associated with large contact forces in direction T:

- the cutting tool may stall (if it does not break);
- a slight motion may develop in the manipulator's end-point motion along direction R, which might exceed the desired tolerance.

A small value for stiffness in direction T (relative to the stiffness in direction R) guarantees the desired contact forces in direction T. The larger the roughness of the surface, the smaller K must be in direction T. The frequency spectrum of the roughness of the surface and the desired translational speed of the manipulator end-point along the surface determine the frequency range of operation, ω_0 . Given the stiffness in both directions, a designer can arrive at proper values for J and C to guarantee ω_0 and stability. At each point on the

trajectory, a controller must be redesigned in the joint-angle coordinate frame such that the desired target impedance of the form (2.2) is achieved in the global coordinate frame. The rotation of the cutter causes some high-frequency disturbances in the manipulator. The contact force measurement is also noisy. ω_0 must be selected to be lower than the frequency range of the cutter disturbances and the force measurement noise. The satisfaction of equation (2.2) prevents the system from responding to these disturbances and noises. (See page 15 for a short discussion on disturbances.)

2.4.3 Turning a Crank

Consider the case in which a manipulator turns a crank or opens a valve, as shown in Figure 2-5-a.

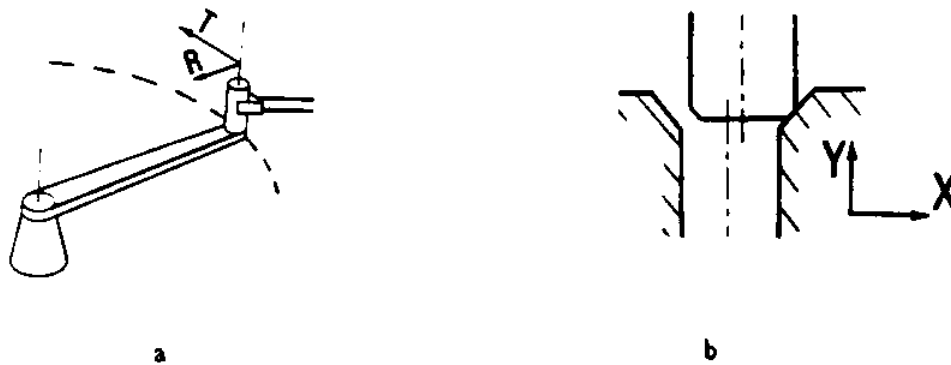


Figure 2-5: a: Manipulator Turning a Crank
b: Peg and Hole

The objective is to design a closed-loop positioning system so the manipulator will have a large stiffness in direction T; this will cause the manipulator to turn the crank by overcoming the external loads (friction). It is necessary to consider a small stiffness in direction R, because if there is any discrepancy between the real trajectory of the crank handle and the commanded trajectory, no large contact force in direction R will result. Note that the crank handle cannot move in direction R and a small disagreement with the prescribed trajectory of the crank handle will cause a large force if the stiffness in direction R is large. The frequency content in the command signal requires a proper value for ω_0 . The stiffness values in different directions, a suitable value for ω_0 and the desire for stability imply proper values for K, J and C.

2.4.4 Peg-in-Hole

The peg-in-hole task is generic to many assembly operations such as inserting a rod into a hole or a computer board into a slot. There are many strategies for this task (see for example [57]); most assume that the manipulators are capable of producing compliant motion. We are not giving a complete solution to the peg-in-hole problem. This is just a simplified example to illustrate the use of this method in such maneuvers. Once the peg is located at the position shown in Figure 2-5-b, then a small stiffness in direction X must be selected. If there is any misalignment between the peg axis and the hole axis, a small stiffness in direction X causes the manipulator end-point to align itself with the axis of the hole. If the stiffness in direction X is large, the manipulator end-point will not move in direction X, and large contact forces will result. A large stiffness must be selected for direction Y to guarantee a positioning system that will reject the friction forces in direction Y and insert the peg into the hole.

2.5 Representations of Target Dynamics

This section represents other forms of the target dynamics. Equation (2.2) in the time domain can be described by equation (2.5).

$$J \ddot{\Delta Y}(t) + C \dot{\Delta Y}(t) + K \Delta Y(t) = \Delta D(t) \quad (2.5)$$

J, K and C are non-singular matrices.

$\Delta Y(t)$ and $\Delta D(t)$ are $n \times 1$ vectors. Even though we use the time-domain representation of the target dynamics in our design method, we plan to guarantee the achievement of the target dynamics in the frequency domain. We also select the parameters of equation (2.2) to guarantee the design specifications in the frequency domain. Selection of J, C and K to represent a frequency-domain design specification implies shaping the steady-state behavior of the system in response to all frequency components of the imposed motion command. An alternative approach is to specify J, C and K to represent some design specifications in the time-domain [20]. The target dynamics (2.2) in state-space are shown by equations (2.6) and (2.7).

$$\begin{bmatrix} \dot{\Delta Y}(t) \\ \ddot{\Delta Y}(t) \end{bmatrix} = \underbrace{\begin{bmatrix} 0_{nn} & I_{nn} \\ -J^{-1}K & -J^{-1}C \end{bmatrix}}_{A_t} \begin{bmatrix} \Delta Y(t) \\ \dot{\Delta Y}(t) \end{bmatrix} + \underbrace{\begin{bmatrix} 0_{nn} \\ J^{-1} \end{bmatrix}}_{B_t} \Delta D(t) \quad (2.6)$$

$$\Delta Y(t) = \underbrace{\begin{bmatrix} I_{nn} & 0_{nn} \end{bmatrix}}_{C_t} \begin{bmatrix} \Delta Y(t) \\ \dot{\Delta Y}(t) \end{bmatrix} \quad (2.7)$$

$$A_t = 2n \times 2n, \quad B_t = 2n \times n, \quad C_t = n \times 2n$$

$$\text{Rank } B_t \text{ and } C_t = n$$

The transfer function matrix that relates interaction load to interaction-port motion is shown by equations (2.8) and (2.9).

$$\Delta Y(j\omega) = G_t(j\omega) \Delta D(j\omega) \quad (2.8)$$

where:

$$G_t(j\omega) = C_t (j\omega I_{nn} - A_t)^{-1} B_t \quad (2.9)$$

or

$$G_t(s) = [J s^2 + C s + K]^{-1} \text{ where } s = j\omega \quad (2.10)$$

Chapter 3

Eigenstructure Analysis of the Target Dynamics

Since a geometric approach is being considered for compensator design, it is necessary to identify the eigenstructure properties of the target dynamics. Section 3.1 discusses this issue. Section 3.2 explains the concept of *simplicity*, which is the second condition for the mathematical achievability of the target impedance. (The non-singularity of J , C and K is the first condition.) Finally, in Section 3.3 we consider the stability analysis of the target dynamics.

3.1 Geometric Properties

The target dynamics that correlate interaction loads (forces and torques) with system motion (position and orientation) are given in state-space form by equations (2.6) and (2.7). The advantage of this form is that it enables a designer to describe the target dynamics of a system in geometrical terms. A_t contains information concerning the modes (eigenvalues) and the relative distribution of the modes (eigenvectors) among the states. A unique value for A_t can be determined by $2n$ eigenvalues and $2n$ right eigenvectors. B_t represents a rank- n matrix that transforms interaction load to system states; C_t is a rank- n matrix that transforms system states to system motion.

The target dynamics in equation (2.2) imply a closed-loop behavior for the dynamic system. Our goal is to make the dynamic system (e.g., a manipulator) behave according to equation (2.2) for all $0 < \omega < \omega_0$. Note that in general the closed-loop behavior of a system cannot be shaped arbitrarily over an arbitrary frequency range. The target dynamics in equation (2.6) and (2.7) offer a set of eigenvalues and eigenvectors to model the internal dynamic behavior of the target dynamics. Construction of the eigenstructure of the dynamic system (e.g., a manipulator or an underwater vehicle) according to the eigenstructure of the target dynamics is the first step in our design method. There are two issues of concern in this step. The first issue addresses the achievement of the eigenstructure of the target dynamics; there is no a-priori guarantee that the eigenstructure of the dynamic system can be

constructed according to the eigenstructure of the target dynamics. This limitation in the construction of the eigenstructure is explained in Chapter 5. The second issue concerns the achievement of the target dynamics for some bounded frequency range. Normally, the construction of the eigenstructure of the dynamic system according to that of the target dynamics does not guarantee that the closed-loop dynamic system behaves dynamically as equation (2.2) for all $0 < \omega < \omega_0$. The above two issues are answered in Chapter 5. We will prove that the eigenstructure of the target dynamics is achievable and we explain how this achievement is interpreted. The achievement of the eigenstructure of the target dynamics is because of appropriate choice of the target dynamics. We also prove that the achievement of the eigenstructure of the target dynamics is required to guarantee that the closed-loop system will behave dynamically like equation (2.2) for all $0 < \omega < \omega_0$. Knowing the eigenstructure of the target dynamics is necessary for our design method.

Each eigenvalue of the target impedance, λ_i , and its corresponding right eigenvector, z_i , can be computed from equation (3.1).

$$\begin{aligned} (\lambda_i I_{2n2n} - A_t) z_i &= 0_{2n} & i &= 1, 2, \dots, 2n \\ z_i &\neq 0_{2n} \end{aligned} \quad (3.1)$$

Substituting for A_t from equation (2.6) in equation (3.1) results in equation (3.2), which can be used to compute the eigenvalues and right eigenvectors of the target dynamics.

$$\begin{bmatrix} \lambda_i I_{nn} & -I_{nn} \\ J^{-1}K & \lambda_i I_{nn} + J^{-1}C \end{bmatrix} \begin{bmatrix} q_i \\ p_i \end{bmatrix} = 0_{2n} \quad i = 1, 2, \dots, 2n \quad (3.2)$$

where: $z_i = \begin{bmatrix} q_i \\ p_i \end{bmatrix} \neq 0_{2n}$

q_i and p_i are $n \times 1$ vectors. To produce a non-zero solution for z_i , equation (3.3) must be satisfied [54].

$$\det \begin{bmatrix} \lambda_i I_{nn} & -I_{nn} \\ J^{-1}K & \lambda_i I_{nn} + J^{-1}C \end{bmatrix} = 0 \quad i = 1, 2, \dots, 2n \quad (3.3)$$

Equation (3.3) yields the eigenvalues of the target dynamics. Equations (3.4) and (3.5), which come from equation (3.2), result in vectors p_i and q_i :

$$p_i = \lambda_i q_i \quad (3.4)$$

$$[J \lambda_i^2 + C \lambda_i + K] q_i = 0_n \quad i = 1, 2, \dots, 2n \quad (3.5)$$

$$q_i \neq 0_n .$$

To produce a non-zero solution for q_i , equation (3.6) must be satisfied.

$$\det D(\lambda_i) = 0 \quad i = 1, 2, \dots, 2n \quad (3.6)$$

$$\text{where: } D(\lambda) = J \lambda^2 + C \lambda + K$$

$D(\lambda)$ is the *matrix polynomial* [12, 11, 13] associated with the target dynamics of equation (2.2). Equation (3.6) can also be produced by algebraic manipulation of equation (3.3). q_i is called the right latent vector of $D(\lambda_i)$ associated with λ_i . If J , C and K are symmetric matrices, it can be verified that the right- and the left-latent vectors of $D(\lambda)$ are equal. Therefore, for symmetric J , C and K :

$$r_i = q_i \quad (3.7)$$

$$\text{where: } r_i^T D(\lambda_i) = 0_n^T \quad i = 1, 2, \dots, 2n$$

$$r_i^T \neq 0_n^T .$$

We wish to design a model-based compensator to guarantee that the manipulator dynamics behave according to equation (2.2) for all $0 < \omega < \omega_0$. Since dynamic models for manipulators are often specified in the joint-angle coordinate frame, it is helpful to recast equations (2.6) and (2.7) in the joint-angle coordinate frame. Equations (2.6) and (2.7) represent a state-space relationship between end-point motion and interaction load in the global coordinate frame. The transformation of end-point motion and interaction load from the global coordinate frame to the joint-angle coordinate frame is given in reference [56]; it results in the following equation:

$$\Delta Y(t) = J_c \Delta \Theta(t) \quad (3.8)$$

where J_c is the Jacobian of the matrix that transforms joint-angle coordinates to global coordinates. Equation (2.2) represents a dynamic behavior in the neighborhood of an equilibrium point; $\Delta Y(t)$ and $\Delta D(t)$ are small incrementals away from an equilibrium point (a point with zero speed in space). Knowing this, we can write:

$$\dot{\Delta Y}(t) = J_c \dot{\Delta \Theta}(t) . \quad (3.9)$$

Combining equations (3.8) and (3.9) results in equation (3.10).

$$\begin{bmatrix} \Delta Y(t) \\ \dot{\Delta Y}(t) \end{bmatrix} = \begin{bmatrix} J_c & 0_{nn} \\ 0_{nn} & J_c \end{bmatrix} \begin{bmatrix} \Delta \theta(t) \\ \dot{\Delta \theta}(t) \end{bmatrix} \quad (3.10)$$

Using equation (3.10), the target dynamics in the joint-angle coordinate frame can be written as:

$$\begin{bmatrix} \dot{\Delta \theta}(t) \\ \ddot{\Delta \theta}(t) \end{bmatrix} = \begin{bmatrix} 0_{nn} & I_{nn} \\ -J_c^{-1} J^{-1} K J_c & -J_c^{-1} J^{-1} C J_c \end{bmatrix} \begin{bmatrix} \Delta \theta(t) \\ \dot{\Delta \theta}(t) \end{bmatrix} + \begin{bmatrix} 0_{nn} \\ J_c^{-1} J^{-1} \end{bmatrix} \Delta D(t) \quad (3.11)$$

$$\Delta \theta(t) = \begin{bmatrix} I_{nn} & 0_{nn} \end{bmatrix} \begin{bmatrix} \Delta \theta(t) \\ \dot{\Delta \theta}(t) \end{bmatrix} .$$

$\Delta D(t)$ in equation (3.11) is still expressed in the global coordinate frame. If v_i is the right eigenvector of the target dynamics in the joint-angle coordinate frame, then:

$$v_i = \begin{bmatrix} J_c^{-1} & 0_{nn} \\ 0_{nn} & J_c^{-1} \end{bmatrix} z_i = \begin{bmatrix} J_c^{-1} q_i \\ \lambda_i J_c^{-1} q_i \end{bmatrix} \quad (3.12)$$

where q_i is the right latent vector of $D(\lambda_i)$. The $2n$ eigenvectors of equation (3.12) form a $2n \times 2n$ matrix V :

$$V = [v_1 \quad v_2 \quad \dots \quad v_{2n}] . \quad (3.13)$$

V is a basis for the state-space representation of the target dynamics in the joint-angle coordinate frame. V shows how the desired modes are coupled among the states of the target dynamics. The $2n$ eigenvalues resulting from equation (3.3) are invariant under any linear transformation and form a self-conjugate constant set $\Lambda = \{ \lambda_i : i = 1, 2, \dots, 2n \}$.

Λ and V taken together describe the eigenstructure of the desired impedance in the joint-angle coordinate frame. The realization of the target dynamics in state-space form is not unique; each representation offers a different V .

3.2 Simplicity of the Target Dynamics

Impedances that always yield a complete set of right eigenvectors are called *simple*. Having a complete set of right eigenvectors is vital to our controller design methodology. The requirements for the completeness of the set of right eigenvectors are explained in Chapter 5. Multiple eigenvalues in Λ are allowed, while V is restricted to be a full-rank matrix. Distinct eigenvalues result in independent right eigenvectors [40, 41], but multiple eigenvalues in the target dynamics may not result in a complete set of right eigenvectors. If the eigenvalues of the target dynamics are distinct, the requirement on the completeness of the set of right eigenvectors will automatically be fulfilled. Suppose equation (3.3) results in an eigenvalue with a multiplicity of α . For the set of right eigenvectors to be complete, the α right eigenvectors associated with the multiple eigenvalue must be independent. Equation (3.12) shows that the independence of the α right latent vectors associated with an eigenvalue of multiplicity α is a necessary and sufficient condition for the independence of the right eigenvectors of the target dynamics. Appendix B identifies the class of impedances that always yields a complete set of right eigenvectors for the target dynamics despite a multiplicity of eigenvalues. These impedances are called *simple*. The exact definition of the simple impedances are given in Appendix B. Knowing the requirements for the independence of the right eigenvectors of the target dynamics, we can write explicitly the only set of formal conditions that guarantees the structure of the target dynamics will be mathematically achievable:

1. J , C and K must be non-singular matrices.
2. The target dynamics must be simple; all right eigenvectors of the target dynamics must span the entire $2n$ -space.

The target dynamics in equation (2.2) imply a closed-loop behavior for the manipulator dynamics. We plan to make the manipulator behave as equation (2.2) for $0 < \omega < \omega_0$. Note that in general one cannot ask a special closed-loop behavior for the system. This is an inherent limitation of linear controller design theory. We will prove that if the target dynamics of structure (2.2) satisfy the above two conditions, the target dynamics will always be achievable. We will explain this concept of achievability in Chapter 5. These conditions only guarantee that the target dynamics with the structure given by (2.2) are mathematically achievable; they do not assure that a particular set of J , C and K is a good candidate for a system. A target dynamics with the structure given by (2.2) and a particular set of J , C

and K may not satisfy stability robustness, or even stability condition, even though it is mathematically achievable.

3.3 Stability of the Target Dynamics

We consider two issues of importance in analyzing the stability of a dynamic system that interacts with the environment. The first issue concerns the condition under which equation (2.2) offers a stable target dynamics. The stability of the target dynamics is not enough to assure the stability of the dynamic system and its environment taken as a whole. This brings up the second issue: the global stability of the dynamic system and its environment.

The target dynamics of a system must be stable. Note that stability is not a condition for achievability. We claim that unstable target dynamics are achievable as long as they are simple and J , C and K are non-singular matrices. Stability of the target dynamics depends on the values of J , C and K . One sufficient condition for the stability of the target dynamics is explained in Appendix A. According to this condition, if J , C and K are symmetric, positive definite matrices, then the eigenvalues of the target dynamics lie in the left half complex plane. If K and/or C are symmetric, positive, semi-definite matrices, then some or all eigenvalues will be on the imaginary axis. (These cases are considered unstable.)

If a dynamic system interacts with the environment while satisfying equation (2.5) with symmetric, positive definite J , C and K , the overall system consisting of the environment and the dynamic system will be stable. In other words, if the controller achieves the target dynamics of (2.2) for all $0 < \omega < \infty$, then the overall system (dynamic system and environment) will be stable. This shows that the target impedance has desirable properties. The global stability is proved in Appendix A. The global stability is not a result of the design method, but of the form that we chose for the target dynamics. If the controller does not guarantee equation (2.2) for all $0 < \omega < \infty$ and yields a behavior "approximately" like the target impedance for a bounded frequency range, then the global stability is not guaranteed. Appendix A also gives a sufficient condition for global stability as a function of this approximation.

Chapter 4

Dynamic Behavior of the Manipulators

This chapter is devoted to the Lagrangian derivation of the dynamic model for manipulators and their actuators suitable for impedance control. Section 4.1 presents the steps toward this derivation, while Section 4.2 explains the restrictions and uncertainties associated with the dynamic model. From the standpoint of formalism, some readers may find our treatment superficial; references [23, 24, 53] offer more leisurely developments of this derivation.

4.1 Mathematical Modelling

Dynamic equations that describe the behavior of manipulators are inherently non-linear. Two classes of non-linearities are treated by the manipulator dynamics. One class is associated with the change in the geometrical configuration of the manipulator, while the second is associated with non-differentiable non-linearities, such as dry friction, backlash, etc. In this derivation, we consider only the former, differentiable non-linearities.

Let the joint angles in the manipulator be the system's coordinates. These coordinates vary arbitrarily and independently of each other without violating any constraints that might act on the system. This simply implies that the coordinates are generalized coordinates and the manipulators are holonomic systems. If $M(\Theta)$ is the inertia matrix of a manipulator, then the kinetic co-energy, $T(\Theta, \dot{\Theta})$, can be expressed in quadratic form by equation (4.1).

$$T(\Theta, \dot{\Theta}) = \frac{1}{2} \dot{\Theta}(t)^T M(\Theta) \dot{\Theta}(t) \quad (4.1)$$

where $\Theta(t) = [\theta_1(t), \theta_2(t), \dots, \theta_n(t)]^T$ is the vector of coordinates. $M(\Theta)$ is always a symmetric, positive definite matrix. Lagrange's equations (4.2) are used to derive the dynamic equations [4].

$$\frac{d}{dt} \left[\frac{\partial T(\Theta, \dot{\Theta})}{\partial \dot{\theta}_i(t)} \right] - \frac{\partial T(\Theta, \dot{\Theta})}{\partial \theta_i(t)} + \frac{\partial P(\Theta)}{\partial \theta_i(t)} = f_i(t) \quad i = 1, 2, \dots, n \quad (4.2)$$

$T(\Theta, \dot{\Theta})$ = kinetic co-energy
 $P(\Theta)$ = potential energy from gravitational force
 $f_i(t)$ = generalized force
 $\theta_i(t)$ = generalized coordinate

Equations (4.3), (4.5) and (4.7) are derived to simplify the terms in the set of differential equations represented by (4.2).

$$\left[\frac{d}{dt} \left[\frac{\partial T(\Theta, \dot{\Theta})}{\partial \dot{\theta}_1(t)} \right], \frac{d}{dt} \left[\frac{\partial T(\Theta, \dot{\Theta})}{\partial \dot{\theta}_2(t)} \right], \dots, \frac{d}{dt} \left[\frac{\partial T(\Theta, \dot{\Theta})}{\partial \dot{\theta}_n(t)} \right] \right]^T = M(\Theta) \ddot{\Theta}(t) + \left[\frac{d}{dt} M(\Theta) \right] \dot{\Theta}(t) \quad (4.3)$$

where $\frac{d}{dt} M(\Theta)$ is given by equation (4.4)

$$\frac{d}{dt} M(\Theta) = \frac{\partial M(\Theta)}{\partial \theta_1(t)} \dot{\theta}_1(t) + \frac{\partial M(\Theta)}{\partial \theta_2(t)} \dot{\theta}_2(t) + \dots + \frac{\partial M(\Theta)}{\partial \theta_n(t)} \dot{\theta}_n(t) \quad (4.4)$$

$$- \left[\frac{\partial T(\Theta, \dot{\Theta})}{\partial \theta_1(t)}, \frac{\partial T(\Theta, \dot{\Theta})}{\partial \theta_2(t)}, \dots, \frac{\partial T(\Theta, \dot{\Theta})}{\partial \theta_n(t)} \right]^T = - Q(\Theta, \dot{\Theta}) \dot{\Theta}(t) \quad (4.5)$$

where $Q(\Theta, \dot{\Theta})$ is an $n \times n$ matrix and is given by equation (4.6).

$$Q(\Theta, \dot{\Theta}) = \frac{1}{2} \begin{bmatrix} \dot{\Theta}(t)^T & \frac{\partial M(\Theta)}{\partial \theta_1(t)} \\ \dot{\Theta}(t)^T & \frac{\partial M(\Theta)}{\partial \theta_2(t)} \\ \vdots & \vdots \\ \dot{\Theta}(t)^T & \frac{\partial M(\Theta)}{\partial \theta_n(t)} \end{bmatrix} \quad (4.6)$$

$$\left[\frac{\partial P(\Theta)}{\partial \theta_1(t)}, \frac{\partial P(\Theta)}{\partial \theta_2(t)}, \dots, \frac{\partial P(\Theta)}{\partial \theta_n(t)} \right]^T = F_g(\Theta) \quad (4.7)$$

Substituting equations (4.3), (4.5) and (4.7) into equation (4.2) yields the following set of differential equations, (4.8), for the manipulators.

$$M(\Theta) \ddot{\Theta}(t) + \left[\frac{d}{dt} M(\Theta) - Q(\Theta, \dot{\Theta}) \right] \dot{\Theta}(t) + F_g(\Theta) = F(t) \quad (4.8)$$

where $Q(\Theta, \dot{\Theta})$ and $\frac{d}{dt} M(\Theta)$ are given by equation (4.6) and (4.4). Vector $F(t)$ in equation (4.9) represents the generalized force.

$$F(t) = [f_1(t), f_2(t), \dots, f_n(t)]^T \quad (4.9)$$

The term $\left[\frac{d}{dt} M(\Theta) - Q(\Theta, \dot{\Theta}) \right] \dot{\Theta}(t)$ is associated with gyroscopic forces (e.g., Coriolis forces or Lorentz forces). The n -dimensional vector of $F_g(\Theta)$ is associated with the gravitational forces on the manipulators.

In most constrained manipulations, the motion of a manipulator is very slow; the system operates at "near stall" conditions, mostly because of dynamic and kinematic constraints. For example in grinding, arc welding and metal cutting, the state of the art of current technology is the limiting factor in the speed of such operations. The orders of magnitude of the gyroscopic terms are much smaller than the inertia and the gravity terms in constrained maneuvers; this suggests the elimination of the gyroscopic terms from the differential equations of the motion. This elimination is mathematically equivalent to the linearization of the gyroscopic terms in the neighborhood of an equilibrium point (zero velocity). This point is characterized by the vector Θ_0 . At this stage, the assumption that the manipulator moves slowly does not imply any specific restraint on the inputs to the system. In general, there is no unique characterization associated with the inputs that can generate large-velocity terms. The above assumption rejects all inputs that could give rise to velocity terms. The discussion on page 41 clarifies the conditions on the inputs that will guarantee small velocities. At this stage, it is sufficient to assume that all velocity terms are close to zero. This automatically ensures that the inputs will satisfy the conditions. Equation (4.10) is true at equilibrium.

$$F_g(\Theta_0) = F_0 \quad (4.10)$$

If $\Delta\Theta(t)$ is the perturbation of the generalized coordinate from Θ_0 and $\Delta F(t)$ is the perturbation of the generalized force from F_0 , then the linearized equation of motion is:

$$M(\Theta_0) \ddot{\Delta\Theta}(t) + GR(\Theta_0) \dot{\Delta\Theta}(t) = \Delta F(t) \quad (4.11)$$

where $GR(\Theta_0)$ is an $n \times n$ matrix that can be computed from the following equation:

$$GR(\Theta_0) = \left[\begin{array}{ccc} \frac{\partial F_f(\Theta)}{\partial \theta_1(t)} & \frac{\partial F_f(\Theta)}{\partial \theta_2(t)} & \dots & \frac{\partial F_f(\Theta)}{\partial \theta_n(t)} \end{array} \right]^T \text{ computed at } \Theta = \Theta_0. \quad (4.12)$$

Since the velocity terms in $\left[\frac{d}{dt} M(\Theta) - Q(\Theta, \dot{\Theta}) \right] \dot{\Theta}(t)$ are of the form $\dot{\theta}_i(t)^2$ or $\dot{\theta}_i(t)\dot{\theta}_j(t)$, the linearized form of the gyroscopic terms around the equilibrium point, Θ_0 , vanish from the linearized equations. The linearized form of the gyroscopic term around the non-zero-velocity operating point ($\Theta = \Theta_0$, $\dot{\Theta} = \dot{\Theta}_0$) in general is not zero. Since the target dynamics are specified in the vicinity of the equilibrium point, Θ_0 , we will continue the analysis with the linearized model at the zero-velocity equilibrium point (equation (4.11)).

$M(\Theta_0)$ and $GR(\Theta_0)$ are functions of the configuration of the system, and once the manipulator moves from one point to another point, they change. We plan to update $M(\Theta_0)$ and $GR(\Theta_0)$ as Θ_0 changes. Equation (4.11) represents the dynamic behavior of a manipulator when its motion is slow. Gravity and the inertia of the system are two effects that practitioners always observe in the behavior of the manipulators at low speeds; gravity dominates the motion of the system at very low frequencies, while inertia affects the behavior of the system in the higher frequency range. The generalized force, $\Delta F(t)$, can be expressed by equation (4.13).

$$\Delta F(t) = T_s \Delta T(t) + \Delta N(t) \quad (4.13)$$

$$\Delta N(t) = J_c^T \Delta D(t)$$

where:

$$\Delta T(t) = [\delta t_1(t), \delta t_2(t), \dots, \delta t_n(t)]^T \quad \text{is the perturbation of the actuator torques;}$$

$$\Delta N(t) = [\delta n_1(t), \delta n_2(t), \dots, \delta n_n(t)]^T \quad \text{is the perturbation of the torque loads on the actuators;}$$

$$\Delta D(t) = [\delta d_1(t), \delta d_2(t), \dots, \delta d_n(t)]^T \quad \text{is the perturbation of the interaction load in the global coordinate frame; and}$$

$$J_c \quad \text{is the Jacobian.}$$

T_s is a non-singular square matrix which represents the effect of $\Delta T(t)$ on the coordinates. If the coordinates are independently driven by actuators, then $T_s = I_{nn}$. An example of a non-unity T_s arises when $\Delta \Theta(t)$ is measured absolutely while some actuators are not driving the joint angles from a stationary base. Substituting equation (4.13) in equation (4.11) yields equation (4.14) for the linearized dynamics of the manipulators.

$$M(\theta_0) \ddot{\Delta\theta}(t) + GR(\theta_0) \Delta\theta(t) = T_s \Delta T(t) + \Delta N(t) \quad (4.14)$$

The form of equation (4.14) that describes the behavior of the manipulator in the neighborhood of an equilibrium point in state-space is given by equation (4.15):

$$\begin{bmatrix} \dot{\Delta\theta}(t) \\ \ddot{\Delta\theta}(t) \end{bmatrix} = \begin{bmatrix} 0_{nn} & I_{nn} \\ -M^{-1}(\theta_0)GR(\theta_0) & 0_{nn} \end{bmatrix} \begin{bmatrix} \Delta\theta(t) \\ \dot{\Delta\theta}(t) \end{bmatrix} + \begin{bmatrix} 0_{nn} \\ M^{-1}(\theta_0)T_s \end{bmatrix} \Delta T(t) + \begin{bmatrix} 0_{nn} \\ M^{-1}(\theta_0)J_c^T \end{bmatrix} \Delta D(t) \quad (4.15)$$

where $\Delta\theta(t) = [\delta\theta_1(t), \delta\theta_2(t), \dots, \delta\theta_n(t)]^T$ expresses the perturbed joint-angles.

Equation (4.16) approximates the dynamic behavior of each actuator.

$$\frac{\dot{\delta t_i(t)}}{\lambda_{ai}} + \delta t_i(t) = \delta u_i(t) \quad i = 1, 2, \dots, n \quad (4.16)$$

where:

- λ_{ai} = bandwidth of each actuator
- $\delta u_i(t)$ = input perturbation of each actuator
- $\delta t_i(t)$ = output-torque perturbation of each actuator

Note that equation (4.16) is scaled to produce one unit of torque for each unit of input at equilibrium. Such scaling is common and can always be compensated for at the end of the design procedure by adjusting the open-loop transfer function matrix. The set of differential equations describing the actuation of the manipulator is approximated by equation (4.17).

$$\dot{\Delta T}(t) = A_s \Delta T(t) + B_s \Delta U(t) \quad (4.17)$$

where:

$$A_s = \text{diag}(-\lambda_{a1}, -\lambda_{a2}, \dots, -\lambda_{an})$$

$$B_s = \text{diag}(\lambda_{a1}, \lambda_{a2}, \dots, \lambda_{an})$$

$$\Delta U(t) = [\delta u_1(t), \delta u_2(t), \dots, \delta u_n(t)]^T$$

$$\Delta T(t) = [\delta t_1(t), \delta t_2(t), \dots, \delta t_n(t)]^T$$

Combining equations (4.15) and (4.17) yields equation (4.18) for the dynamics of the manipulator and the actuators.

$$\underbrace{\begin{bmatrix} \Delta \dot{\Theta}(t) \\ \Delta \ddot{\Theta}(t) \\ \Delta \dot{T}(t) \end{bmatrix}}_{\Delta \dot{X}(t)} = \underbrace{\begin{bmatrix} 0_{nn} & I_{nn} & 0_{nn} \\ -M^{-1}(\Theta_0)GR(\Theta_0) & 0_{nn} & M^{-1}(\Theta_0)T_s \\ 0_{nn} & 0_{nn} & A_s \end{bmatrix}}_A \underbrace{\begin{bmatrix} \Delta \Theta(t) \\ \Delta \dot{\Theta}(t) \\ \Delta T(t) \end{bmatrix}}_{\Delta X(t)} + \underbrace{\begin{bmatrix} 0_{nn} \\ 0_{nn} \\ B_s \end{bmatrix}}_B \Delta U(t) + \underbrace{\begin{bmatrix} 0_{nn} \\ M^{-1}(\Theta_0)J_c^T \\ 0_{nn} \end{bmatrix}}_L \Delta D(t) \quad (4.18)$$

If $C = [I_{nn} \quad 0_{nn} \quad 0_{nn}]$, then:

$$\Delta \dot{X}(t) = A \Delta X(t) + B \Delta U(t) + L \Delta D(t) \quad (4.19)$$

$$\Delta \Theta(t) = C \Delta X(t) \quad (4.20)$$

where: $\Delta X(t) \in \mathbb{R}^{3n}$; $\Delta U(t)$, $\Delta D(t)$ and $\Delta \Theta(t) \in \mathbb{R}^n$;

(A, B) is a controllable pair; and
 (A, C) is an observable pair.

Loosely speaking, if the bandwidths of the actuators are much greater than ω_0 in all directions, then the actuator dynamics can be neglected in the dynamic equations (4.18). Neglecting all actuator dynamics results in 2n-state differential equations for the manipulator. Conversely, if an actuator bandwidth is smaller than ω_0 in a given direction, then the actuator dynamics cannot be neglected. Matrix A has 2n eigenvalues associated with the manipulator dynamics and n eigenvalues describing the actuator's bandwidth. If the transfer function matrix that maps $\Delta U(j\omega)$ to $\Delta \Theta(j\omega)$ is $G_p(j\omega)$ and the transfer function matrix that maps $\Delta D(j\omega)$ to $\Delta \Theta(j\omega)$ is $G_p^d(j\omega)$ then the following equations are true:

$$\Delta \Theta(j\omega) = G_p(j\omega) \Delta U(j\omega)$$

$$\Delta\Theta(j\omega) = G_e(j\omega) \Delta D(j\omega)$$

where:

$$G_p(j\omega) = C (j\omega I_{3n3n} - A)^{-1} B \tag{4.21}$$

$$G_p^o(j\omega) = C (j\omega I_{3n3n} - A)^{-1} L . \tag{4.22}$$

Pair (A, L) is not controllable. In forming $G_p^o(j\omega)$, the modes in the uncontrollable space (actuator modes) are cancelled out, so $G_p^o(j\omega)$ becomes a 2n-order system.

The mathematical model given by equation (4.18) is a fair approximation of the non-linear dynamics represented by equation (4.8) as long as $\Delta D(t)$ and $\Delta U(t)$ are bounded in magnitude and frequency. Equation (4.18) is the linearized version of a set of non-linear differential equations in the neighborhood of an arbitrary zero-velocity operating point. The model is therefore valid as long as the velocity terms are close to zero. The smaller the magnitude of the inputs, the closer the model will be to reality, because small inputs result in small velocities as long as the frequency range of operation of the inputs is bounded. The target behavior is specified as an impedance with $\Delta D(t)$ as the system's response to the imposed motion. The block diagram in Figure 4-1 shows how the dynamic system and the environment interact with each other in the ideal case when the target impedance is achieved for all $0 < \omega < \infty$.

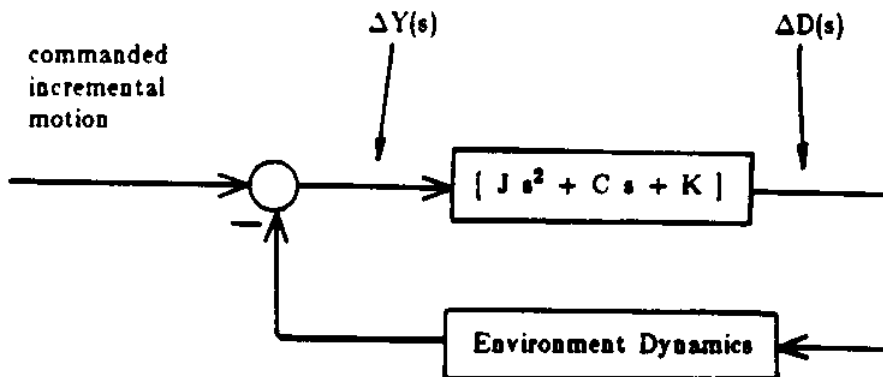


Figure 4-1: The interaction of the dynamic system and environment in the ideal case when the target impedance is achieved for all $0 < \omega < \infty$

The imposed motion is equal to algebraic addition of the commanded incremental motion from the operator and environmental motion. We assume that the environment can be modelled as a linear system; therefore, $\Delta D(t)$ will have bounded frequency range if the

imposed motion from the operator is bounded in frequency range. A slightly more elaborate block diagram is shown in Figure A-1 in Appendix A. Since $\Delta U(t)$ and $\Delta D(t)$ contain most of their energy in the bounded frequency range $0 < \omega < \omega_0$ (ω_0 is introduced in Chapter 2), then by selecting inputs of small magnitude, a designer will never face large velocities in the manipulator dynamics. Note that by confining the frequency range of $\Delta U(t)$ and $\Delta D(t)$ to all $0 < \omega < \omega_0$ and the magnitudes of $\Delta U(t)$ and $\Delta D(t)$ to very small values, a designer eliminates all inputs that could give rise to significant joint-angle velocities.

4.2 Model Uncertainties

Even though some mathematical models reliably represent the dynamics of a system, no nominal model can imitate a dynamic system completely. No mathematical model is more than an approximation of reality; none is absolutely true. The mathematical model given by equation (4.18) will yield a rational approximation of the dynamic system for a certain range of $\Delta U(t)$ and $\Delta D(t)$ which is bounded in magnitude and frequency. Outside this range, the model will depart from reality. The difference in behavior between the model and the real system in various operating regions must be taken into account through a meaningful mathematical method that allows for differences between ideal and real systems. Such discrepancies are called *model uncertainties*.

Let $G'_p(j\omega)$ represent the true dynamics of the system. Satisfying the condition on the input magnitudes, equation (4.23) can be written to show the relationship between the nominal model, $G_p(j\omega)$, and the true dynamics, $G'_p(j\omega)$, by means of $E(j\omega)$ [33].

$$G'_p(j\omega) = G_p(j\omega) [I_{nn} + E(j\omega)] \quad (4.23)$$

$$\sigma_{\max}[E(j\omega)] < e(\omega) \quad \text{for all } \omega \geq 0 \quad (4.24)$$

$E(j\omega)^*$ is called the unstructured model uncertainty because equation (4.23) does not imply any mechanism or structure that gives rise to $E(j\omega)$. $e(\cdot)$ is a positive scalar function which

* The maximum singular value of $E(j\omega)$ is defined as:

$$\sigma_{\max}[E(j\omega)] = \max \frac{\| E(j\omega) x \|}{\| x \|}$$

$x \neq 0_n$ and $\|\cdot\|$ denotes the Euclidean norm [12].

confines $G'_p(j\omega)$ to a neighborhood of $G_p(j\omega)$ with magnitude $e(\omega)$. Equation (4.23) is not the only representation of the true model. We assume that $G'_p(j\omega)$ in equation (4.23) remains a strictly proper finite system. We also assume that $G'_p(j\omega)$ has the same number of unstable modes as $G_p(j\omega)$. The unstable modes of $G_p(j\omega)$ and $G'_p(j\omega)$ need not be identical. Therefore, $E(j\omega)$ may be an unstable operator. The above condition implies that $G_p(j\omega)$ must contain unstable modes of the system (if there are any).

When equation (4.23) is used to represent various unmodelled dynamics of manipulators, the limiting function $e(\omega)$ has the form shown in Figure 4-2. $e(\omega)$ is a bound for unstructured uncertainties. It is non-zero for all frequencies.

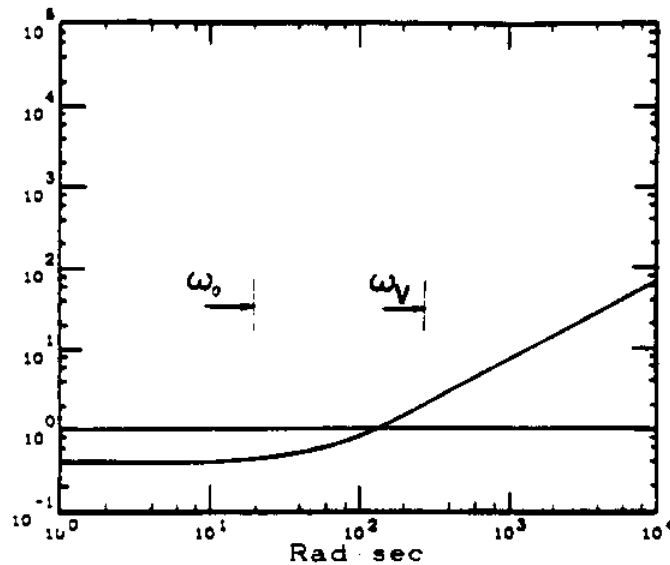


Figure 4-2: $e(\omega)$ is a conservative and educated guess about the difference between the model of the system and the real system.

$e(\omega)$ is usually smaller than unity at low frequencies and increases to unity and above at high frequencies. High-frequency dynamics caused by time delays, electrical resonances, structural dynamics, etc., always exist, but are neglected. This causes equation (4.18) to significantly contradict reality at high frequencies. Lack of knowledge about the precise inertia matrix, the size of the inputs, the effects of perturbations from operating points, nonlinearities such as saturation, etc., give rise to an $e(\omega)$ at all frequencies, while high-frequency unmodelled dynamics contribute significantly to the magnitude of $e(\omega)$ at high frequencies. Saturation is inherently non-linear but can be modelled as open-loop gain reduction for all frequencies.

Since $e(\omega)$ assumes a single worst-case magnitude applicable in all directions, it is helpful

to determine the slowest unmodelled mode in the manipulator. Let the frequency range associated with this mode be ω_v . A good estimation of ω_v allows the designer to determine the frequency range for which the model is nearly valid. (No model is absolutely valid.) This estimation is necessary because it is meaningless to consider equation (2.2) as expressing the target dynamics for all $0 < \omega < \omega_o$ when the frequency range for which the model can be trusted is unknown. Models must be nearly valid for the entire frequency range through which the target dynamics are expected to occur, i.e., $\omega_o < \omega_v$. Figure 4-2 shows the relative sizes of ω_o and ω_v . The upper bound for ω_o can be selected from equation (4.25):

$$\omega_v = c \omega_o \tag{4.25}$$

where c is a constant number whose size depends on the damping of the unmodelled mode. A well-damped unmodelled mode requires a small c (perhaps somewhere between 5 and 10), while an under-damped mode requires a large c (could be as large as 100). ω_v and a conservative guess for c assign an upper bound for ω_o . To meet stability robustness specifications, it is necessary to have a conservative guess for $e(\omega)$ for all $0 < \omega < \infty$. This is because our stability robustness test is a sufficient condition which must be satisfied for all $0 < \omega < \infty$. (This is explained in Chapter 5 and Appendix E.) Experience, a good understanding of the system, and high-performance experimental equipment will enable a designer to make a good guess as to the magnitude for $e(\omega)$ for a wide frequency range. $e(\omega)$ is an educated guess about the difference between the model of the system and the real system which must be supplied by the designer. Here we assume that a conservative guess for $e(\omega)$ is given, along with equation (4.18), to represent the model uncertainty in the system.

To recapitulate, the model in equation (4.18) is considered nearly valid as long as the following conditions are satisfied:

- $\Delta D(t)$ and $\Delta U(t)$ must contain components whose frequency spectra are within ω_o . ω_o must be selected so that $\omega_o < \omega_v$; this is because of the significant difference between the model and the reality of the system for $\omega_v < \omega < \infty$.
- $\Delta D(t)$ and $\Delta U(t)$ must be small enough in magnitude to meet the linearization conditions. (In theory, $\Delta D(t)$ and $\Delta U(t)$ must approach zero.)

Note that most constrained manipulation is quite slow and that the system operates at a near stall. (The slow motion does not imply narrow range of frequencies.) The commands are small in magnitude and they contain bounded frequency components. For example a slow

transition from free to constrained motion (e.g., a manipulator encounters a wall) in principle may contain large (but bounded) frequencies. The nature of constrained manipulations means that the conditions on the magnitude and frequency of the inputs are spontaneously satisfied, and equation (4.18) can be used as a model of the manipulator. (In fact, the natural confinement of the inputs in magnitude and frequency is a strong motivation to linearize the differential equations (4.8).) In unconstrained manipulations, the end-point moves quickly. The inputs are not confined in magnitude and might contain high-frequency components. In many unconstrained maneuvers, the speed of operation is one of the most significant specifications that must be met. The model represented by equation (4.18) is not valid for these types of manipulations.

Chapter 5

Compensator Design

This chapter presents a controller design technique such that a manipulator that obeys dynamic equation (4.18) behaves dynamically like equation (2.2) for all $0 < \omega < \omega_0$. Since we plan to shape a frequency domain relationship between $\Delta D(t)$ and $\Delta Y(t)$, we must not consider the dependence of $\Delta D(t)$ on the dynamics of the environment in this analysis. This allows us to preserve $\Delta D(t)$ so we can arrive at a relationship between $\Delta D(t)$ and $\Delta Y(t)$. Theorem 2 in Appendix A considers the global stability of the manipulator and its environment taken together, based on the dependence of $\Delta D(t)$ on the dynamics of the environment.

Section 5.1 explains the overall design method, the first stage of which requires the measurement of all states of the system, $\Delta X(t)$, and interaction loads, $\Delta D(t)$. Section 5.2 offers a geometric design method to achieve the state-feedback gain. In Section 5.3 we consider the role of force-feedforward gain. Finally, in Section 5.4 we arrive at the design parameters for stability robustness.

5.1 Background

Our analysis of the compensator design for impedance control consists of two stages. During the first stage, it is assumed that all states, $\Delta X(t)$, and interaction loads, $\Delta D(t)$, in equation (4.18) can be measured. The states of the system are joint-angles, joint-angle rates, and actuator torques. There are no acceleration measurements. Suppose the control law in equation (4.19) is chosen so that:

$$\Delta U(t) = -G \Delta X(t) + G_d \Delta D(t) \quad (5.1)$$

$$G = n \times 3n \quad G_d = n \times n .$$

Substituting $\Delta U(t)$ in equation (4.19) yields equation (5.2).

$$\dot{\Delta X}(t) = (A - B G) \Delta X(t) + (L + B G_d) \Delta D(t) \quad (5.2)$$

$$\Delta\theta(j\omega) = G_{c1}(j\omega) \Delta D(j\omega) \quad (5.4)$$

where:

$$G_{c1}(j\omega) = C (j\omega I_{3n \times 3n} - A + B G)^{-1} (L + B G_d) \quad (5.5)$$

$$J_c G_{c1}(j\omega) = G_t(j\omega) \quad (5.6)$$

$J_c G_{c1}(j\omega)$ represents the transfer-function matrix that maps the interaction load, $\Delta D(j\omega)$, to the end-point motion, $\Delta Y(j\omega)$, in the global coordinate frame.

At the second stage of the design, it is assumed that only the first n states of $\Delta X(t)$ (i.e., $\Delta\theta(t)$) and all states of $\Delta D(t)$ are available for measurement. Even though we are not obliged to make such an assumption, we feel more confident offering a final compensator design for impedance control based on the most reliable and extensive set of available measurements.

A new geometric method for full-state observer design is offered to recover the design of the first stage. The geometric recovery procedure allows the designer to achieve the target impedance using only the joint angles, $\Delta\theta(t)$, and the interaction load, $\Delta D(t)$. Chapter 5 is devoted to the first design stage, while Chapter 7 explains the second stage of the design.

5.2 State-Feedback Design

G is designed to guarantee the eigenstructure represented by V (given by equation (3.13)) and Λ (given on page 32) and the stability robustness specification. The complex number s_i and the complex vector u_i that satisfy equation (5.7) are the closed-loop eigenvalue and the right closed-loop eigenvector of equation (5.2).

$$s_i u_i = (A - B G) u_i \quad i = 1, 2, \dots, 3n \quad (5.7)$$

$$u_i \neq 0_{3n}$$

u_i is $3n \times 1$ vector. For convenience, matrix U is formed such that it contains all right closed-loop eigenvectors, u_i , as its columns, and self-conjugate set S is formed such that it contains all closed-loop eigenvalues as its members.

$$U = [u_1 \quad u_2 \quad \dots \quad u_{3n}] \quad (5.8)$$

$$S = \{ s_i : i = 1, 2, \dots, 3n \} \quad (5.9)$$

The object is to design G so that $(A - B G)$ contains the eigenstructure represented by Λ and V . Aside from the case of a single input system, the specification of closed-loop eigenvalues does not uniquely define G . The source of non-uniqueness is the freedom offered by state feedback, beyond eigenvalue assignment, in selecting the associated right closed-loop eigenvectors (or left closed-loop eigenvectors) and generalized eigenvectors from an allowable space. Arbitrary eigenvector assignment in general is not possible. Each closed-loop eigenvector is confined to an allowable sub-space. This allowable sub-space is given in Sections 5.2.1 and 5.2.2. The restriction on the construction of the closed-loop eigenvectors simply implies that one cannot specify all members of each right eigenvector arbitrarily. Only some partitions of each eigenvector in general can be constructed according to design specifications. A unique value for G is determined by the arbitrary pole-placement of S and by the eigenvector construction of U in the allowable sub-space [9, 10, 44, 45, 27, 39]. In other words, a unique value of G can be designed so that :

- the $2n$ dominant closed-loop eigenvalues in S are placed at locations assigned by Λ . The n remaining actuator eigenvalues are moved as far to the left as the stability robustness specifications will allow. (This will be explained in Section 5.4.);
- U is constructed in the allowable sub-space, so that the dominant partition of U contains V .

Since u_i and v_i belong to different spaces, it is necessary to partition U . Here we describe the dominant partition of U and explain how U can be constructed such that it contains V . Partitioning U yields:

$$U = \begin{bmatrix} U_{11} & U_{12} \\ U_{21} & U_{22} \end{bmatrix} \quad (5.10)$$

where : $U_{11} = 2n \times 2n$ $U_{12} = 2n \times n$ $U_{21} = n \times 2n$ $U_{22} = n \times n$.

Assume also that $U = [U_1 \quad U_2]$ where :

$$U_1 = \begin{bmatrix} U_{11} \\ U_{21} \end{bmatrix} , \quad U_2 = \begin{bmatrix} U_{12} \\ U_{22} \end{bmatrix} .$$

U_1 is the set of right closed-loop eigenvectors associated with the $2n$ dominant closed-loop eigenvalues represented by Λ . U_2 is the set of right closed-loop eigenvectors associated

with the n actuator closed-loop eigenvalues. U_{11} shows the contribution of the $2n$ dominant closed-loop eigenvalues to the manipulator states $(\Delta\theta(t), \dot{\Delta\theta}(t))$, while U_{21} shows the effect of the $2n$ dominant eigenvalues on the actuator states $\Delta T(t)$. We construct U_1 such that $U_{11}=V$. In general, because of limitations on eigenstructure construction, a designer cannot form the closed-loop eigenvectors arbitrarily. But in this case, it is possible to construct U_1 so that $U_{11}=V$. In other words, V , which is the set of the right eigenvectors of the target dynamics of (2.6), is in the allowable sub-space determined by the open-loop dynamics. The existence of the right eigenvectors of the target impedance in the allowable sub-space determined by the open-loop dynamics given by equation (4.19) is a significant factor in achieving the target impedance. If V were not in the allowable sub-space, the achievement of V and A , and consequently, the target dynamics of equation (2.6) would not be possible by state-feedback design. This allowable subspace is given in Sections 5.2.1 and 5.2.2. Once U_{11} is constructed to be exactly like V , no choice will remain in constructing U_{21} .

U_{12} shows the effect of non-dominant closed-loop eigenvalues on the manipulator states. U_{22} is the more significant partition of U_2 because it allows the achievement of the uncoupled closed-loop dynamics for the actuators. Once U_{22} is constructed to achieve the uncoupled closed-loop behavior for the actuators, no choice will remain in construction of U_{12} . This issue is explained in Section 5.2.2. Because of the mentioned limitation on construction of eigenvectors, only some partitions of eigenvectors can be constructed arbitrarily. Designers must construct those partitions of eigenvectors that have a more significant role in the closed-loop behavior. In our case, U_{11} and U_{22} are more significant partitions of U_1 and U_2 , respectively. The exact construction of U_{11} and U_{22} and the placement of the $3n$ poles of S are the free choices that linear state-feedback control offers for achieving a unique gain, G . Sections 5.2.1 and 5.2.2 explain how this freedom can be used.

5.2.1 Manipulator Eigenstructure

This section identifies how the manipulator eigenstructure can be constructed. Using equation (5.7), equation (5.11) can be written to express the right closed-loop eigenvector, u_i , associated with the $2n$ dominant eigenvalues. From equation (5.7):

$$\begin{pmatrix} s_i I_{3n3n} - A \\ u_i \neq 0_{3n} \end{pmatrix} u_i + B G u_i = 0_{3n} \quad i = 1, 2, \dots, 2n . \quad (5.11)$$

Since s_i is selected from set A , then $s_i = \lambda_i$. Equation (5.11) can also be written as:

$$\left[\begin{array}{cc} (\lambda_i I_{3n3n} - A) & -B \end{array} \right] \begin{bmatrix} u_i \\ -G u_i \end{bmatrix} = 0_{4n} \quad i = 1, 2, \dots, 2n . \quad (5.12)$$

If $m_i = -G u_i$ where m_i is $n \times 1$ vector then:

$$\left[\begin{array}{cc} (\lambda_i I_{3n3n} - A) & -B \end{array} \right] \begin{bmatrix} u_i \\ m_i \end{bmatrix} = 0_{4n} \quad i = 1, 2, \dots, 2n . \quad (5.13)$$

Equation (5.13) states that $[u_i^T \quad m_i^T]^T$ is in the right null-space of $[(\lambda_i I_{3n3n} - A) \quad -B]$. Since the dimension of the right null-space of $[(\lambda_i I_{3n3n} - A) \quad -B]$ is at least n [54], $[u_i^T \quad m_i^T]^T$ is confined in an n -dimensional sub-space spanned by null vectors of $[(\lambda_i I_{3n3n} - A) \quad -B]$. Because of this restriction on $[u_i^T \quad m_i^T]^T$, not all members of u_i can be selected arbitrarily. u_i must be selected such that $[u_i^T \quad m_i^T]^T$ lies in the null-space of $[(\lambda_i I_{3n3n} - A) \quad -B]$. There is another way of arriving at this confinement. If s_i does not belong to the spectrum of A , then equation (5.14) can be generated from equation (5.7):

$$u_i = - (s_i I_{3n3n} - A)^{-1} B G u_i \quad i = 1, 2, \dots, 2n . \quad (5.14)$$

Since s_i is selected from set Λ , then $s_i = \lambda_i$. u_i can also be expressed by equation (5.15).

$$u_i = (\lambda_i I_{3n3n} - A)^{-1} B m_i \quad i = 1, 2, \dots, 2n \quad (5.15)$$

$$\text{where : } m_i = -G u_i \quad m_i \text{ is } n \times 1 \text{ vector} \quad (5.16)$$

$$\text{Let: } N_i = (\lambda_i I_{3n3n} - A)^{-1} B \quad i = 1, 2, \dots, 2n ; \quad (5.17)$$

$$\text{then : } u_i = N_i m_i \quad i = 1, 2, \dots, 2n . \quad (5.18)$$

Equation (5.18) mathematically justifies the limitation on the construction of the closed-loop eigenvector mentioned previously [16]. Each closed-loop eigenvector, u_i , associated with λ_i must reside in the column space of N_i , which is a function of the closed-loop eigenvalue λ_i and the open-loop dynamics of the manipulator (A,B). This is an important constraint on the construction of the right closed-loop eigenvector, u_i , which is trapped in the n -dimensional sub-space established by columns of N_i .

Because of the confinement of u_i in an n -dimensional subspace, in general, it can be expected that only n members of u_i can be selected arbitrarily. But we are interested in construction of u_i such that its first $2n$ members are like v_i . We show that a vector, u_i , (along with an m_i) exists such that $[u_i^T \quad m_i^T]^T$ is in the null-space of

$[(\lambda_i I_{3n3n} - A) \quad -B]$ and its first $2n$ members are the same as v_i . Consider u_i and m_i given by equations (5.19) and (5.20).

$$u_i = \begin{bmatrix} I_{nn} \\ \lambda_i I_{nn} \\ T_s^{-1} [M(\theta_o) \lambda_i^2 + GR(\theta_o)] \end{bmatrix} \begin{bmatrix} J_c^{-1} q_i \end{bmatrix} \quad i = 1, 2, \dots, 2n \quad (5.19)$$

$$m_i = B_a^{-1} (\lambda_i I_{nn} - A_a) T_s^{-1} [M(\theta_o) \lambda_i^2 + GR(\theta_o)] J_c^{-1} q_i \quad i = 1, 2, \dots, 2n \quad (5.20)$$

The first $2n$ members of u_i are the same as v_i . Form $[(s_i I_{3n3n} - A) \quad -B]$:

$$[(s_i I_{3n3n} - A) \quad -B] = \begin{bmatrix} s_i I_{nn} & -I_{nn} & 0_{nn} & 0_{nn} \\ M^{-1}(\theta_o) GR(\theta_o) & s_i I_{nn} & -M^{-1}(\theta_o) T_s & 0_{nn} \\ 0_{nn} & 0_{nn} & (s_i I_{nn} - A_a) & -B_a \end{bmatrix}. \quad (5.21)$$

Substituting for $[(s_i I_{3n3n} - A) \quad -B]$ from equation (5.21) when $s_i = \lambda_i$, and u_i and m_i from equations (5.19) and (5.20) into equation (5.13), shows that $[u_i^T \quad m_i^T]^T$ is in the null-space of $[(\lambda_i I_{3n3n} - A) \quad -B]$. This substitution shows that u_i , which is given by equation (5.19), is achievable. Since u_i ($i=1,2,\dots,2n$) must be in the right null space of $[(\lambda_i I_{3n3n} - A) \quad -B]$, then no option would remain to construct the last n members of u_i , if the first $2n$ members of u_i are constructed like v_i .

5.2.2 Actuator Eigenstructure

We offer a similar treatment for the actuator eigenvalues and their right corresponding eigenvectors. The actuators in the manipulators are dynamically uncoupled. It is a good practice to preserve this uncoupling in the dynamics of the actuators in the closed-loop case, too. The uncoupling of the closed-loop actuator dynamics allows the designers to achieve different bandwidths for actuators such that they are consistent with their hardware.

It has already been mentioned that U_{22} is the significant partition of U_2 . To achieve the uncoupling of the actuators, U_{22} is chosen to be an identity matrix. Since each right closed-loop eigenvector is confined to an n -dimensional subspace in $3n$ -dimensional space,

constructing U_2 such that $U_{22} = I_{nn}$ is always possible. At this stage, we have not mentioned where the n actuator closed-loop eigenvalues must be located. This will depend on the stability robustness specifications. Section 5.4 is devoted to this matter. For continuity in all material concerning the design of G , readers can assume that the closed-loop eigenvalues of the actuators are located deeper in the left half complex plane than any complex number offered by A . At this point, it does not matter how far from the origin these eigenvalues are located. Section 5.4 clarifies how a designer can use this freedom as to the closed-loop eigenvalues of the actuators to satisfy the robustness specifications. If $m_i = -G u_i$, equation (5.7) can be written as:

$$\begin{bmatrix} (s_i I_{3n3n} - A) & -B \end{bmatrix} \begin{bmatrix} u_i \\ m_i \end{bmatrix} = 0_{4n} \quad i = 2n+1, 2n+2, \dots, 3n. \quad (5.22)$$

$$\text{Let: } U_{22} = [g_1 \quad g_2 \quad \dots \quad g_n] \quad (5.23)$$

where g_i is $n \times 1$ vector and $U_{22} = I_{nn}$. If u_i and m_i are selected according to equations (5.24) and (5.25),

$$u_i = \begin{bmatrix} [M(\theta_0) s_i^2 + GR(\theta_0)]^{-1} T_s \\ [M(\theta_0) s_i^2 + GR(\theta_0)]^{-1} T_s s_i \\ I_{nn} \end{bmatrix} \begin{bmatrix} g_i \end{bmatrix} \quad i = 2n+1, 2n+2, \dots, 3n. \quad (5.24)$$

$$m_i = B_s^{-1} [s_i I_{nn} - A_s] g_i \quad i = 2n+1, 2n+2, \dots, 3n \quad (5.25)$$

then substituting u_i and m_i from equations (5.24) and (5.25) into equation (5.22) and $[(s_i I_{3n3n} - A) \quad -B]$ from equation (5.21) into equation (5.22) shows that $[u_i^T \quad m_i^T]^T$ is in the right null-space of $[(s_i I_{3n3n} - A) \quad -B]$. This shows that u_i , which is given by equation (5.24), is achievable. The last members of u_i are like g_i , which guarantees the uncoupling of the closed-loop actuator dynamics. Note that the inverse of $[M(\theta_0) s_i^2 + GR(\theta_0)]$ always exists as long as s_i is not equal to any eigenvalues of A . One can always multiply u_i by $[M(\theta_0) s_i^2 + GR(\theta_0)]$ to ease this condition. Since u_i ($i=2n+1, 2n+2, \dots, 3n$) must be in the right null space of $[(s_i I_{3n3n} - A) \quad -B]$, then no option would remain to construct the first $2n$ members of u_i , if the last n members of u_i are constructed like v_i .

5.2.3 Computation of G

Once the m_i 's and u_i 's are computed from equations (5.19), (5.20), (5.24) and (5.25), then equation (5.16) can be used to derive equation (5.26) for G.

$$G = - [m_1 \quad m_2 \quad \dots \quad m_{3n}] [u_1 \quad u_2 \quad \dots \quad u_{3n}]^{-1} \quad (5.26)$$

Or equivalently:

$$G = - [m_1 \quad m_2 \quad \dots \quad m_{3n}] U^{-1} \quad (5.27)$$

Equation (5.27) requires that U (given by equation (5.10)) is a full rank matrix. Since the target dynamics are simple, then U_{11} , which is equal to V, is a full rank matrix. This means that U_1 is a $2n$ -rank matrix. Matrix U_2 must be constructed such that $[U_1 \quad U_2]$ is a full rank matrix. We do not give a general procedure to construct U_2 such that $[U_1 \quad U_2]$ is a full rank matrix. But since there is freedom in the selection of the eigenvalues and eigenvectors of the actuators, one can always use this freedom to modify U_2 such that $[U_1 \quad U_2]$ is a full rank matrix. Here we prove that if all closed-loop eigenvalues of the actuators approach infinity at any angle in the left half complex plane, then U is a full rank matrix. It can be verified that as actuator eigenvalues approach negative large numbers, each of the upper $2n$ members of each right eigenvector in equation (5.24) approaches a small number, while the last n members stay constant. This implies that the members of U_{12} of matrix U in equation (5.10) will be much smaller than U_{22} . Suppose $[U_1 \quad U_2]$ is not a full rank matrix. Then there exists at least one column in U_2 which belongs to the column space of U_1 (U_1 is a full rank matrix) as eigenvalues of the actuators approach infinity at any angles in the left half complex plane. Since, in the limit, all members of U_{12} are almost zero, this leads to the dependence of the columns of U_{11} . This is a contradiction because U_{11} is a full rank matrix. The above discussion proves the existence of U^{-1} only when all the eigenvalues of the actuators approach infinity in a stable sense. In practice, we plan to locate the actuator eigenvalues deeper in the left half complex plane than any complex number offered by λ . If U is a full rank matrix, then U^{-1} can be computed as:

$$\begin{bmatrix} [U_{11} - U_{12}U_{22}^{-1}U_{21}]^{-1} & -U_{11}^{-1}U_{12} [U_{22} - U_{21}U_{11}^{-1}U_{12}]^{-1} \\ -U_{22}^{-1}U_{21} [U_{11} - U_{12}U_{22}^{-1}U_{21}]^{-1} & [U_{22} - U_{21}U_{11}^{-1}U_{12}]^{-1} \end{bmatrix} \quad (5.28)$$

Note that we do not consider the independence of the columns of U as a condition for the achievability of the target impedance. This is because one can always use the freedom in

choosing the eigenvalues of the actuators to construct U_2 such that $[U_1 \ U_2]$ is full rank as long as U_1 is a full rank matrix, which will be true if the target impedance is simple. Since U and S are self conjugate, the G will always be a real matrix [39].

5.3 Force-Feedforward Design

Section 5.2 provides a method for designing the state-feedback gain, G , to guarantee the eigenstructure of the target dynamics given by Λ and V . Assuring that the eigenstructure of the target dynamics is achievable does not imply that the target dynamics given by equation (2.2) can be achieved. The following theorem formally states the conditions under which a designer can guarantee that the system will follow the target dynamics, given by equation (2.2), governing the closed-loop behavior of the manipulators for all $0 < \omega < \omega_b$. $(0, \omega_b)$ is the bounded frequency range in which the system may operate.

5.3.1 Theorem

The state-space representation of the dynamic system given by equation (4.18), with state-feedback gain G and force-feedforward gain G_d , is given by equations (5.29) and (5.30).

$$\dot{\Delta X}(t) = (A - B G) \Delta X(t) + (L + B G_d) \Delta D(t) \quad (5.29)$$

$$\Delta \theta(t) = C \Delta X(t) \quad (5.30)$$

$$G = n \times 3n, \quad G_d = n \times n, \quad \Delta \theta(t) \text{ and } \Delta D(t) \in R^n$$

The closed-loop transfer-function matrix that maps $\Delta D(j\omega)$ to $\Delta \theta(j\omega)$ is given by equation (5.31).

$$G_{cl}(j\omega) = C (j\omega I_{3n3n} - A + B G)^{-1} (L + B G_d) \quad (5.31)$$

$$\text{where:} \quad \Delta \theta(j\omega) = G_{cl}(j\omega) \Delta D(j\omega)$$

Suppose all actuator closed-loop eigenvalues are selected to satisfy inequality (5.32):

$$|s_i| > \rho \quad \text{real}(s_i) < 0 \quad i = 2n+1, 2n+2, \dots, 3n, \quad (5.32)$$

where ρ is a positive scalar.

- If ρ approaches ∞ ,

- and if G is designed according to Section 5.2 to guarantee the target eigenstructure V and Λ for the closed-loop system,

then a unique value for G_d can be obtained such that limit (5.33) is true for all ω in the bounded interval $(0, \omega_b)$.

$$\lim_{\rho \rightarrow \infty} J_c G_{cl}(j\omega) = G_t(j\omega) \quad (5.33)$$

Comment

This theorem does not prescribe any value for G_d . It justifies the conditions under which limit (5.33) is true for all $0 < \omega < \omega_b$ without regard to stability robustness. According to this theorem, the satisfaction of inequality (5.32) when ρ approaches ∞ and the selection of G such that V and Λ are guaranteed, ensure a unique value for G_d that leads to limit (5.33) for all $0 < \omega < \omega_b$. The proof is given in Appendix D.

5.3.2 Computation of G_d

Theorem 5.3.1 can be used to compute G_d . Since, for fast actuator eigenvalues a unique value for G_d guarantees that limit (5.33) is true for all $0 < \omega < \omega_b$, limit (5.33) can be used to compute G_d at some frequency in the bounded interval $(0, \omega_b)$. Assume $\omega = 0$ and all eigenvalues of the actuators are located in the left half complex plane farther than any complex number given by Λ . Then from limit (5.33):

$$\text{where } J_c G_{cl}(0) = G_T(0); \quad (5.34)$$

$$G_{cl}(0) = C (-A + B G)^{-1} L_p; \quad \text{and} \quad (5.35)$$

$$G_t(0) = K^{-1}. \quad (5.36)$$

K is non-singular and L_p is given by equation (D.2) in Appendix D. Substituting for $G_{cl}(0)$ and $G_t(0)$ in equation (5.34) results in equation (5.37).

$$J_c C (-A + B G)^{-1} L_p = K^{-1} \quad (5.37)$$

Assume that:

$$G = [G_1 \quad G_2 \quad G_3]$$

where: $G_1 = n \times n$, $G_2 = n \times n$, $G_3 = n \times n$.

Compute $(-A + B G)^{-1}$ as follows:

$$(-A + B G) = \begin{bmatrix} 0_{nn} & -I_{nn} & 0_{nn} \\ M^{-1}(\theta_0)GR(\theta_0) & 0_{nn} & -M^{-1}(\theta_0) T_s \\ B_s G_1 & B_s G_2 & B_s G_3 - A_s \end{bmatrix} \quad (5.38)$$

$$(-A + B G)^{-1} = \begin{bmatrix} \Xi G_2 \\ -I_{nn} \\ T_s^{-1} GR(\theta_0) \Xi G_2 \end{bmatrix} \quad (5.39)$$

$$\begin{bmatrix} \Xi [G_3 + I_{nn}] T_s^{-1} M(\theta_0) & \Xi B_s^{-1} \\ 0_{nn} & 0_{nn} \\ -[G_3 + I_{nn}]^{-1} G_1 \Xi [G_3 + I_{nn}] T_s^{-1} M(\theta_0) & T_s^{-1} GR(\theta_0) \Xi B_s^{-1} \end{bmatrix}$$

where:

$$\Xi = [(G_3 + I_{nn}) T_s^{-1} GR(\theta_0) + G_1]^{-1}.$$

Substituting equation (5.39) in equation (5.37) and solving for G_d produces:

$$G_d = [(G_3 + I_{nn}) T_s^{-1} GR(\theta_0) + G_1] J_c^{-1} K^{-1} - (G_3 + I_{nn}) T_s^{-1} J_c^T. \quad (5.40)$$

5.3.3 Summary of the Design Method

The four following steps can be used to design the feedback and feedforward gains for a given θ_0 .

1- Use equation (5.19) to compute $2n$ closed-loop eigenvector, u_i , associated with the dominant modes. Use equation (5.20) to compute m_i , ($i = 1, 2, \dots, 2n$) which identifies the

location of u_i in its allowable sub-space. q_i and λ_i are given by equations (3.2) or (3.5). The first $2n$ members of u_i are like v_i , so one can also use equations (3.1) and (3.12) to compute the first $2n$ members of u_i . This terminates the construction of dominant modes.

2- Use equation (5.24) to compute a closed-loop eigenvector, u_i , associated with the actuators. Use equation (5.25) to compute m_i , ($i = 2n+1, 2n+2, \dots, 3n$) which identifies the location of u_i in its allowable sub-space. This terminates the construction of non-dominant modes.

3- Use equation (5.26) to compute the state-feedback gain G . The first $n \times n$ partition of G is the joint-angle feedback-gain while the second and the third $n \times n$ partition of G are the velocity and torque feedback-gains.

4- Use equation (5.40) to compute the force-feedforward gain.

5.3.4 Selection of the J-Matrix

If the conditions of the theorem are satisfied, a unique value for G_d can be found such that limit (D.23) is true for all $0 < \omega < \omega_b$. Even though Section 5.3.2 offers a better equation for G_d , one can use equation (D.23) to compute G_d . Equation (D.23) shows another interesting result. If the desired inertia, J , is selected according to equation (5.41):

$$J = J_c^{-T} M(\Theta_0) J_c^{-1} \quad (5.41)$$

then substituting equation (5.41) in equation (D.23) results in $G_d = 0$. This simply means that if the target inertia, J , is chosen according to equation (5.41), then no force measurement is needed to achieve the target dynamics (2.2). This result is significant, since force measurements are not available for many commercial manipulators. The force measurement can be eliminated if the desired frequency range of operation, ω_o , is small enough that it can be parametrized by choosing J according to equation (5.41).

We do not prescribe a unique value for the J-matrix to parametrize ω_o . In fact, there exist an infinite number of matrices that can be selected for J to parametrize ω_o . The size of J is important, not its structure. (One can consider the size of the J-matrix in terms of its singular values.) Here, we summarize some options for the J-matrix. One method is given on page 19 by considering $J = \gamma_1 K$. A designer can also choose the J-matrix to be γI_{nn} , where γ is a positive scalar. Equation (5.41) motivates us to use equation (5.42) to select matrix J .

$$J = \gamma J_c^{-T} M(\Theta_0) J_c^{-1} \quad (5.42)$$

where γ is a positive scalar. Choosing J according to equation (5.42) has the advantage of consistency with the natural behavior of the manipulator because $J_c^{-T} M(\Theta_0) J_c^{-1}$ is the manipulator inertia matrix in the global coordinate frame. γ in equation (5.42) scales the natural inertia of the manipulator the same way in all directions. Note that when γ is not unity in equation (5.42), G_d will not be zero.

5.4 Stability Robustness and the Eigenstructure of the Actuators

In this section we arrive at a design parameter for stability robustness. Given a nominal model, $G_p(j\omega)$, in equation (4.21), an error function, $E(j\omega)$, is given according to equation (4.23) to represent the uncertainties in the system. If the state-feedback gain, G , is used to stabilize the nominal model, $G_p(j\omega)$, then the real model, $G_r(j\omega)$, will also be stable if inequality (5.43) is satisfied.

$$\sigma_{\min} [G_o(j\omega)]^* > e(\omega) \quad \text{for all } 0 < \omega < \infty \quad (5.43)$$

$$\text{where: } G_o(j\omega) = I_{nn} + [G(j\omega I_{nn} - I_{nn})^{-1} B]^{-1}$$

$$\text{and } e(\omega) \geq \sigma_{\max} [E(j\omega)]$$

References [49, 33] leisurely explain this concept in greater depth. Appendix E gives a summary of the derivation of inequality (5.43).

The object is to design G so that inequality (5.43) is satisfied. Figure 6-6-b shows a case in which inequality (5.43) is satisfied. The closed-loop eigenstructure of the n actuators is the only freedom left in the design of G . Theorem 5.3.1 states that if all the closed-loop eigenvalues of the target dynamics approach $-\infty$, then the target dynamics represented by equation (2.2) can be achieved for all $0 < \omega < \omega_b$. Placement of the closed-loop actuator eigenvalues deep in the left half complex plane is not trivial. A trade-off must occur between

*The minimum singular value of $G_o(j\omega)$ is defined as:

$$\sigma_{\min} [G_o(j\omega)] = \min \frac{ \| G_o(j\omega) x \| }{ \| x \| }$$

$x \neq 0_n$ and $\| \cdot \|$ denotes the Euclidean norm [12].

performance through a wide frequency range and stability robustness.

Suppose the closed-loop eigenvalues of the actuators are located at $\alpha\lambda_{a1}, \alpha\lambda_{a2}, \dots, \alpha\lambda_{an}$. Scaling all closed-loop actuator eigenvalues to one number preserves bandwidth ratios for the actuators that are consistent with the hardware. The farther from the origin the n closed-loop eigenvalues of the actuators are located, the larger will be $G (j\omega I_{nn} - I_{nn})^{-1} B$. Figure 5-2 shows how $G (j\omega I_{nn} - I_{nn})^{-1} B$ is affected by the locations of the closed-loop eigenvalues. We show that two design factors contribute in stability robustness; ω_0 and α .

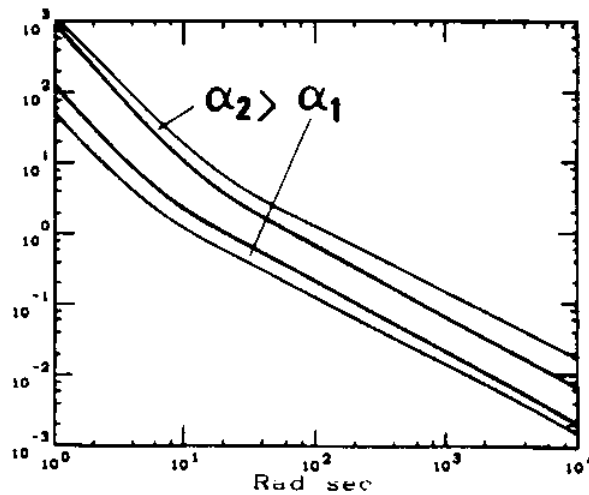


Figure 5-2: σ_{\max} and σ_{\min} of $G (j\omega I_{nn} - I_{nn})^{-1} B$ for Various Actuator Closed-Loop Eigenvalues

Note that the closed-loop actuator eigenvalues that are far from the origin act as gains for $G (j\omega I_{nn} - I_{nn})^{-1} B$. Large values for these eigenvalues shift $G (j\omega I_{nn} - I_{nn})^{-1} B$ up. This is true only when the closed-loop actuator eigenvalues are located much farther from the origin than any complex number offered by A . Since closed-loop actuator eigenvalues that are far from the origin result in a large $G (j\omega I_{nn} - I_{nn})^{-1} B$ for a wide frequency range, inequality (5.43) may not be satisfied for all $0 < \omega < \infty$. This is true because a large $G (j\omega I_{nn} - I_{nn})^{-1} B$ for a wide frequency range allows $G_o(j\omega)$ to remain very close to unity for a wide frequency range, which may, in return, cause a violation of inequality (5.43) if $e(\omega)$ does not also remain close to unity for a wide frequency range. Figure 6-5-b shows a case in which inequality (5.43) is not satisfied. On the other hand, according to theorem 5.3.1, the larger α is selected to be, the closer $J_c G_c(j\omega)$ will be to $G_t(j\omega)$ for all $0 < \omega < \omega_b$. So the closed-loop actuator eigenvalues must be placed in the left half complex plane as far as

possible without violating the stability robustness specification. In selecting α , $G_o(j\omega)$ must preserve stability robustness specifications at all frequencies. We do not offer any value for α ; it is the designer's choice. Selecting a good value for α requires experience and an understanding of the system. α must be large enough to guarantee that the performance specifications will be met, but small enough to guarantee that the stability robustness specifications will also be fulfilled. Theorem 5.3.1 clarifies how a large α can guarantee the performance specifications for a bounded frequency range.

Given J , C and K , the locations of the eigenvalues of the actuators can be altered to meet the stability robustness specifications. If the designer can meet neither stability robustness nor performance specifications with only one set of actuator closed-loop dynamics, then the designer must compromise on the set of performance specifications or model the high-frequency dynamics for the manipulators. In other words, if the actuator closed-loop eigenvalues are required to be in the neighborhood of the complex numbers of Λ to meet the stability robustness specifications at high frequencies, then it is necessary to model the manipulator more precisely at high frequencies or to reconsider the set of performance specifications. The parameter in the set of performance specifications that can be altered most effectively to meet the stability robustness specifications is ω_o , the frequency range in which the relationship between interaction load and displacement is approximately independent of frequency: $\Delta D(j\omega) \approx K \Delta Y(j\omega)$. Shaping the loop transfer function $G (sI_{nn} - A)^{-1} B$ for all $0 < \omega < \omega_o$ is the requirement to produce this frequency-independent relationship. On the other hand, one cannot shape $G (sI_{nn} - A)^{-1} B$ arbitrarily for an arbitrary frequency range because inequality (5.43) must be satisfied for all $0 < \omega < \infty$. Satisfying inequality (5.43) at low frequencies is trivial because of the small size of $e(\omega)$. At larger frequencies, $G (sI_{nn} - A)^{-1} B$ must become small to satisfy inequality (5.43). Therefore, the smaller ω_o is selected to be, the more robustness to high-frequency unmodelled dynamics can be achieved. Since ω_o is parametrized by J , it is necessary to consider a larger J (and consequently a smaller ω_o) as a compromise to meet the stability robustness specifications at high frequencies. Of course, the K -matrix can also be altered to change ω_o . The following summarizes the effects of ω_o and α on stability robustness.

	More stability		Less stability
Increasing ω_o or α	> robustness in>	robustness in
	uncertainties of the		high frequency
	modelled dynamics		unmodelled dynamics

Decreasing ω_0 or α > **Less stability**
robustness in
uncertainties of the
modelled dynamics

..... > **More stability**
robustness in
high frequency
unmodelled dynamics

Chapter 6

Examples

6.1 Example 1

Consider the planar manipulator with two degrees of freedom shown in Figure 6-1. Both of its joint angles are powered from the stationary base. The second link is driven by an actuator on the base via a relatively stiff chain. The mass, length and moment of inertia of each link are represented by δm_1 , δx_1 and i_1 . The variables i_1 and i_2 are the moments of inertia of the links relative to their end-points. δl_2 locates the center of mass of the second link.

$$\begin{aligned} \delta m_2 &= .7464/32.2 \text{ lbf. sec}^2/\text{ft} \\ \delta x_1 &= 1 \text{ ft} \\ \delta x_2 &= .91667 \text{ ft} \\ i_1 &= .00403 \text{ lbf. ft. sec}^2 \\ i_2 &= .0074381 \text{ lbf. ft. sec}^2 \\ \delta l_2 &= .34375 \text{ ft} \\ \theta_1 &= 30^\circ \\ \theta_2 &= 45^\circ \end{aligned}$$

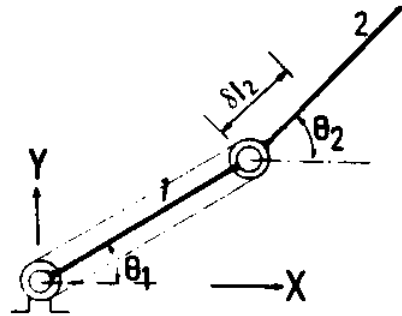


Figure 6-1: Manipulator with Two Degrees of Freedom

The inertia matrix and Jacobian are:

$$M(\theta_0) = \begin{bmatrix} i_1 + \delta m_2 \delta x_1^2 & \delta m_2 \delta x_1 \delta l_2 \cos(\theta_2 - \theta_1) \\ \delta m_2 \delta x_1 \delta l_2 \cos(\theta_2 - \theta_1) & i_2 \end{bmatrix}$$

$$J_c = \begin{bmatrix} -\delta x_1 \sin(\theta_1) & -\delta x_2 \sin(\theta_2) \\ \delta x_1 \cos(\theta_1) & \delta x_2 \cos(\theta_2) \end{bmatrix}$$

Substituting the numerical values for each variable in the inertia matrix and the Jacobian matrix gives:

$$M(\theta_0) = \begin{bmatrix} 2.7210\text{D-}02 & 7.6967\text{D-}03 \\ 7.6967\text{D-}03 & 7.4381\text{D-}03 \end{bmatrix} \quad J_c = \begin{bmatrix} -5.0000\text{D-}01 & -6.4818\text{D-}01 \\ 8.6603\text{D-}01 & 6.4818\text{D-}01 \end{bmatrix}$$

Since the manipulator is mounted horizontally, gravity does not affect it. The actuator driving θ_1 has a bandwidth of 8 rad/sec, while the other actuator has a bandwidth of 10 rad/sec. The actuator dynamics can be expressed by matrices A_a and B_a according to equation (4.17). Since θ_2 is not the relative angle between the two links and since the actuators are powering the system from a stationary base, $T_1=I_n$ in equations (4.13) and (4.15).

$$A_a = \begin{bmatrix} -8. & 0. \\ 0. & -10. \end{bmatrix} \quad B_a = \begin{bmatrix} 8. & 0. \\ 0. & 10. \end{bmatrix}$$

A, B and C in equations (4.19) and (4.20) can be written as :

$$A = \begin{bmatrix} 0. & 0. & 1. & 0. & 0. & 0. \\ 0. & 0. & 0. & 1. & 0. & 0. \\ 0. & 0. & 0. & 0. & 5.1959D+01 & -5.3766D+01 \\ 0. & 0. & 0. & 0. & -5.3766D+01 & 1.9008D+02 \\ 0. & 0. & 0. & 0. & -8. & 0. \\ 0. & 0. & 0. & 0. & 0. & -10. \end{bmatrix}$$

$$B = \begin{bmatrix} 0. & 0. & 0. & 0. \\ 0. & 0. & 0. & 0. \\ 0. & 0. & 8.870 & 10.148 \\ 0. & 0. & -96.323 & -10.143 \\ 8. & 0. & 0. & 0. \\ 0. & 10. & 0. & 0. \end{bmatrix} \quad L = \begin{bmatrix} 8.870 & 10.148 \\ -96.323 & -10.143 \end{bmatrix} \quad C = \begin{bmatrix} 1. & 0. & 0. & 0. & 0. & 0. \\ 0. & 1. & 0. & 0. & 0. & 0. \end{bmatrix}$$

The designer must provide not only the nominal model for the manipulator, but also the bound for the uncertainties, $e(\omega)$. The model uncertainty for this example is given by $e(\omega)$ in Figures 4-2. $e(\omega)$ takes the value of .4 at low frequencies and rises to 2 at 35 hertz. The first unmodelled mode that represents a bending dynamic of the manipulator takes place at 35 hertz (220 rad/sec) with $e(220)=2$. The large magnitude of $e(\omega)$ at 220 rad/sec shows that the unmodelled mode is under-damped. Most space manipulators have under-damped structural modes. The large values for $e(\omega)$ at high frequencies for under-damped, unmodelled modes force designers to design low-bandwidth systems to avoid possible instabilities. According to this model uncertainty, the dynamic model is nearly valid for an approximate range of 10 hertz.

We will now consider four different cases. In Cases 1 and 2, the actuator dynamics are considered in modelling the manipulator, while in Cases 3 and 4, the actuators are fast

enough to be neglected in the modelling of the system. Because of this approximation, the feedback gains, G , are smaller in Cases 3 and 4 than in Cases 1 and 2. We show how the smaller size of G in Cases 3 and 4 results in more robustness to high-frequency unmodelled dynamics.

In Case 1, we examine the role of α , which is introduced on page 60. α measures the location of the closed-loop eigenvalues of the actuators. In Case 2, a smaller ω_0 is desired, which motivates us to use equation (5.41) for the target inertia matrix. We have shown (page 58) that if equation (5.41) is used for the target inertia and if the actuator eigenvalues are placed far in the left half complex plane, then force-feedforward can be eliminated. Cases 3 and 4 repeat the design specifications of Cases 1 and 2 with fast actuators. In Cases 3 and 4, we consider the role of G in stability robustness.

Case 1

The design specifications in the global cartesian coordinate frame are:

- stiffness in direction X = .615 lbf/ft for $0 < \omega < 6.283$ rad/sec (1 hertz);
- stiffness in direction Y = 12.3 lbf/ft for $0 < \omega < 6.283$ rad/sec.

Note that the desired frequency range of operation is selected within the range for which the model is nearly valid. The stiffness ratio is about 20. The low stiffness in direction X generates a "soft" positioning system for the end-point along direction X, while a larger stiffness in direction Y guarantees a relatively "stiff" positioning system in that direction. Note that the natural behavior of the manipulator in the configuration shown in Figure 6-1 opposes the desired performance specification. In other words, the inertia of the manipulator in the global cartesian frame, $J_c^{-T} M(\Theta_0) J_c^{-1}$, makes it much easier to keep the manipulator "softer" in direction Y than in direction X. The following diagonal target dynamics are proposed to parametrize the design specifications.

$$K = \begin{bmatrix} 0.615 & 0.0 \\ 0.000 & 12.3 \end{bmatrix} \quad C = \begin{bmatrix} 7.9965D-02 & 0.0000D+00 \\ 0.0000D+00 & 1.2388D+00 \end{bmatrix} \quad J = \begin{bmatrix} 2.4725D-03 & 0.0000D+00 \\ 0.0000D+00 & 2.9670D-02 \end{bmatrix}$$

The diagonal inertia matrix and the diagonal damping matrix are selected such that the stiffness value for each direction guarantees the desired behavior within a frequency range of 6.283 rad/sec. Note that since we choose a diagonal target dynamics, selection of J - and C - matrices for a given K -matrix is trivial. We choose each member of C and J such that, at each direction, a slightly over-damped, stable, second-order impedance results. The transfer function of the target dynamics $G_t(s)$ is:

$$\begin{bmatrix} 1.6250 \frac{1}{(s/12.62 + 1)(s/19.72 + 1)} & 0 \\ 0 & 0.0812 \frac{1}{(s/16.2 + 1)(s/25.4 + 1)} \end{bmatrix}$$

Figure 6-2-a shows how the equation that expresses the target dynamics of the system, $G_t(s) = [J s^2 + C s + K]^{-1}$, represents the desired stiffness values and frequency range of operation.

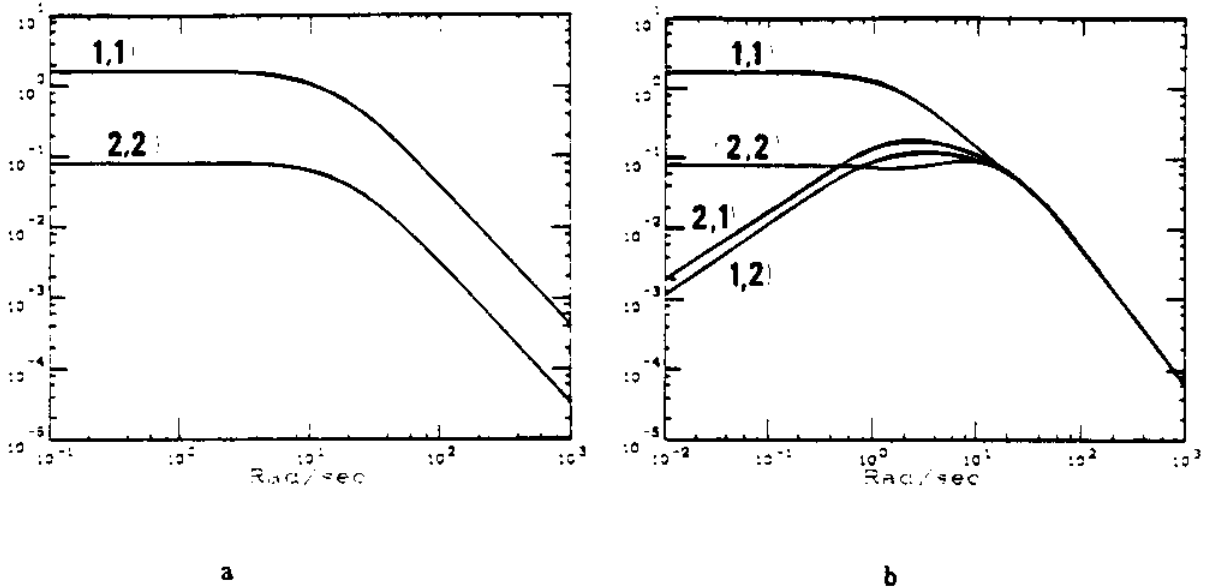


Figure 6-2: a: The Target Dynamics, $G_t(j\omega)$, in Case 1
 b: The Target Dynamics, $G_t(j\omega)$, in Case 2
 The numbers in the parentheses indicate the row and column of each member of the matrix, respectively.

The eigenstructure of the target dynamics can be represented by V (equation (3.13)) and by Λ which is defined on page 32:

$$\Lambda = \{ -12.621, -19.72, -16.294, -25.459 \}$$

$$V = \begin{bmatrix} 2.7321 & 2.7321 & 2.7321 & 2.7321 \\ -3.6502 & -3.6502 & -2.1075 & -2.1075 \\ -34.4812 & -53.8768 & -44.5150 & -69.5547 \\ 46.0696 & 71.9837 & 34.3382 & 53.6535 \end{bmatrix}$$

For $\alpha=5$, the closed-loop eigenvalues of the actuators are located at -40 and -50. This preserves the bandwidth ratio of 8/10 for the actuators. The set of closed-loop eigenvalues, S , is given by:

$$S = \{ -12.621, -19.72, -16.294, -25.459, -40., -50. \} .$$

Using equations (5.19) and (5.24) in Chapter 5, U can be computed to be:

$$U = \begin{bmatrix} 2.7321 & 2.7321 & 2.7321 & 2.7321 & 3.2475D-02 & -2.1506D-02 \\ -3.6502 & -3.6502 & -2.1075 & -2.1075 & -3.3604D-02 & 7.6031D-02 \\ -34.4812 & -53.8768 & -44.5150 & -69.5547 & -1.2990 & 1.0753 \\ 46.0696 & 71.9837 & 34.3382 & 53.6535 & 1.3441 & -3.8016 \\ 7.3663 & 17.9840 & 15.4295 & 37.6697 & 1.0000 & 0.0000 \\ -0.9753 & -2.3812 & 1.4209 & 3.4690 & 0.0000 & 1.0000 \end{bmatrix}$$

Note that the first 4×4 members of U are identical to V. Equations (5.20) and (5.25) can be used to compute m_i ($i = 1, 2, \dots, 6$) as follows:

$$\begin{bmatrix} -4.2549 & -26.3472 & -15.9958 & -82.2082 & -4.0000 & 0.0000 \\ 0.2556 & 2.3146 & -0.8943 & -5.3627 & 0.0000 & -4.0000 \end{bmatrix}$$

The state-feedback gain, G, can be computed via equation (5.26).

$$G = \begin{bmatrix} 70.2275 & 36.2133 & 8.0851 & 3.5328 & 8.6901 & 3.4930 \\ 13.9391 & 12.4491 & 1.7793 & 1.6355 & 0.0786 & 7.6573 \end{bmatrix}$$

The force-feedforward gain can be computed via equation (5.40).

$$G_d = \begin{bmatrix} 104.0860 & -1.2679 \\ -6.3087 & -4.7171 \end{bmatrix}$$

The size of α is limited by the stability robustness specifications. Figure 6-3 shows that large values for α will lead to a violation of the stability robustness specifications (inequality (5.43)) at high frequencies. The system violates the stability robustness specifications for $\alpha=10$, and meets the stability robustness specifications for $\alpha=5$. Large values of α result in large G which leads to large values of $G (sI_{nn} - A)^{-1} B$. Figure 6-4 shows the closed-loop transfer function $J_c G_{cl}(s)$ for various values of α . The larger α is selected to be, the closer the closed-loop transfer function $J_c G_{cl}(s)$ will be to $G_c(s)$ for a bounded frequency range. For small values of α , the members of $J_c G_{cl}(s)$ will exhibit strong coupling; therefore, satisfaction of the performance specifications is not guaranteed at low frequencies. On the other hand, large values of α result in a trivial coupling between the members of $J_c G_{cl}(s)$ at low frequencies (as long as $G_o(j\omega) = I_{nn} + [G(j\omega I_{nn} - A)^{-1} B]^{-1}$ does not violate the stability robustness specifications). Even though a large α ensures better performance, it produces large values for the state-feedback gain, G, and the force-feedforward gain, G_d .

The transfer function matrix $J_c G_{cl}(s)$ is shown below for $\alpha=5$.

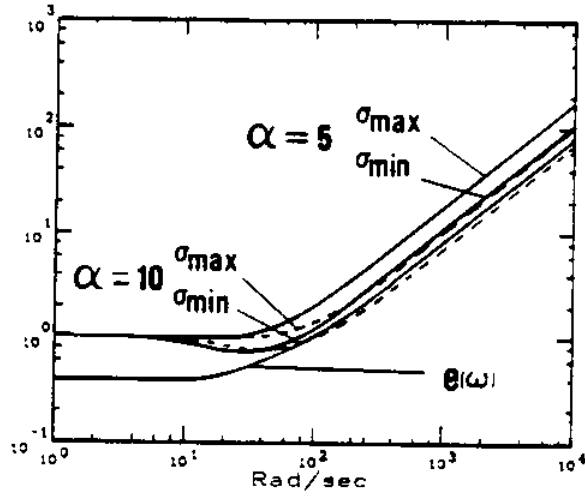


Figure 6-3: σ_{\max} and σ_{\min} of $G_o(j\omega)$ for $\alpha=5$ and $\alpha=10$

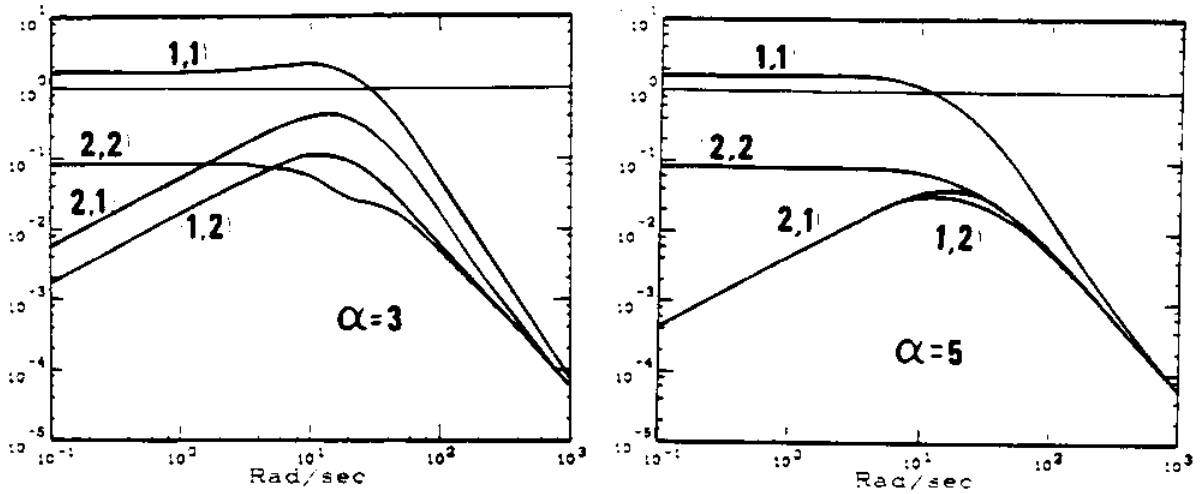


Figure 6-4: The Closed-Loop Transfer Function Matrix, $J_c G_{cl}(j\omega)$, in Case 1

$$\begin{bmatrix} 1.6250 \frac{(s/310 + 1)(s/46 + 1)}{(s/12.62 + 1)(s/19.72 + 1)} & -4.42D-03 \frac{s(s/41 + 1)}{(s/12.62 + 1)(s/19.72 + 1)} \\ -4.28D-03 \frac{s(s/65.8 + 1)}{(s/16.2 + 1)(s/25.46 + 1)} & 0.0812 \frac{(s/32 + 1)(s/37 + 1)}{(s/16.2 + 1)(s/25.4 + 1)} \end{bmatrix}$$

The off-diagonal members of $J_c G_{cl}(j\omega)$ for $\alpha=5$ are much smaller than the diagonal members and therefore, the plot of $J_c G_{cl}(j\omega)$ in Figure 6-4 resembles the target dynamics in Figure 6-2-a for all $0 < \omega < \omega_o$.

Note that the elemental zeros at the origin of the complex plane cause the off-diagonal members of $J_c G_{cl}(s)$ to be very small at low frequencies. The elemental zeros are located outside the operating frequency range and do not contribute to the dynamics in the frequency range of operation. If α is selected to be large, then all non-zero elemental zeros will be very large, and as α approaches ∞ , all non-zero elemental zeros will approach ∞ , all off-diagonal terms will approach zero, and $J_c G_{cl}(s)$ will approach $G_t(s)$. On the other hand, α cannot be selected to be a large number since this would violate the stability robustness specifications. α must be selected to be large enough to insure that the performance specifications will be met, but small enough so that $G_o(j\omega)$ will not violate the stability robustness specifications.

Case 2

Now suppose the performance specifications have been changed as follows:

- stiffness in direction X = .61538 lbf/ft for $0 < \omega < .6283$ rad/sec (0.1 hertz);
- stiffness in direction Y = 12.308 lbf/ft for $0 < \omega < .6283$ rad/sec.

The stiffness values are the same as for Case 1, but the frequency range of operation is smaller. In fact, this is almost the case of static stiffness. If we take $J_c^{-T} M(\Theta_o) J_c^{-1}$ to be equal to the target inertia, then we might be able to achieve the target dynamics without any force-feedforward gain. Using equation (5.41) for the target inertia matrix results in:

$$J = J_c^{-T} M(\Theta_o) J_c^{-1} ,$$

or:

$$J = \begin{bmatrix} 1.4869D-01 & 1.3925D-01 \\ 1.3925D-01 & 1.4750D-01 \end{bmatrix} .$$

The following damping matrix is proposed to produce a stable impedance:

$$C = \begin{bmatrix} 0.55 & 0.9 \\ 1.40 & 2.5 \end{bmatrix} .$$

C is not a symmetric, positive, definite matrix, but the target dynamics are stable. (See Appendix A for the sufficient conditions for the stability of the target dynamics.) Figure 6-2-b shows how the plot of $G_t(s) = [J s^2 + C s + K]^{-1}$ represents the desired stiffness

values and frequency range of operation. As Figure 6-2-b shows, using $J_c^{-T} M(\Theta_0) J_c^{-1}$ as the target inertia matrix produces a very narrow frequency range of operation, about the size required by the performance specifications. As explained on page 20, even though J and C are not diagonal matrices, the target dynamics exhibit an approximate uncoupled behavior for $0 < \omega < .6283$ rad/sec. For all $0 < \omega < \omega_0$, the off-diagonal members of $G_i(j\omega)$ are much smaller than the diagonal members. The eigenstructure of the proposed dynamics is represented by Λ and V :

$$\Lambda = \{ -26.062, -20.427, -1.2812, -4.3664 \},$$

$$V = \begin{bmatrix} -0.6205 & -0.8052 & 19.0481 & 6.0533 \\ -1.0641 & -0.9216 & -23.9070 & -6.5449 \\ 16.1711 & 16.4487 & -24.4041 & -26.4311 \\ 27.7331 & 18.8259 & 30.6292 & 28.5777 \end{bmatrix}$$

U can be computed by equation (5.19) and (5.24) to achieve the target dynamics.

$$U = \begin{bmatrix} -0.6205 & -0.8052 & 19.0481 & 6.0533 & 8.1187D-05 & -5.3766D-05 \\ -1.0641 & -0.9216 & -23.9070 & -6.5449 & -8.4009D-05 & 1.9008D-04 \\ 16.1711 & 16.4487 & -24.4041 & -26.4311 & -6.4949D-02 & 5.3766D-02 \\ 27.7331 & 18.8259 & 30.6292 & 28.5777 & 6.7207D-02 & -1.9008D-01 \\ -17.0306 & -12.1023 & 0.5487 & 2.1799 & 1.0000D+00 & 0.0000D+00 \\ -8.6198 & -5.4464 & -0.0512 & -0.0399 & 0.0000D+00 & 1.0000D+00 \end{bmatrix}$$

The first 4×4 sub-matrix of U is identical to V. The smallest value of α that guarantees the achievement of the desired stiffness for $0 < \omega < .6283$ rad/sec without a force-feedforward gain is 100. This is the proposed value for J that causes G_d to approach zero for large values of α . $J_c G_{cl}(s)$ is shown in Figure 6-5-a for $\alpha=100$. Figure 6-5-b shows $G_o(j\omega)$ for $\alpha=100$, which violates the stability robustness specification. Nor does $J_c G_{cl}(s)$ converge to $G_i(s)$ for smaller values of α . Since no α guarantees the stability robustness and performance specifications at the same time, the design specifications cannot be met. If the structural unmodelled dynamics were to occur at higher frequencies, then the design specifications could be met without force-feedback. Using the above target inertia matrix requires a large α to meet the performance specifications without a force-feedforward gain. If a force-feedforward gain is allowed, then the above performance specifications can be met by a small α which will ensure the stability robustness specifications as well.

Case 3

In this case, the bandwidths of the actuators are about 40 hertz. The performance specifications are similar to those of Case 1:

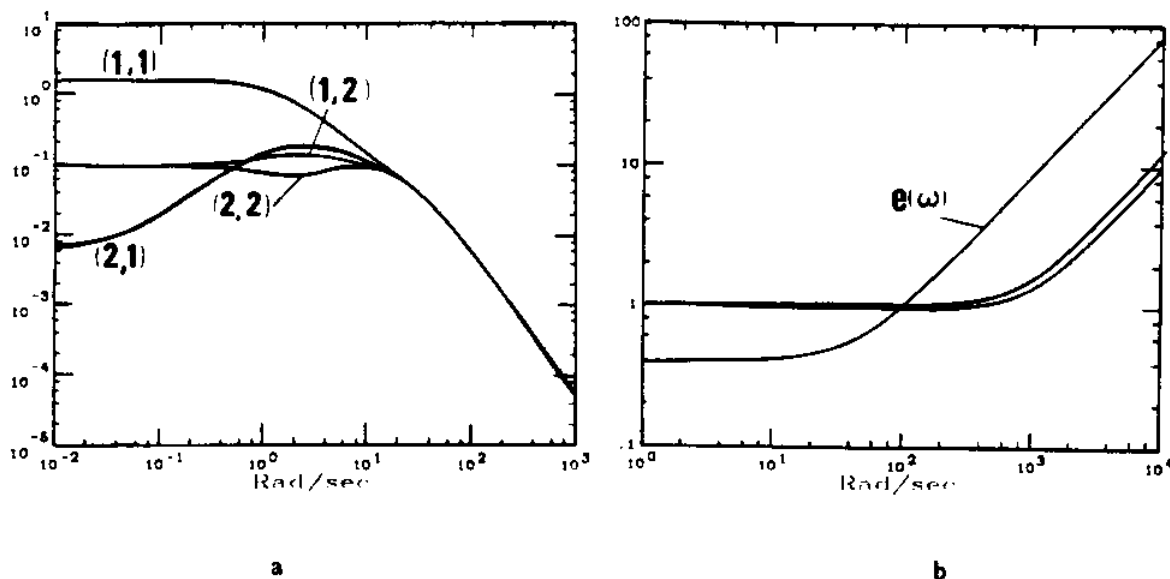


Figure 6-5: a: The Closed-Loop Transfer Function Matrix, $J_c G_{cl}(j\omega)$
 b: σ_{max} and σ_{min} of $G_0(j\omega)$ in Case 2

- stiffness in direction X = .61538 lbf/ft for $0 < \omega < 6.283$ rad/sec;
- stiffness in direction Y = 12.308 lbf/ft for $0 < \omega < 6.283$ rad/sec.

Since the bandwidths of the actuators are much larger than the frequency range of operation, the dynamics of the actuators can be neglected. The manipulator is modelled according to the equations given in Appendix C. A, B, L and C in equation (C.1) can be written as:

$$A = \begin{bmatrix} 0. & 0. & 1. & 0. \\ 0. & 0. & 0. & 1. \\ 0. & 0. & 0. & 0. \\ 0. & 0. & 0. & 0. \end{bmatrix} \quad L = \begin{bmatrix} 0. & 0. \\ 0. & 0. \\ 5.1959D+01 & -5.3766D+01 \\ -5.3766D+01 & 1.9008D+02 \end{bmatrix}$$

$$B = \begin{bmatrix} 0.0000D+00 & 0.0000D+00 \\ 0.0000D+00 & 0.0000D+00 \\ 5.1959D+01 & -5.3766D+01 \\ -5.3766D+01 & 1.9008D+02 \end{bmatrix} \quad C = \begin{bmatrix} 1. & 0. & 0. & 0. \\ 0. & 1. & 0. & 0. \end{bmatrix}$$

The target dynamics in Case 1 are selected to parametrize the performance specifications. The eigenstructure of the target dynamics can be represented by V (Equation (3.13)) and by A, which is given on page 32:

$$A = \{ -12.621 \quad -19.720 \quad -16.294 \quad -25.459 \}.$$

$$V = \begin{bmatrix} 0.2158 & -4.8722 & 0.1674 & -4.8661 \\ -0.2883 & 6.5097 & -0.1291 & 3.7537 \\ -2.7235 & 96.0812 & -2.7269 & 123.8854 \\ 3.6388 & -128.3721 & 2.1035 & -95.5635 \end{bmatrix}$$

The set of closed-loop eigenvalues, S , is equal to Λ . Using equation (C.2) in Appendix C, U can be computed to be:

$$U = \begin{bmatrix} 0.2158 & -4.8722 & 0.1674 & -4.8661 \\ -0.2883 & 6.5097 & -0.1291 & 3.7537 \\ -2.7235 & 96.0812 & -2.7269 & 123.8854 \\ 3.6388 & -128.3721 & 2.1035 & -95.5635 \end{bmatrix}$$

Note that U and V are identical. Equation (C.3) can be used to compute m_i , ($i=1,2,3,4$):

$$\begin{bmatrix} 0.5818 & -32.0718 & 0.9452 & -67.0943 \\ -0.0770 & 4.2465 & 0.0870 & -6.1788 \end{bmatrix}$$

The state-feedback gain, G , and the force-feedforward gain, G_d , can be computed via equations (C.4) and (C.5).

$$G = \begin{bmatrix} 15.1237 & 8.1663 & 1.3537 & 0.6035 \\ 2.6847 & 2.4269 & 0.2925 & 0.2732 \end{bmatrix}$$

$$G_d = \begin{bmatrix} 19.2034 & 1.0928 \\ -1.8282 & -0.4678 \end{bmatrix}$$

The transfer function matrix $J_c G_{cl}(s)$ is:

$$\begin{bmatrix} 1.6250 \frac{1}{(s/12.62 + 1)(s/19.72 + 1)} & 0 \\ 0 & 0.0812 \frac{1}{(s/16.2 + 1)(s/25.4 + 1)} \end{bmatrix}$$

$J_c G_{cl}(s)$ is shown in Figure 6-6-a. Note that neglecting the actuator dynamics eliminates the freedom to adjust $G_o(j\omega)$, which is shown in Figure 6-6-b. If $G_o(j\omega)$ violates the stability robustness specifications, then the target inertia matrix must be selected so that $G_o(j\omega)$ can meet the stability robustness specifications.

A comparison of $G_o(j\omega)$ in Figures 6-3 and 6-6-b reveals that the system in Figure 6-6-b has more robustness to high-frequency uncertainties than the system in Figure 6-3. The system in Figure 6-3, however, is more robust to low-frequency uncertainties than the one in Figure 6-6-b. This difference is because of the size of the state-feedback gain, G . A large G causes a larger bandwidth for $G(j\omega I_{nb} - A)^{-1}B$, which allows $G_o(j\omega)$ to remain close to unity

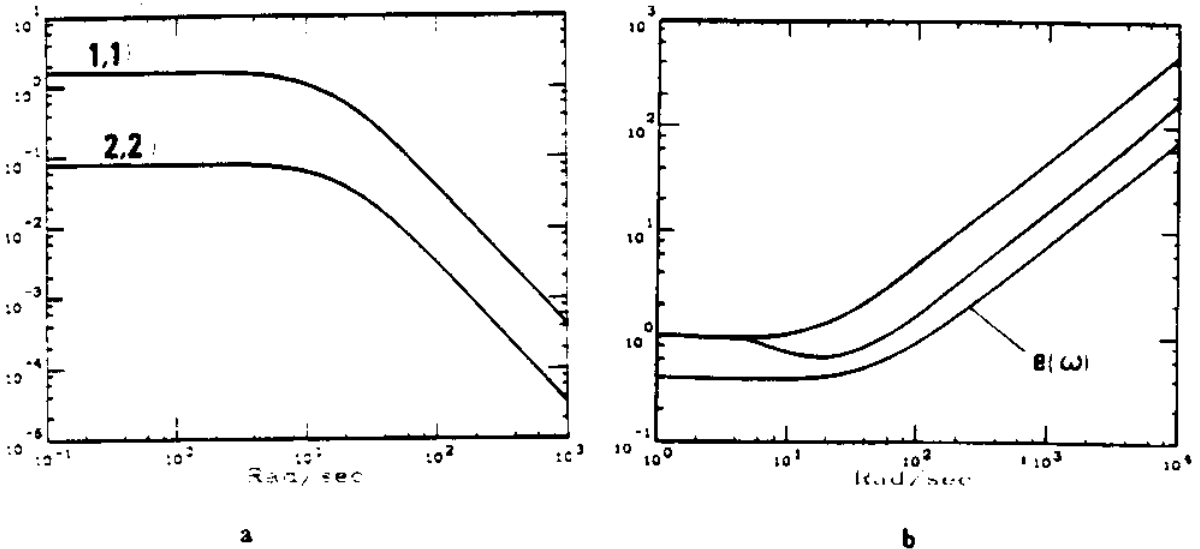


Figure 6-6: a: The Closed-Loop Transfer Function, $J_c G_{cl}(j\omega)$
 b: σ_{max} and σ_{min} of $G_o(j\omega)$ in Case 3

for a wider frequency range thus causing less robustness to high-frequency uncertainties and more robustness to low-frequency uncertainties. In Case 1, G is selected to be large to move the actuator eigenvalues deeper into the left half complex plane. In Case 3, since the actuators are fast, G is no longer a large matrix. We consider the size of a matrix in terms of its singular values.

Case 4

In this case, the actuators are very fast (40 hertz), and the dynamic equation presented in Case 3 is valid. The performance specifications are those in Case 2:

- stiffness in direction X = .61538 lbf/ft for $0 < \omega < .6283$ rad/sec;
- stiffness in direction Y = 12.308 lbf/ft for $0 < \omega < .6283$ rad/sec.

It is suggested that the performance specifications be achieved without force-feedforward gain. The target dynamics of Case 2 are used to parametrize the performance specifications. Using equation (C.4) from Appendix C a designer can arrive at a state-feedback gain, G , and a force-feedforward gain, G_d . Because of the choice of target inertia matrix, G_d is zero while

$$G = \begin{bmatrix} 9.3846 & 7.1083 & 1.0166 & 0.5040 \\ 7.1083 & 5.4295 & 0.6227 & 0.3151 \end{bmatrix}$$

The closed-loop transfer function, $J_c G_{cl}(j\omega)$, and $G_o(j\omega)$ are shown in Figure 6-7. Since ω_o in

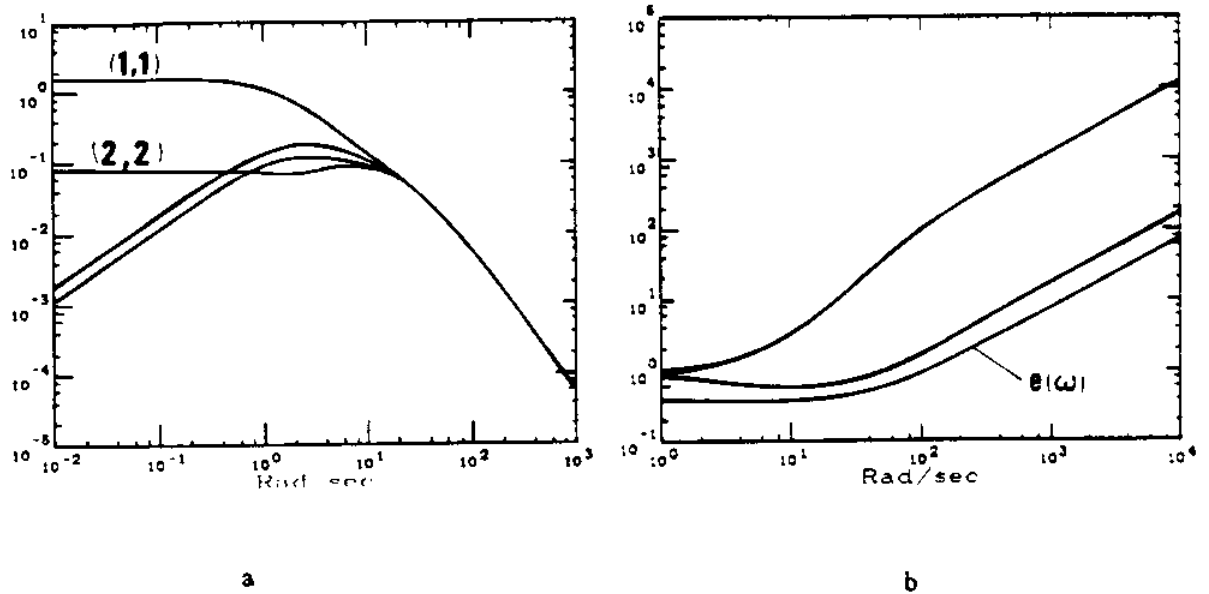


Figure 6-7: a: The Closed-Loop Transfer Function, $J_c G_c(j\omega)$
 b: σ_{min} and σ_{max} of $G_o(j\omega)$ in Case 4

Case 4 is less than ω_o in Case 3, the system in Case 4 has more robustness at high frequencies than the system in Case 3. Thus, if the actuators are fast and the model uncertainties happen at frequencies much higher than ω_o , it is possible to meet the design specifications without a force-feedforward gain, as long as the desired frequency range of operation is small enough to be parametrized by the target inertia represented by equation (5.41).

The design specifications of Case 2 and 4 are the same. Since the actuators in Case 2 were not fast enough, we could not meet the performance specifications without violating the performance specifications.

6.2 Example 2

Consider the parallelogram shown in Figure 6-8, which is mounted on the end-point of a large manipulator. The mass, length and moment of inertia relative to the center of mass of each link of the parallelogram are represented by δm_i , δx_i and i_i . If the location of the center of mass on each link is shown by δl_i , then the members of the inertia matrix $M(\theta_o)$ are:

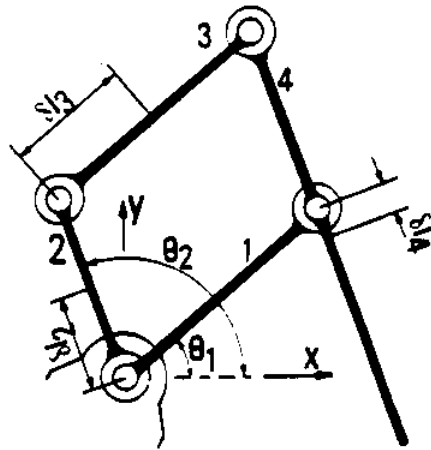


Figure 6-8: Parallelogram

$$M(\Theta_o)^{11} = \delta m_1 \delta l_1^2 + i_1 + \delta m_3 \delta l_3^2 + i_3 + \delta m_4 \delta x_1^2$$

$$M(\Theta_o)^{12} = (\delta m_3 \delta x_2 \delta l_3 - \delta m_4 \delta x_1 \delta l_4) \text{Cos}(\theta_2 - \theta_1)$$

$$M(\Theta_o)^{22} = \delta m_2 \delta l_2^2 + i_2 + \delta m_4 \delta l_4^2 + i_4 + \delta m_3 \delta x_2^2 .$$

The Jacobian is :

$$J_c = \begin{bmatrix} -\delta x_1 \text{Sin}(\theta_1) & (\delta x_4 - \delta x_2) \text{Sin}(\theta_2) \\ \delta x_1 \text{Cos}(\theta_1) & -(\delta x_4 - \delta x_2) \text{Cos}(\theta_2) \end{bmatrix}$$

If the following equality [1] is satisfied:

$$\delta m_3 \delta x_2 \delta l_3 - \delta m_4 \delta x_1 \delta l_4 = 0 ,$$

then the inertia matrix is not only diagonal, but also independent of joint angles; the cross-coupled velocity terms vanish from the equations of motion (4.8). With the following approximate data*:

$$\delta m_1 = 3.169/32.2 \text{ lbf. sec}^2/\text{ft} \quad \delta x_1 = 8\text{in} \quad \delta l_1 = 4\text{in} \quad i_1 = 0.42 \text{ lbf. sec}^2 \text{ ft}$$

$$\delta m_2 = 1.570/32.2 \text{ lbf. sec}^2/\text{ft} \quad \delta x_2 = 6\text{in} \quad \delta l_2 = 3\text{in} \quad i_2 = 0.13 \text{ lbf. sec}^2 \text{ ft}$$

* Such a parallelogram has been built by I. H. Ro and H. Asada at the Laboratory of Manufacturing and Productivity, MIT.

$$\begin{aligned} \delta m_3 &= 2.586/32.2 \text{ lbf sec}^2/\text{ft} & \delta x_3 &= 8\text{in} & \delta l_3 &= 4\text{in} & i_3 &= 0.33 \text{ lbf}\cdot\text{sec}^2\cdot\text{ft} \\ \delta m_4 &= 7.760/32.2 \text{ lbf sec}^2/\text{ft} & \delta x_4 &= 14\text{in} & \delta l_4 &= 1\text{in} & i_4 &= 1.68 \text{ lbf}\cdot\text{sec}^2\cdot\text{ft} \\ \theta_1 &= 40^\circ & \theta_2 &= 110^\circ \end{aligned}$$

the inertia matrix and Jacobian are:

$$M(\Theta_0) = \begin{bmatrix} 1.5030\text{D}-01 & 0.0000\text{D}+00 \\ 0.0000\text{D}+00 & 8.1000\text{D}-02 \end{bmatrix} \quad J_c = \begin{bmatrix} -4.2853\text{D}-01 & 6.2646\text{D}-01 \\ 5.1070\text{D}-01 & 2.2801\text{D}-01 \end{bmatrix}$$

The bandwidths of the actuators are 12.8 and 16 rad/sec. The dynamics of the system under the conditions expressed in Chapter 4 can be represented by A, B and C in equations (4.19) and (4.20):

$$A = \begin{bmatrix} 0. & 0. & 1. & 0. & 0. & 0. \\ 0. & 0. & 0. & 1. & 0. & 0. \\ 0. & 0. & 0. & 0. & 6.6534 & 0. \\ 0. & 0. & 0. & 0. & 0. & 12.346 \\ 0. & 0. & 0. & 0. & -12.8 & 0. \\ 0. & 0. & 0. & 0. & 0. & -16.0 \end{bmatrix}$$

$$B = \begin{bmatrix} 0. & 0. & 0. & 0. \\ 0. & 0. & 0. & 0. \\ 0. & 0. & -2.8511 & 3.3978 \\ 0. & 0. & 7.7341 & 2.8150 \\ 12.8 & 0. & 0. & 0. \\ 0. & 16.0 & 0. & 0. \end{bmatrix} \quad C = \begin{bmatrix} 1. & 0. & 0. & 0. & 0. & 0. \\ 0. & 1. & 0. & 0. & 0. & 0. \end{bmatrix}$$

The uncertainty of the dynamic model given by $e(\omega)$ is shown in Figure 6-10-b. We consider two cases. The target stiffness is the same in both cases, but ω_0 is different. This example shows the trade-off between ω_0 and stability robustness to high-frequency unmodelled dynamics.

Case 1

The design specifications in the global coordinate frame are:

- stiffness in direction X = .615 lbf/ft for $0 < \omega < 6.283$ rad/sec (1 hertz);
- stiffness in direction Y = 50 lbf/ft for $0 < \omega < 6.283$ rad/sec (1 hertz).

Note that the large stiffness in direction Y guarantees a very stiff positioning system in direction Y (.02 ft deviation for 1 lbf of the external force), while the low stiffness in direction X allows the manipulator to accommodate the interaction loads. The following

target impedance is proposed to parametrize the design specifications:

$$K = \begin{bmatrix} 0.615 & 0.0 \\ 0.000 & 50.0 \end{bmatrix} \quad J = \begin{bmatrix} 4.9451D-03 & 0.0000D+00 \\ 0.0000D+00 & 2.4107D-01 \end{bmatrix} \quad C = \begin{bmatrix} 1.1309D-01 & 0.0000 \\ 0.0000D+00 & 7.1172 \end{bmatrix}$$

The inertia matrix is selected to ensure the desired stiffness for a frequency range of 6.283 rad/sec. The damping matrix of the target dynamics is selected to guarantee the stability of the target dynamics. The transfer function of the target dynamics, $G_t(s)$, is:

$$\begin{bmatrix} 1.62501 \frac{1}{(s/8.924 + 1)(s/13.944 + 1)} & 0 \\ 0 & 0.02 \frac{1}{(s/11.521 + 1)(s/18.002 + 1)} \end{bmatrix}$$

Figure 6-9-a shows the diagonal members of $G_t(s) = [J s^2 + C s + K]^{-1}$.

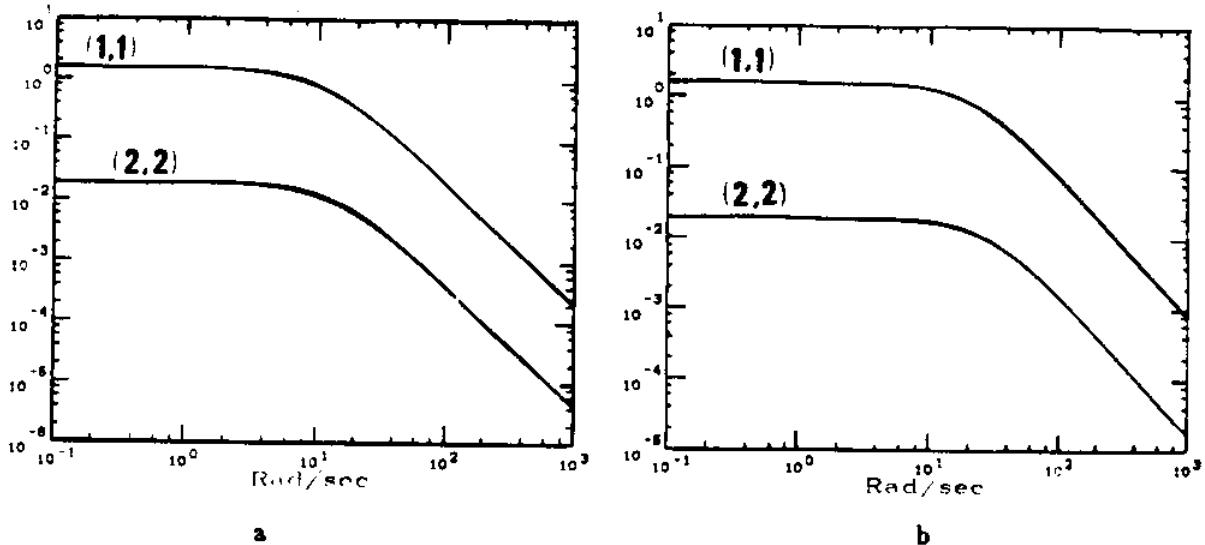


Figure 6-9: a: The Target Dynamics in Case 1
b: The Target Dynamics in Case 2

The eigenstructure of the target dynamics can be represented by V from equation (3.1) and by Λ , which is given on page 32:

$$\Lambda = \{ -8.9244, -13.944, -11.521, -18.0021 \}$$

$$V = \begin{bmatrix} -0.5460 & -0.5460 & 1.5000 & 1.5000 \\ 1.2228 & 1.2228 & 1.0261 & 1.0261 \\ 4.8723 & 7.6130 & -17.2820 & -27.0031 \\ -10.9128 & -17.0513 & -11.8216 & -18.4712 \end{bmatrix}$$

For $\alpha = 3$, the closed-loop eigenvalues of the actuators are located at -48 and -38.4. This preserves the bandwidth ratio 16/12.8 for the actuators. The set of closed-loop eigenvalues is:

$$S = \{ -8.9244, -13.944, 11.521, -18.0021, -48, -38.4 \}$$

Using equations (5.19) and (5.24) in Chapter 5, U can be computed to be:

$$U = \begin{bmatrix} -0.5460 & -0.5460 & 1.5000 & 1.5000 & 4.5121D-03 & 0.0000D+00 \\ 1.2228 & 1.2228 & 1.0261 & 1.0261 & 0.0000D-00 & 5.3584D-00 \\ 4.8723 & 7.6130 & -17.2820 & -27.0031 & -1.7326D-01 & 0.0000D+00 \\ -10.9128 & -17.0513 & -11.8216 & -18.4712 & 0.0000D+00 & -2.5720D-01 \\ -6.5354 & -15.9555 & 29.9264 & 73.0625 & 1.0000D+00 & 0.0000D+00 \\ 7.8886 & 19.2593 & 11.0322 & 26.9341 & 0.0000D+00 & 1.0000D+00 \end{bmatrix}$$

The first 4x4 members of U are identical to V. Equations (5.20) and (5.25) can be used to compute m_i , ($i = 1, 2, \dots, 6$) as follows:

$$\begin{bmatrix} -1.9788 & 1.4264 & 2.9896 & -29.6934 & -2.0000 & 0.0000 \\ 3.4885 & 2.4744 & 3.0881 & -3.3702 & 0.0000 & -2.0000 \end{bmatrix}$$

The state-feedback gain G can be computed via equation (5.26).

$$G = \begin{bmatrix} 84.2459 & 11.7245 & 14.7614 & 1.1806 & 4.1775 & 0.2408 \\ 12.0022 & 35.2393 & 1.2800 & 6.6925 & 0.1676 & 3.5325 \end{bmatrix}$$

The force-feedforward gain can be computed via equation (5.40).

$$G_d = \begin{bmatrix} -49.3760 & 0.0689 \\ 56.6071 & -0.0359 \end{bmatrix}$$

The transfer function matrix $J_c G_{cl}(s)$ is shown below.

$$\begin{bmatrix} 1.6250 \frac{(s/1520 + 1)(s/40.4 + 1)}{(s/8.9244 + 1)(s/13.944 + 1)} & 1.17D^{-4} \frac{s(s/86.7 + 1)}{(s/8.9244 + 1)(s/13.944 + 1)} \\ 1.17D^{-3} \frac{s(s/1423.9 + 1)}{(s/18.002 + 1)(s/11.521 + 1)} & 0.02 \frac{(s/44.95 + 1)(s/71.55 + 1)}{(s/18.002 + 1)(s/11.521 + 1)} \end{bmatrix}$$

$J_c G_{cl}(j\omega)$ and $G_o(j\omega)$ are shown in Figure 6-10 for $\alpha=3$. Large values for α cause $G_o(j\omega)$ to remain close to unity for a wide frequency range. This will bring less stability robustness to high-frequency unmodelled dynamics, but the closed-loop transfer function matrix $J_c G_{cl}(j\omega)$ will be closer to $G_t(j\omega)$.

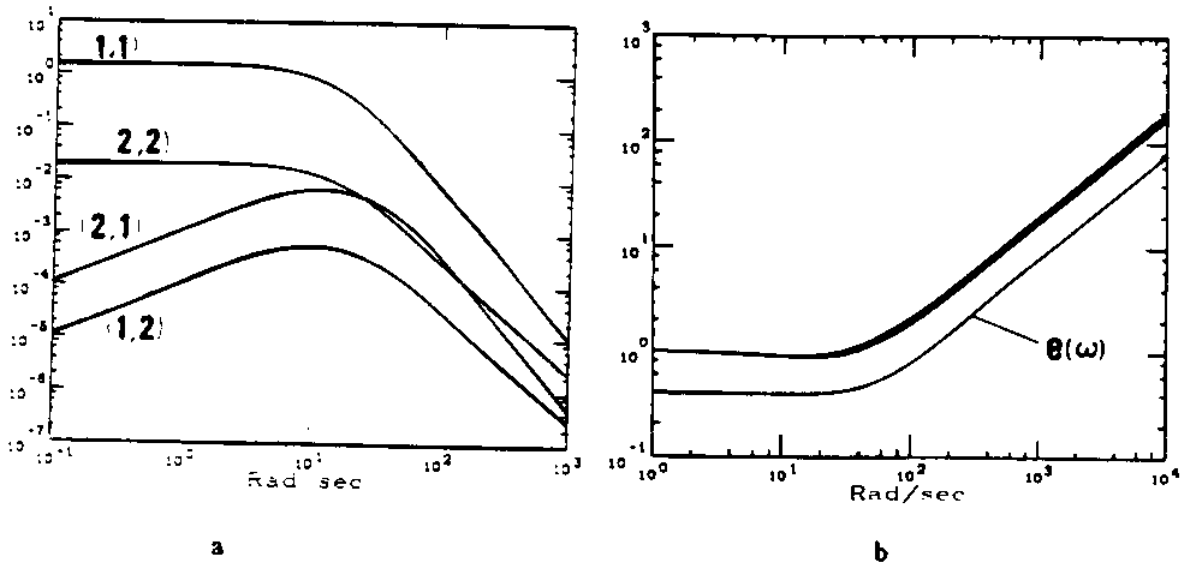


Figure 6-10: a: The Closed-Loop Transfer Function Matrix, $J_c G_c(j\omega)$
 b: σ_{max} and σ_{min} of $G_o(j\omega)$ in Case 1

Case 2

In this case, an increase in the frequency range of operation to 15 rad/sec is desired. Since we chose a diagonal target dynamics, selection of the J- and C-matrices for a given K-matrix is trivial. The following target dynamics are proposed:

$$K = \begin{bmatrix} 0.615 & 0.0 \\ 0.000 & 50.0 \end{bmatrix} \quad J = \begin{bmatrix} 1.2363D-03 & 0.0000D+00 \\ 0.0000D+00 & 6.0268D-02 \end{bmatrix} \quad C = \begin{bmatrix} 5.6544D-02 & 0.0000 \\ 0.0000D+00 & 3.5586 \end{bmatrix}$$

$G_i(j\omega)$ in this case is shown in Figure 6-9-b. Figure 6-11-a shows the closed-loop transfer function $J_c G_c(j\omega)$ for $\alpha=3$. Figure 6-11-b shows that the system in Case 2 is less robust to high-frequency uncertainties than the system of Case 1. This is because ω_o in Case 2 is selected to be wider than ω_o in Case 1. A large target inertia matrix (which implies a narrow ω_o) produces a narrow bandwidth for $G(j\omega - A)^{-1} B$, which allows $G_o(j\omega)$ to become larger than unity at lower frequencies. This will cause more robustness to high-frequency uncertainties and less robustness to low-frequency uncertainties. On the other hand, a small target-inertia matrix (which implies a large ω_o) produces a large bandwidth for $G(j\omega - A)^{-1} B$, which in turn causes $G_o(j\omega)$ to stay very close to unity for a wide frequency range. This will cause a poor stability robustness to high-frequency uncertainties and stronger stability robustness to low-frequency uncertainties.

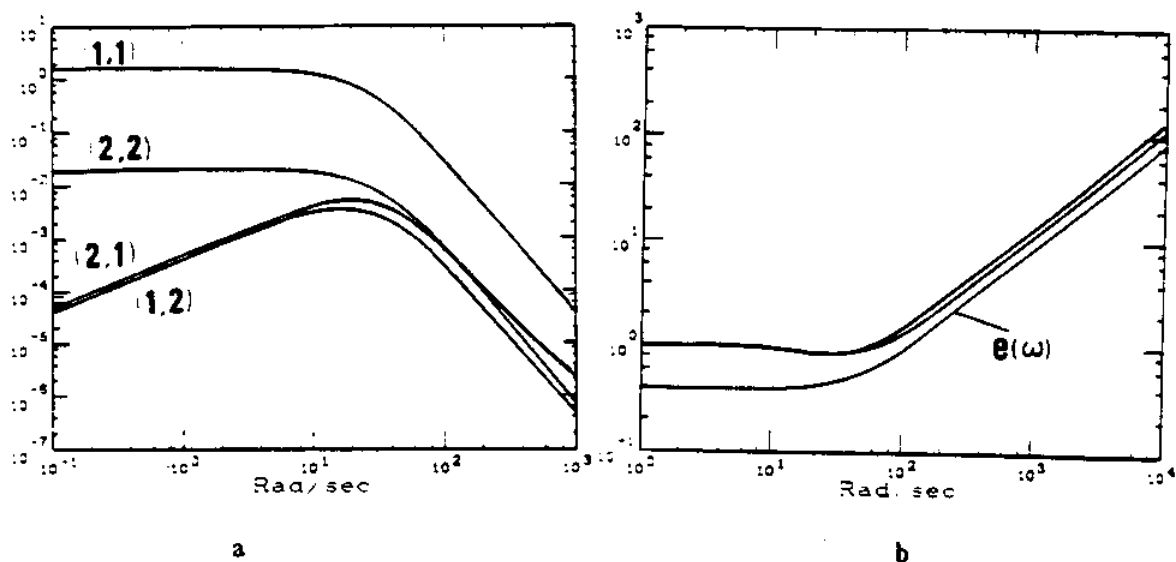


Figure 6-11: a: The Closed-Loop Transfer Function Matrix, $J_c G_{cl}(s)$
 b: σ_{\max} and σ_{\min} of $G_o(j\omega)$ in Case 2

6.3 Simulation

As mentioned earlier in Section 2.4.1, we provide a simple case of a simulated system in which it is shown that conventional controller design specifications which work for the unconstrained case, do not work for the constrained case. The proposed impedance control, however, is shown to work in both unconstrained and constrained cases, including the transition from one to the other. The proposed impedance also allows for control of the behavior of the system (e.g., monitoring the interaction force) by changing the parameters of the impedance. In Section 2.4.1, we explained that if a submersible vehicle is connected to a structure via some stiff cables or flexible connectors, the system of the vehicle and cables may achieve large stiffness for a wide frequency range. If the cables are selected to be very stiff, their stiffness will be dominant compared with the inertia of the vehicle. The stiffness of the cables will be the only dominant dynamics in a wide frequency range. Throughout this frequency range, the system of the vehicle and the cables will behave like a very stiff spring and external loads from water motion, manipulator motion and other disturbances do not affect the vehicle motion in this frequency range.

We conducted several dynamic/3D-graphic simulations of the constrained maneuvers of

underwater vehicles and manipulators to observe the quality of maneuvers in which impedance control and other controllers are employed. The simulation consists of the dynamics of a six degree of freedom vehicle, cables (up to four cables), and environmental effects such as water drag. A 3D-graphic representation of the vehicle with cables is depicted on a vector display which is updated by the dynamic simulation at the rate of fifty hertz. The physical characteristics of a particular submersible vehicle called Recon 5* (now being used at MIT for control experiments) are used as physical parameters in this simulation. This vehicle has five thrusters, weighs approximately 900 lbs., and is 6 feet long. Here we compare some time domain results of a maneuver performance with two different controllers. We did not include any model uncertainties in the simulation; the simulation was performed solely to observe the behavior of the vehicle under different controllers. The first controller guarantees an impedance control for the vehicle while the second controller allows a perfect positioning system for the vehicle with two hertz bandwidth. The first controller was designed according to the design method of Section 5.3.3 to guarantee the target impedance given in equation (2.2). The second controller is a model-based compensator designed according to specifications suitable for unconstrained maneuvers. This compensator contains integrators in each input channel to reject the disturbances up to 2 hertz. The LQG/LTR method was used to achieve this controller. Here we explain the result of the simple constrained maneuver shown in Figure 6-12.

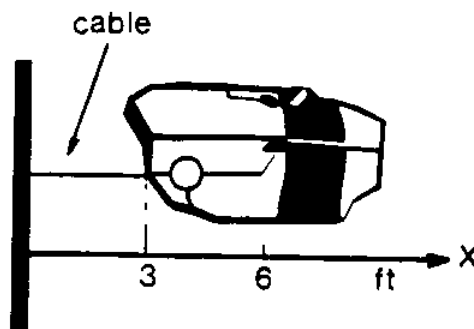


Figure 6-12: An Underwater Vehicle Connected with a Three-foot Cable to a Structure

The object is to move the vehicle in direction X to produce tension in the cable. First we

* Recon 5 (Sea Grant I) is an unmanned underwater vehicle given to MIT by the Perry family.

consider a maneuver using impedance control. J is chosen according to equation (5.41) to eliminate the need for force-feedforward. Because of the selection of J according to equation (5.41), ω_0 will be different depending on the orientation of the vehicle. C is modified by the computer to guarantee a slightly over-damped system. The time history of the command position in the X-direction is given by plot a in Figure 6-13. Plots b and c in Figure 6-13 show the cable tension and vehicle position in direction X. The position reference inputs and the members of the K-matrix are commanded via analog signals to the computers.

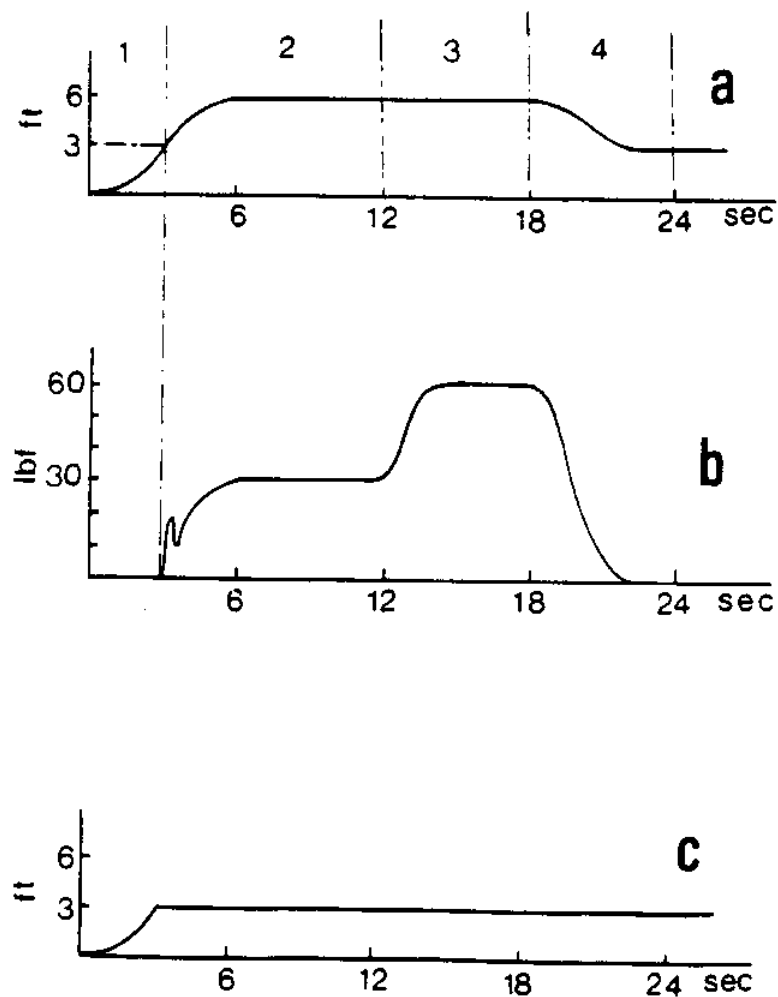


Figure 6-13: Response of the vehicle under impedance control:
a: Input Command, b: Cable Tension,
c: Vehicle Position

Here is the summary of a simple one-dimensional maneuver:

Region 1: In this region, the vehicle slowly approaches along direction X. The high feedback-gain allows the vehicle to follow the reference input. There is no cable tension in this region. K in equation (2.2) is chosen to be 10 lbf/ft.

Region 2: The vehicle encounters the cable. Since the cable is very stiff, a sudden tension occurs upon impact. An overshoot in the cable tension occurs because of the small velocity of approach of the vehicle at the moment of contact. The slower the vehicle approaches in direction X, the smaller the overshoot (at the very start of region 2) in the cable tension will be. If the vehicle hits the cable with a large forward velocity and the reference input is not large, then the undershoot (right after the overshoot) of the cable tension might fall to zero. A similar situation occurs when a manipulator approaches a stiff wall. That is, if a manipulator hits the wall with a large forward velocity and the reference input is not large, then the undershoot of the contact force might fall to zero and the end-point might separate from the wall. Since the command position is three feet beyond the cable length at steady state, the cable tension is 30 lbf. Region 2 shows how the impedance control method allows for a relatively smooth transition period from the unconstrained to the constrained situation.

Region 3: In this region, K is increased slowly from 10lbf/ft to 20lbf/ft by an analog input to the computer while the reference input is kept constant. Because of the selection of J according to equation (5.41), ω_0 will be different depending on the orientation of the vehicle. C is modified by the computer to guarantee a slightly over-damped system. Since the command is kept constant, doubling K also doubles the cable tension; $\Delta D(j\omega) = K \Delta Y(j\omega)$. This region shows the significant capability that impedance control offers for monitoring the behavior of the vehicle at the interaction port. In this simulation, a human monitors the behavior of the vehicle by choosing the "right" K via an analog input signal to the computer. A computer can also be used to monitor K according to some "hidden logic". Having control of the impedance of the vehicle at the interaction port reveals the potential of using supervisory control [52] to monitor the vehicle behavior in complicated tasks.

Region 4: In this region, the input reference-position is commanded to correspond to the cable length. This will give a zero cable tension in steady-state.

Figure 6-14 shows the behavior of the system when the second controller is used. The time history of the command position in the X-direction is given by plot a in Figure 6-14.

Plot b shows the vehicle position in direction X. The reference input is again commanded via an analog signal to the computer.

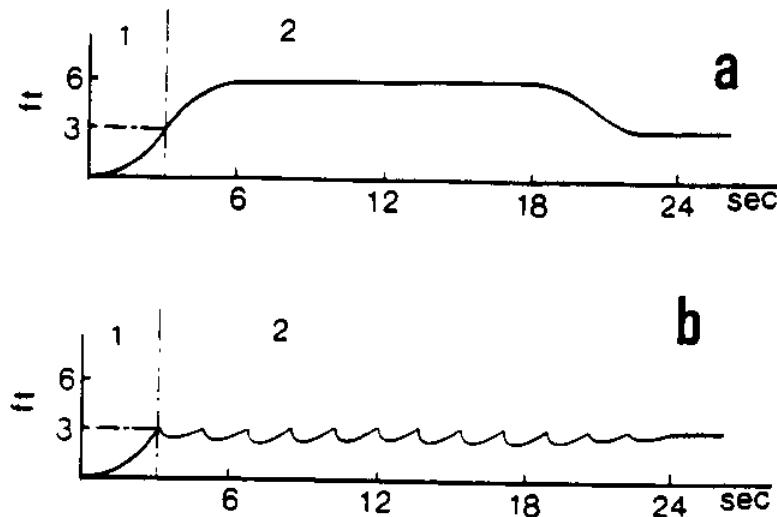


Figure 6-14: Response of the vehicle under pure positioning system
a: Input Command, b: Vehicle Position

Region 1: In this region, the vehicle slowly approaches along the direction X. The high feedback-gain allows the vehicle to follow the reference input almost instantaneously. There is no cable tension in this region. This region shows the successful maneuver of the vehicle in an unconstrained environment.

Region 2: In this region, the vehicle encounters the cable. As soon as the vehicle interacts with the cable, the dynamics of the system will change and stability will no longer be guaranteed. The designer in this case has no control over the impedance of the vehicle. The undesirable behavior of the vehicle in this region depends on the dynamics and characteristics of the environment and controller. Plot b in Figure 6-14 shows the limit cycle developed in the vehicle motion. In some cases, depending on the orientation of the vehicle, the limit cycle does not converge and instability results.

This simple simulation shows the superiority of the impedance control over a conventional positioning system in constrained maneuvers. In the impedance control method,

the designer guarantees not only the positioning capability for the vehicle, but also an ability to monitor the internal dynamics of the vehicle. This ability allows the operator to govern the behavior of the system on the interaction port. Figure 6-13 shows how the operator can position the vehicle while the cable tension is also controlled. The above simulation simply shows how control of the impedance of a system allows for monitoring the behavior of the system in a structured way.

6.4 Experiment

A simple experiment was conducted on a planar positioning table (X-Y table) to verify the application of impedance control to constrained maneuvers. The positioning table consists of a platform driven by two DC motors via two lead-screw mechanisms [Figure 6-15a.] The goal of the overall project is to develop a positioning system with different stiffnesses and different bandwidths along the two axes of a global cartesian coordinate frame by an on-line computer. The axes of this global coordinate frame do not necessarily coincide with the axes of the motors.*

In this section, we are interested to observe the transient behavior of the table from unconstrained maneuvers to constrained maneuvers when equation (2.2) is guaranteed for the system. To show this transient behavior, we just explain the result of an experiment when only one axis is employed (one dimensional case). Figure 6-15b shows this simple set-up. A wide bandwidth force sensor is mounted on the platform to measure the contact force along two orthogonal directions [15]. A computer algorithm with .01 sec sampling time was designed (according to the procedure given on page 57) and implemented on a microcomputer to control the impedance of the table. The controller is able to accept the stiffness, bandwidth and damping coefficient (three items of the set of performance specifications given by Figure 2-1). The platform was commanded to move beyond a solid surface. Figure 6-16a is the periodic ramp position command generated by the computer to the system. Figure 6-16b is the contact force. For this experiment, K is chosen to be 3.5 lbf/in while the bandwidth of the system is 4 hertz.

As long as the force sensor is not in touch with the stiff wall, the contact force is zero.

*This experiment is a small part of a greater project of the robotic deburring conducted by GE & MIT under supervision of Professor Bruce Kramer.

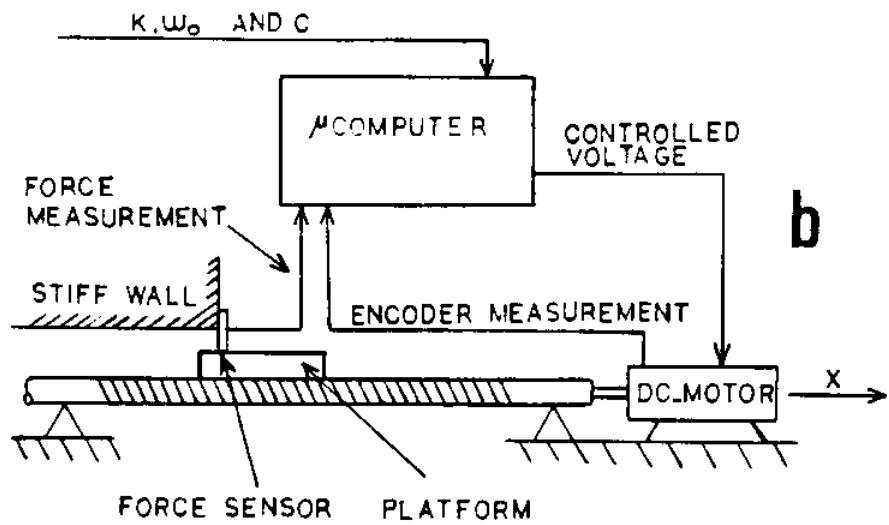
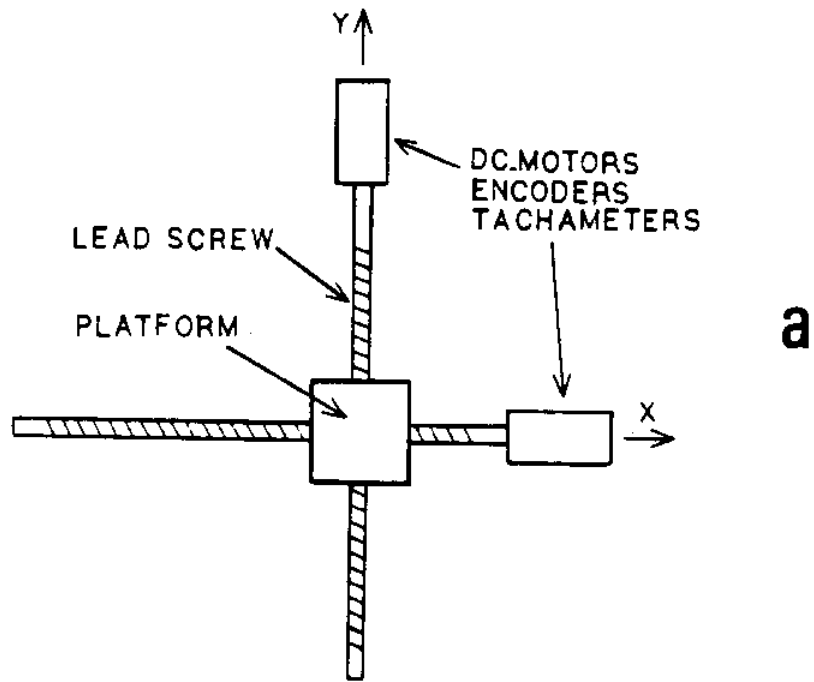


Figure 6-15: a: Planar Positioning Table
b: One-dimensional Case

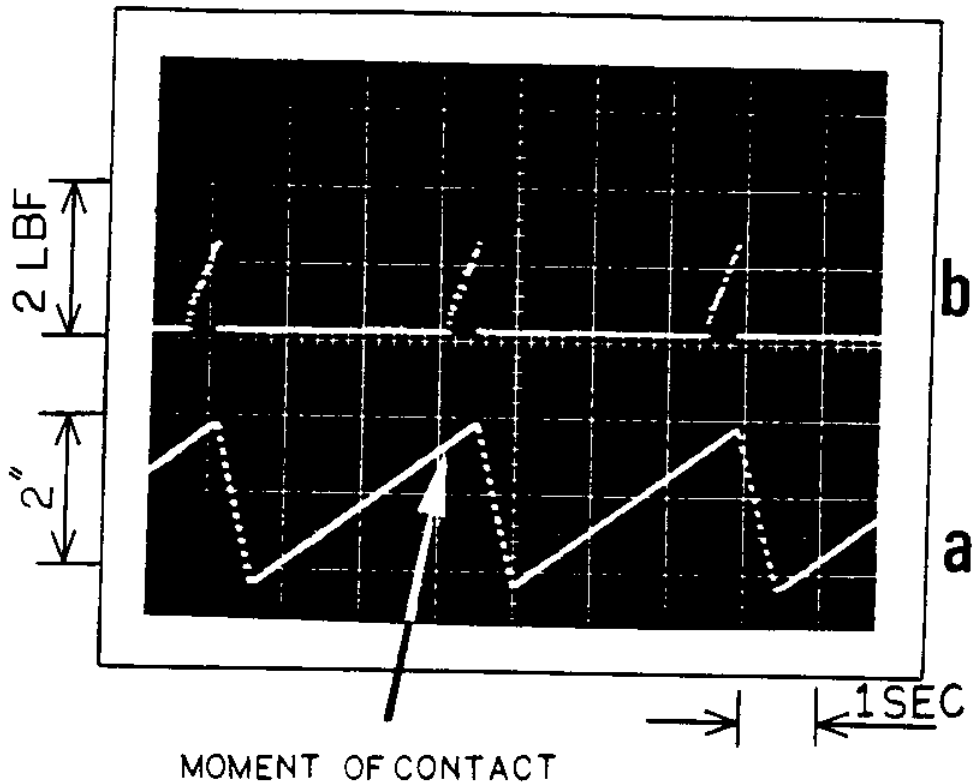


Figure 6-16: a: Command Position
b: Contact Force

After the force sensor touches the stiff wall, the contact force increases proportionally to the commanded input ($\Delta D(t) = K \Delta Y(t)$). Since the input position command is a ramp function, the contact force is also a ramp function. Enhancement of the algorithm to include both axes of the positioning table and sensitivity analysis of the system parameters are on-going projects in Laboratory of Manufacturing and Productivity at MIT.

Chapter 7

An Approach to Loop Transfer Recovery Using Eigenstructure Assignment

7.1 Introduction

This chapter stands by itself; it is not necessarily a part of a design technique for impedance control, but it provides a new method for designing an observer that can estimate the measurable states of the system. Section 7.7 explains how this chapter applies to impedance control. This chapter is to be presented at the American Control Conference in Boston, June 1985.

One method of model-based compensator design for linear multivariable systems consists of state-feedback design and observer design [2]. A key step in recent work in multivariable synthesis involves selecting an observer gain so the final loop-transfer function is the same as the state-feedback loop-transfer function [7], [14]. This is called Loop-Transfer Recovery (LTR). This paper shows how identification of the eigenstructure of the compensators that achieve LTR makes possible a design procedure for observer gain [35]. This procedure is based on the eigenstructure assignment of the observers. The sufficient condition for LTR and the stability of the closed-loop system is that the plant be minimum-phase. The limitation of this method might arise when the plant has multiple transmission zeros.

Historically, the LTR method is the consequence of attempts by Doyle and Stein to improve the robustness of linear quadratic gaussian (LQG) regulators [8], [7]. However, the method has more general applications than to the robustness of the LQG regulators [14]. In their seminal work, Doyle and Stein address the problem of finding the steady-state observer gain that assures the recovery of the loop transfer function resulting from full state feedback. First, they demonstrate a key lemma that gives a sufficient condition for the steady-state observer gain such that LTR takes place. To compute the gain, they show that the infinite time-horizon Kalman filter formalism with "small" white measurement-noise covariance yields an observer gain that satisfies the sufficient condition for loop transfer recovery. In this paper, we present a method for computing observer gain that obviates the need for Kalman filter formalism. The goal of this paper is to analyze the eigenstructure properties of the

LTR method for the general class of feedback control systems that use model-based compensators. After examining the eigenstructure of LTR, a design methodology for LTR via eigenstructure assignment will be given.

Nomenclature

A, B & C plant parameters
 d_i & d_o input and output disturbances
 $x(t), u(t)$ & $y(t)$... states, input and output of the system
 $\hat{x}(t)$ & $\hat{y}(t)$ states and output of the observer
 $e(t)$ error signal of the observer
 $G_p(s)$ transfer function matrix of the plant
 λ_i eigenvalues of (A-BG)
 μ_i eigenvalues of (A-HC)
 s_i transmission zeros of (A,B,C)
 σ_i transmission zeros of (A,B,G)
G state-feedback gain
 $K(s)$ transfer function matrix of the compensator
 ρ positive scalar
 v_i^T left eigenvector of (A-HC)
 u_i right eigenvector of (A-BG)
W square non-singular $m \times m$ matrix
 z_i^T zero direction of the transmission zero
 $-w_i^T$ input direction of the transmission zero
j maximum number of the finite transmission zeros
 x_i^T left eigenvector of (A-BG-HC)
 $\Phi_{oi}(s)$ open-loop characteristic equation of the plant
 $\Phi_{ci}(s)$ closed-loop characteristic equation of the observer
n order of the system
m rank of matrices B and C
P(s) precompensator

7.2 Background

We will deal with the standard feedback configuration shown in Figure 7-1, which consists of: plant model $G_p(s)$; compensator $K(s)$, forced by command $r(t)$; measurement noise $n(t)$; and the disturbances $d_i(t)$ and $d_o(t)$. The precompensator, $P(s)$, is used to filter the input for command following. Throughout this paper, we assume that the plant can be described by equations (7.1) and (7.2).

$$\dot{x}(t) = A x(t) + B u(t) + B d_i(t) \quad (7.1)$$

$$y(t) = C x(t) + d_o(t) + n(t) \quad (7.2)$$

where:

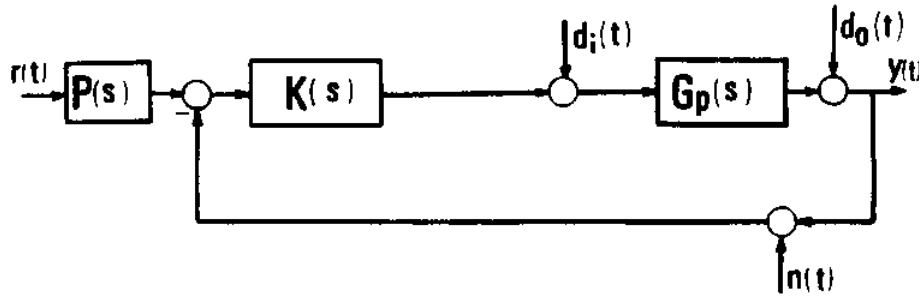


Figure 7-1: Standard Closed-Loop System

$x(t) \in \mathbb{R}^n$, $u(t), y(t), d_i(t), d_o(t)$ and $n(t) \in \mathbb{R}^m$
 $[A, B]$ is a stabilizable (controllable) pair
 $[A, C]$ is a detectable (observable) pair
 $\text{rank}(B) = \text{rank}(C) = m$

Once we specify the plant model, $G_p(s)$, we must find $K(s)$ so that: 1) the nominal feedback design, $y(s) = G_p(s)[I_{mm} + K(s)G_p(s)]^{-1} d_i(s)$, is stable; 2) the perturbed system in the presence of bounded unstructured uncertainties is stable; 3) application-dependent design specifications are achieved. The design specifications can be expressed as frequency-dependent constraints on the loop transfer function, $K(s)G_p(s)$. The standard practice is to shape the loop transfer function, $K(s)G_p(s)$, so it does not violate the frequency-dependent constraints [7]. The loop-shaping problem can be considered to be a design trade-off among performance objectives, stability in the face of unstructured uncertainties [33, 49], and performance limitations imposed by the gain/phase relationship. Here we assume that $n(t)$ is a noise signal that operates over a frequency range beyond the frequency range of $r(t)$, $d_i(t)$ and $d_o(t)$. We also use a precompensator, $P(s)$, to shape the input for command following. Therefore, the performance objectives are considered as only input disturbance rejection over a bounded frequency range. The design specifications may be frequency-dependent constraints on $G_p(s)K(s)$, which is the loop transfer function broken at the output of the plant, rather than on $K(s)G_p(s)$, which is the loop transfer function broken at the input to the plant. Applying the design specifications to $G_p(s)K(s)$ implies rejection of output disturbances. Since Doyle and Stein first applied LTR to the loop transfer function, $K(s)G_p(s)$, for consistency and continuity, we will also assume throughout this article that all design specifications apply to $K(s)G_p(s)$.

One method of designing $K(s)$ consists of two stages. The first stage concerns state-feedback design. A state-feedback gain, G , is designed so that the loop transfer function,

$G(sI_{nn}-A)^{-1}B$, which is shown in Figure 7-2, meets the frequency-dependent design specifications and satisfies equation (7.3) to guarantee stability.

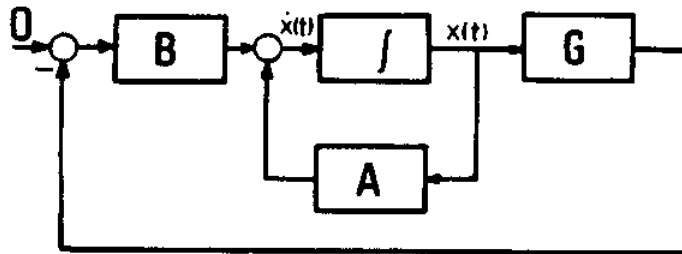


Figure 7-2: State-Feedback Configuration

$$(\lambda_i I_{nn} - A + B G) u_i = 0_n, \quad i = 1, 2, \dots, n \quad (7.3)$$

$$\text{real} (\lambda_i) < 0, \quad u_i \neq 0_n$$

λ_i is the closed-loop state-feedback eigenvalue, while u_i is the $n \times 1$ right closed-loop eigenvector of the system. Controllability of $[A,B]$ guarantees the existence of G in equation (7.3). At this stage, one can determine whether or not state-feedback design can meet the design specifications. In this paper, we assume that G is selected so that equation (7.3) is satisfied and the loop transfer function, $G(sI_{nn}-A)^{-1}B$, which is shown in Figure 7-2 meets the desired frequency-domain design specification. In the second stage of the compensator design, an observer is designed to make the first stage realizable [34, 62]. The observer design is not involved in meeting the specifications for the loop transfer function since all design specifications have been met by the state feedback gain, G . The observer has the structure of the Kalman filter. Combining the state-feedback and observer designs (Figure 7-3) yields the unique compensator transfer-function matrix given by equation (7.4).

$$K(s) = G (s I_{nn} - A + B G + H C)^{-1} H \quad (7.4)$$

The idea behind observer design is to find the steady-state filter gain, H , such that the loop transfer function, $K(s)G_p(s)$, in Figure 7-1 maintains the same loop shape (for a bounded frequency range) that $G(sI_{nn}-A)^{-1}B$ achieved via state-feedback design in the first stage. A technique for designing H to meet this criterion was offered by Doyle and Stein [7]. Since by this method, $K(s)G_p(s)$ preserves the loop-shape achieved by $G(sI_{nn}-A)^{-1}B$, the final design in Figure 7-1 meets the specifications that were already met by state-feedback design. (The

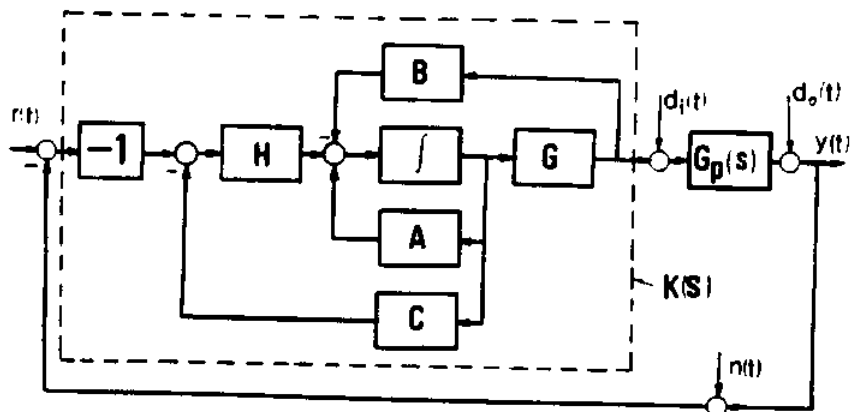


Figure 7-3: Closed-Loop System

title "loop transfer recovery" comes from this idea.) For stability of the observer, equation (7.5) must also be satisfied.

$$v_i^T (\mu_i I_{nn} - A + H C) = 0_n^T, \quad i = 1, 2, \dots, n \quad (7.5)$$

$$\text{real}(\mu_i) < 0, \quad v_i^T \neq 0_n^T$$

μ_i and v_i^T are the observer eigenvalue and left eigenvector, respectively. Observability of $[A,C]$ guarantees the existence of H in equation (7.5). The following lemma, which is proved by Doyle and Stein [7], is central to the design of H :

If H is chosen such that limit (7.6) is true as scalar ρ approaches infinity for any non-singular $m \times m$ W -matrix,

$$\frac{H(\rho)}{\rho} \rightarrow BW \quad (7.6)$$

then $K(s)$, as given by equation (7.4), approaches pointwise toward expression (7.7):

$$G (sI_{nn} - A)^{-1} B [C (sI_{nn} - A)^{-1} B]^{-1}, \quad (7.7)$$

and since $G_p(s) = C (sI_{nn} - A)^{-1} B$, (7.8)

then $K(s) G_p(s)$ will approach $G (sI_{nn} - A)^{-1} B$ pointwise.

The procedure requires only that H be stabilizing and have the asymptotic characteristic of equation (7.6). Doyle and Stein suggested one way to meet this requirement: a steady-state Kalman filter gain [31] with very small measurement-noise covariance. Now suppose we choose H with the following structure:

$$H = \rho B W \quad (7.9)$$

where W is any non-singular $m \times m$ matrix and ρ is a scalar. It can be shown (by the definition of the limit) that the structure of H chosen in equation (7.9) satisfies the limit in equation (7.6) as ρ approaches infinity. In other words, as ρ approaches infinity, ' $H \rightarrow \rho BW$ ' results in ' $H/\rho \rightarrow BW$ '. (The reverse is not true.) Since the structure of H given in equation (7.9) satisfies the limit in (7.6), then if H is chosen to be ρBW , $K(s)G_p(s)$ will approach $G(sI_{nn}-A)^{-1}B$ pointwise, as ρ approaches infinity. Note that the structure of H given by equation (7.9) does not necessarily yield a stable observer. We choose H to be ρBW throughout this paper. The asymptotic finite eigenstructures of both forms given by (7.9) and (7.6) are the same, while the asymptotic infinite eigenstructures are usually different. The form in equation (7.9) usually yields an unstable infinite eigenstructure.

Although this paper is not an exposition of the properties of the transmission zeros of a plant, before stating the theorem, we will remind readers of some definitions and concepts about this matter. (For more information and properties of the transmission zeros, see references [48, 6, 58, 28].) The transmission zeros of a square plant are defined to be the set of complex numbers s_i that satisfy inequality (7.10).

$$\text{rank} \begin{bmatrix} s_i I_{nn} - A & B \\ C & 0_{mm} \end{bmatrix} < n + m \quad (7.10)$$

The necessary and sufficient condition for the truth of inequality (7.10) is given by equation (7.11).

$$\det \begin{bmatrix} s_i I_{nn} - A & B \\ C & 0_{mm} \end{bmatrix} = 0 \quad (7.11)$$

Equation (7.11) yields j finite transmission zeros ($j \leq n-m$). The remaining $(n-j)$ transmission zeros are at infinity. For each finite transmission zero, there is one non-zero left null-vector $[z_i^T \quad -w_i^T]$ (for $i=1,2,\dots,j$) such that:

$$[z_i^T \quad -w_i^T] \begin{bmatrix} s_i I_{nn} - A & B \\ C & 0_{mm} \end{bmatrix} = 0_{n+m}^T \quad (7.12)$$

where: $[z_i^T \quad -w_i^T] \neq 0_{n+m}^T$.

w_i^T is an $m \times 1$ vector, and z_i^T is an $n \times 1$ vector. z_i^T is called left zero direction of the transmission zeros of the plant. If the left eigenvector and left zero direction associated with

a pair of equal-valued eigenvalue and transmission zero are equal, then s_i is an uncontrollable mode of the system. These transmission zeros are called "input decoupling zeros" [37]. Similarly, if the right eigenvector and the right zero direction associated with an equal-valued eigenvalue and transmission zero are equal, then s_i is an unobservable mode of the system. These transmission zeros are called "output decoupling zeros." A similar definition for the transmission zeros of a square plant is given by reference [31]; all complex numbers that are roots of $\Psi(s)$ in the equation:

$$\det G_p(s) = \frac{\Psi(s)}{\Phi_{o1}(s)} \quad (7.13)$$

are transmission zeros of the plant. $\Phi_{o1}(s)$ is the n th-order open-loop characteristic equation. The maximum order of $\Psi(s)$ is j . All transmission zeros of the plant, including the ones that are equal to the eigenvalues of the plant (which may even be the input-decoupling and/or output-decoupling zeros of the system), are roots of $\Psi(s)$ and also satisfy inequality (7.10) and equation (7.11). The equality of equations (7.13) and (7.11) can be shown by careful use of Schur's equality [26].

7.3 Asymptotic Eigenstructure Properties of the LTR Method

We will now explore some eigenstructure properties for LTR when the observer gain satisfies equation (7.9). Knowing the eigenstructure properties of the compensator, we will develop a method for designing H via eigenstructure assignment of the observer. The following theorem gives the eigenstructure properties of the observer when H is chosen according to equation (7.9). Part 1 of the theorem is proved differently in reference [5] and can also be considered to be a special result of the multivariable root locus given by references [42, 51, 29, 28]. The second part of the theorem is the result we will use in the design process.

Theorem

Consider the square linear observer in Figure 7-4:

$$\hat{\dot{x}}(t) = A \hat{x}(t) + H e(t) + B u(t) \quad (7.14)$$

$$e(t) = -C \hat{x}(t) + y(t) \quad (7.15)$$

$$\hat{x}(t) \in \mathbb{R}^n \quad u(t) \text{ and } y(t) \in \mathbb{R}^m$$

with $\text{rank}(B) = \text{rank}(C) = m$.

Then if H is chosen so that:

$$H = \rho B W \quad (7.16)$$

where W is any non-singular square matrix and ρ is a scalar approaching ∞ , then the following statements are true:

1) The finite closed-loop eigenvalues of $(A-HC)$, μ_i , approach finite transmission zeros of the plant, s_i . If the linear plant $[A,B,C]$ has j finite transmission zeros, ($j \leq n-m$), then $(A-HC)$ will have j finite eigenvalues. The remaining closed-loop eigenvalues approach infinity at any angle.

2) The left closed-loop eigenvector v_i^T ($i=1,2,\dots,j$) associated with the finite closed-loop eigenvalue μ_i approaches z_i^T , which satisfies equation (7.17).

$$\begin{bmatrix} z_i^T & -w_i^T \end{bmatrix} \begin{bmatrix} s_i I_{nn} - A & B \\ C & 0_{mm} \end{bmatrix} = 0_{n+m}^T \quad (7.17)$$

$$\begin{bmatrix} z_i^T & -w_i^T \end{bmatrix} \neq 0_{n+m}^T$$

w_i^T is an $m \times 1$ vector and z_i^T is an $n \times 1$ vector. If s_i is not equal to any eigenvalue of A , then z_i^T can be computed from equation (7.17), and the following expression for v_i^T ($i=1,2,\dots,j$) can be obtained:

$$v_i^T = w_i^T [C (s_i I_{nn} - A)^{-1}] \quad (7.18)$$

where w_i^T ($i=1,2,\dots,j$) can be calculated from equation (7.19).

$$w_i^T [C (s_i I_{nn} - A)^{-1} B] = 0_m^T \quad (7.19)$$

$$\text{where: } w_i^T \neq 0_m^T$$

Interpretation. This theorem identifies the asymptotic locations of finite closed-loop eigenvalues and left eigenvectors of the observer. As ρ approaches a large number, j (for $j \leq n-m$) closed-loop eigenvalues will approach finite transmission zeros of the plant, and $(n-j)$ closed-loop eigenvalues will approach infinity at any angle. Since conventional practice in complex variable work is to regard a function as having an equal number of poles and zeros when the zeros at infinity are included, one can claim that all closed-loop eigenvalues

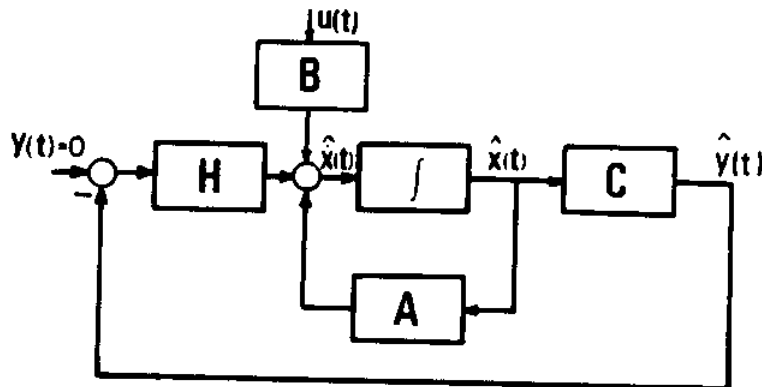


Figure 7-4: Closed-Loop Observer

approach the transmission zeros of the plant. Equation (7.17) states that $[v_i^T \quad -w_i^T]$ is confined in the left null space of the given matrix in equation (7.17) as ρ approaches infinity. In other words, the left null space of the matrix given in equation (7.17) assigns a subspace for limiting location of $[v_i^T \quad -w_i^T]$ when ρ approaches infinity. If s_i is not equal to any eigenvalues of A , the limiting location of v_i^T can be interpreted differently. Equation (7.18) states that the left eigenvector, v_i^T is confined to a sub-space spanned by the rows of $[C(s_i I_{nn} - A)^{-1}]$ if s_i is not equal to any eigenvalues of A . This sub-space is of dimension equal to the rank of C . Therefore, the number of independent output variables determines how large the sub-space corresponding to the left closed-loop eigenvector can be. The orientation of each sub-space associated with each left closed-loop eigenvector, v_i^T depends on the open-loop dynamics of the system $[A, C]$ and the closed-loop observer eigenvalue, μ_i . Construction of the left closed-loop eigenvectors in their allowable m -dimensional sub-space in C^n is the exact freedom that is offered by observer design beyond pole placement [27, 44, 45, 16]. The second part of the theorem identifies the asymptotic m -dimensional sub-space in C^n that confines the left closed-loop eigenvector, v_i^T . The choice of w_i^T in equation (7.18) allows the designer to construct each n -dimensional left closed-loop eigenvector in its allowable m -dimensional sub-space. As ρ approaches a large number, then w_i^T approaches the left null vector of $G_p(s_i)$ in equation (7.19); consequently, each left closed-loop eigenvector v_i^T approaches a final value in its allowable sub-space given by expression (7.18).

Proof:

Part 1: H is chosen according to equation (7.16). The block diagram of the closed-loop observer is shown in Figure 7-5. The loop transfer function at the plant output is given by expression (7.20).

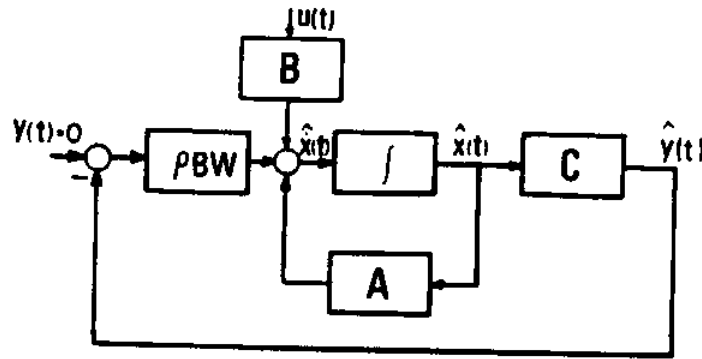


Figure 7-5: Closed-Loop Observer Configuration

$$C (s I_{nn} - A)^{-1} \rho B W \tag{7.20}$$

Equation (7.21) relates the open-loop and closed-loop characteristic equations [36, 47].

$$\det [I_{nn} + C (s I_{nn} - A)^{-1} \rho B W] = \frac{\Phi_{cl}(s)}{\Phi_{ol}(s)} \tag{7.21}$$

where:

$\Phi_{cl}(s)$ = closed-loop characteristic equation of the system in Figure 7-5.

$\Phi_{ol}(s)$ = open-loop characteristic equation of the system in Figure 7-5.

From matrix theory, equality (7.22) is true [26].

$$\det [I_{mm} + C (s I_{nn} - A)^{-1} \rho B W] = I_{mm} + \text{trace}[C(s I_{nn} - A)^{-1} \rho B W] + \dots + \det[C(s I_{nn} - A)^{-1} \rho B W] \tag{7.22}$$

As ρ approaches ∞ , the last term of equation (7.22) grows faster than the other terms. Therefore, approximation (7.23) is true.

$$\det [I_{mm} + C (s I_{nn} - A)^{-1} \rho B W] \approx \det[C(s I_{nn} - A)^{-1} \rho B W] \tag{7.23}$$

Considering approximation (7.23), equation (7.21) can be written as:

$$\det [C (s I_{nn} - A)^{-1} \rho B W] \approx \frac{\Phi_{cl}(s)}{\Phi_{ol}(s)} \tag{7.24}$$

or equivalently:

$$\det [G_p(s)] \det [\rho W] \approx \frac{\Phi_{cl}(s)}{\Phi_{ol}(s)} \tag{7.25}$$

Since $\det [\rho W] \neq 0$, comparing equations (7.13) and (7.25) shows that the roots of $\Psi(s)$ and $\Phi_{cl}(s)$ are the same. In other words, $\Phi_{cl}(s)$ produces all the transmission zeros of the plant, including the ones that are equal to the eigenvalues of A, which can even be decoupling zeros.

Part 2: When H approaches its asymptotic value, the eigenvalues of (A-HC) can no longer be moved via matrix C. This is true because the eigenvalues of (A-HC) are at their limiting locations (i.e., transmission zeros of the plant). Therefore, [(A-HC), B, C] must have unobservable or uncontrollable modes. Since [(A-HC), C] is an observable pair and H is expressed as ρBW , [(A-HC), B] must be an uncontrollable pair. Since [(A-HC), B] is an uncontrollable pair, equations (7.26) and (7.27) are true [37].

$$v_i^T (\mu_i I_{nn} - A + H C) = 0_n^T \quad i = 1, 2, \dots, j \quad (7.26)$$

$$v_i^T B = 0_m^T \quad (7.27)$$

μ_i is the closed-loop observer eigenvalue, and v_i^T is the corresponding left eigenvector. Equation (7.27) states that the left closed-loop eigenvector, v_i^T , from equation (7.26) is in the left null space of B and cannot be affected by the input. Each closed-loop eigenvector, v_i^T (for $i=1,2,\dots,j$) can be expressed by equation (7.28).

$$v_i^T (\mu_i I_{nn} - A) - w_i^T C = 0_n^T \quad (7.28)$$

$$\text{where: } w_i^T = -v_i^T H \quad (7.29)$$

Combining equation (7.28) and equation (7.27) yields equation (7.30). (Note that $s_i = \mu_i$.)

$$\begin{bmatrix} v_i^T & -w_i^T \end{bmatrix} \begin{bmatrix} s_i I_{nn} - A & B \\ C & 0_{mm} \end{bmatrix} = 0_{n+m}^T \quad (7.30)$$

$$\text{where: } \begin{bmatrix} v_i^T & -w_i^T \end{bmatrix} \neq 0_{n+m}^T \text{ for } i=1,2,\dots,j$$

If s_i is not equal to any eigenvalue of A, then from equation (7.30) we can find an expression for the left closed-loop eigenvector of A:

$$v_i^T = w_i^T C (s_i I_{nn} - A)^{-1} \quad i = 1, 2, \dots, j \quad (7.31)$$

where w_i^T can be computed from equation (7.32)

$$w_i^T [C (s_i I_{nn} - A)^{-1} B] = 0_m^T, \quad i=1,2,\dots,j \quad (7.32)$$

$$w_i^T \neq 0_m^T$$

Equation (7.31) shows that the left eigenvectors achievable for the closed-loop observer are confined to the m-dimensional sub-spaces determined by their associated eigenvalues and open-loop dynamics [A, C]. ■

Comment: As ρ approaches ∞ , the j eigenvalues of (A-HC) cancel out the j finite transmission zeros of the plant. A cancellation of an equal-valued closed-loop eigenvalue of the system with a transmission zero happens if the left closed-loop eigenvector of the system is equal to the left zero direction, z_i^T , associated with the transmission zero in equation (7.17). By cancelling [60] we mean they will not appear as poles in the closed-loop transfer function matrix, $C(sI_{nn}-A+HC)^{-1}B$. The transmission zeros of [A, B, C] are the same as those of [(A-HC), B, C], because transmission zeros do not change under feedback. As ρ approaches infinity, the transmission zeros of [(A-HC), B, C] turn into input decoupling zeros, because the system of [(A-HC), B, C] is not controllable at these modes [37].

Corollary 1: *The finite transmission zeros of $K(s)$ are the same as the finite transmission zeros of $G(sI_{nn}-A)^{-1}B$.*

Proof: The transmission zeros of $G(sI_{nn}-A)^{-1}B$ are the complex values σ_i that satisfy the following inequality :

$$\text{rank} \begin{bmatrix} \sigma_i I_{nn} - A & B \\ G & 0_{mm} \end{bmatrix} < n + m . \quad (7.33)$$

Post-multiplying the matrix in inequality (7.33) by the non-singular matrix:

$$\begin{bmatrix} I_{nn} & 0_{nm} \\ G + \rho W C & \rho W \end{bmatrix} \quad (7.34)$$

will result in inequality (7.35) for the transmission zeros of $G(sI_{nn}-A)^{-1}B$:

$$\text{rank} \begin{bmatrix} \sigma_i I_{nn} - A + BG + \rho BWC & \rho BW \\ G & 0_{mm} \end{bmatrix} < n + m \quad (7.35)$$

Substituting H for (ρBW) in inequality (7.35) results in inequality (7.36).

$$\text{rank} \begin{bmatrix} \sigma_i I_{nn} - A + BG + HC & H \\ G & 0_{mm} \end{bmatrix} < n+m \quad (7.36)$$

The complex number, σ_i , that satisfies inequality (7.36) is a transmission zero of $K(s)$ as given by equation (7.4). Therefore, $K(s)$ and $G(sI_{nn} - A)^{-1}B$ have equal transmission zeros. If $G(sI_{nn} - A)^{-1}B$ does not have any finite transmission zeros, then $K(s)$ will not have any finite transmission zeros. ■

Corollary 2: If ρ approaches ∞ , then all the eigenvalues of the compensator $K(s)$ will approach the transmission zeros (including the ones at infinity) of the plant, and the left eigenvectors of $(A - BG - HC)$, x_i^T , will approach z_i^T where z_i^T and s_i ($i=1,2,\dots,j$) satisfy equation (7.37).

$$\begin{bmatrix} z_i^T & -w_i^T \end{bmatrix} \begin{bmatrix} s_i I_{nn} - A & B \\ C & 0_{mm} \end{bmatrix} = 0_{n+m}^T \quad (7.37)$$

$$\begin{bmatrix} z_i^T & -w_i^T \end{bmatrix} \neq 0_{m+n}^T$$

In other words, the eigenvalues of the compensator cancel out the transmission zeros of the plant.

Proof: The transmission zeros of the plant are the set of complex numbers, s_i , that satisfy inequality (7.37). Post-multiplying the matrix in equation (7.37) by the non-singular matrix:

$$\begin{bmatrix} I_{nn} & 0_{nm} \\ G & I_{mm} \end{bmatrix} \quad (7.38)$$

will yield the following equation, which can then be solved to find the finite transmission zeros of the plant:

$$\begin{bmatrix} z_i^T & -w_i^T \end{bmatrix} \begin{bmatrix} s_i I_{nn} - A + BG & B \\ C & 0_{mm} \end{bmatrix} = 0_{n+m}^T \quad (7.39)$$

$$\begin{bmatrix} z_i^T & -w_i^T \end{bmatrix} \neq 0_{n+m}^T \text{ for } i=1, 2, \dots, j.$$

We apply the result of the theorem to system $[(A - BG), B, C]$. According to part 1 of the theorem, if $H = \rho BW$, then as ρ approaches ∞ , the eigenvalues of $(A - BG - HC)$ will

approach the transmission zeros of $\{(A-BG), B, C\}$ computed from equations (7.39). These are also the transmission zeros of the plant given by equation (7.37).

According to part 2 of the theorem, the left closed-loop eigenvectors, x_i^T of the compensator given by equation (7.40):

$$x_i^T (\mu_i I_{nn} - A + BG + HC) = 0_n^T, \quad i=1,2,\dots,j \quad (7.40)$$

$$x_i^T \neq 0_n^T$$

approach z_i^T given by equation (7.39) or equation (7.37). ■

7.4 Comments

1) According to corollary 2, as ρ approaches ∞ , the eigenvalues of $K(s)$ will cancel out the transmission zeros of the plant. According to corollary 1, as ρ approaches ∞ , the transmission zeros of $K(s)$ will approach the transmission zeros of $G(sI_{nn}-A)^{-1}B$. Since the number of transmission zeros of two cascaded systems ($K(s)$ and $G_p(s)$) is the sum of the number of transmission zeros of both systems, the transmission zeros of $K(s)G_p(s)$ are the same as the transmission zeros of $G(sI_{nn}-A)^{-1}B$. Similar arguments can be given for the poles of $K(s)G_p(s)$. The poles of $K(s)$ cancel out the transmission zeros of the plant; therefore, the poles of $K(s)G_p(s)$ will be the same as poles of $G(sI_{nn}-A)^{-1}B$. This argument does not prove the equality of $G(sI_{nn}-A)^{-1}B$ and $K(s)G_p(s)$ as ρ approaches ∞ . Proof of the pointwise equality of $K(s)G_p(s)$ and $G(sI_{nn}-A)^{-1}B$ is best shown by Doyle and Stein in [7]. The above comment concerning pole-zero cancellation explains the eigenstructure mechanism for LTR. Since pole placement and eigenvector construction in the allowable sub-space prescribes a unique value for H , we plan to design the observer gain for the LTR via pole placement and left eigenvector construction.

2) The asymptotic finite eigenstructure for H in both equations (7.6) and (7.9) are the same, but the asymptotic infinite eigenstructures are usually different. The form of H given by equation (7.9) is rarely stabilizing. Since both forms guarantee the pointwise approach of $K(s)G_p(s)$ to $G(sI_{nn}-A)B$, it can be deduced that the pointwise approach of $K(s)G_p(s)$ to $G(sI_{nn}-A)B$ occurs whenever the asymptotic finite eigenstructure is the same as that given by the theorem. Hence, combining any such finite eigenstructure with any stable infinite eigenstructure will result in the approach of $K(s)G_p(s)$ to $G(sI_{nn}-A)B$ in a stable sense.

3) Difficulty in using LTR will arise if the plant has some right half-plane zeros (non-minimum phase plant). In our proposed procedure for LTR, one should place the eigenvalues of (A-HC) at the transmission zeros of the plant. If the plant is non-minimum phase, one would place some eigenvalues of (A-HC) on the right half-plane. The closed-loop system will not be stable if any eigenvalues of (A-HC) are on the right half-plane. According to the separation theorem, the eigenvalues of (A-HC) are also the eigenvalues of the closed-loop system. Therefore, the sufficient condition for LTR and the stability of the closed-loop system is that the plant be minimum-phase. If the plant is non-minimum phase, one should consider the mirror images of the right half-plane zeros as target locations for eigenvalues of (A-HC). In such cases, loop transfer recovery is not guaranteed, but the closed-loop system will be stable.

7.5 Design Method

For observer design, we place j finite eigenvalues of (A-HC) at finite transmission zeros of the plant. The left closed-loop eigenvector, v_i^T , associated with the finite modes must be constructed such that $[v_i^T \ -w_i^T]$ is in the left null space of the matrix given by equation (7.17). The remaining $(n-j)$ closed-loop eigenvalues should be placed far in the left half-plane. Note that the farther the $(n-j)$ infinite eigenvalues of (A-HC) are located from the imaginary axis, the closer $K(s)G_p(s)$ will be to $G(sI_{nn}-A)B$ as shown in the example. The left closed-loop eigenvectors associated with the infinite modes can be computed via equation (7.41).

$$v_i^T = w_i^T C (\mu_i I_{nn} - A)^{-1} \quad i = j+1, j+2, \dots, n \quad (7.41)$$

$$\text{where: } w_i^T = -v_i^T H \quad (7.42)$$

The following steps will lead a designer toward observer design for the recovery procedure:

1) Use equation (7.17) to compute the j target locations of the complex finite eigenvalues of the observer, s_i , and j left null vectors of $[z_i^T \ -w_i^T]$. μ_i must be selected to be equal to s_i . The left closed-loop eigenvector of the observer, v_i^T , must be selected to be equal to z_i^T . If s_i is not equal to any eigenvalue of A , use equations (7.18) and (7.19) to compute the j left closed-loop eigenvectors, v_i^T and w_i^T . w_i^T identifies the location of the left closed-loop eigenvector in its allowable sub-space. This step terminates the construction of the finite eigenstructure of the observer.

2) Place the remaining (n-j) eigenvalues of (A-HC) at locations farther than the finite transmission zeros of the plant. Use equation (7.41) to achieve (n-j) values for v_i^T . The w_i^T for infinite modes are arbitrary and have little importance because their corresponding eigenvalues are selected far in the left half complex plane.

3) Since

$$v_i^T H = -w_i^T \quad , \quad i = 1, 2, \dots, n \quad (7.43)$$

then:

$$\begin{bmatrix} v_1^T \\ v_2^T \\ \vdots \\ v_n^T \end{bmatrix} H = - \begin{bmatrix} w_1^T \\ w_2^T \\ \vdots \\ w_n^T \end{bmatrix} \quad (7.44)$$

Use equation (7.45) to compute H.

$$H = - \begin{bmatrix} v_1^T \\ v_2^T \\ \vdots \\ v_n^T \end{bmatrix}^{-1} \begin{bmatrix} w_1^T \\ w_2^T \\ \vdots \\ w_n^T \end{bmatrix} \quad (7.45)$$

The independence of the n left closed-loop eigenvectors, v_i^T , is a necessary condition to use eigenstructure assignment for LTR. If the left closed-loop eigenvectors are not independent, our approach fails and one must use Doyle and Stein's approach to recover the loop transfer function. The dependency of the left eigenvectors might arise if multiple finite transmission zeros result in equation (7.17). If degeneracy of the matrix in equation (7.17) is equal to the multiplicity of a transmission zero, the existence of n independent, finite, left closed-loop eigenvectors is guaranteed.

7.6 Example

Consider the following example:

$$A = \begin{bmatrix} 0. & 0. & 1. & 0. \\ 0. & 0. & 0. & 1. \\ 0. & 0. & 0. & 0. \\ 0. & 0. & 0. & 0. \end{bmatrix} \quad B = \begin{bmatrix} 0.0 & 0.0 \\ 0.0 & 0.0 \\ 76.0 & -105.0 \\ -105.0 & 280.0 \end{bmatrix}$$

$$C = \begin{bmatrix} 1. & 0. & 1. & 0. \\ 0. & 1. & 0. & 4. \end{bmatrix}$$

Suppose we are given G such that the closed-loop poles are at -19.35, -1.76, -5.57 and -6.12 :

$$G = \begin{bmatrix} 4.7234 & 3.4265 & 0.9923 & 0.6631 \\ 1.1497 & 0.8579 & 0.2633 & 0.1952 \end{bmatrix}.$$

Using equation (7.19), the finite transmission zeros, s_i , and the associated left null-vector directions, w_i^T , can be computed. μ_1 and μ_2 are selected to be equal to s_1 and s_2 .

$$\mu_1 = -1, \mu_2 = -25, w_1^T = [1 \ 0], w_2^T = [0 \ 1]$$

Using equation (7.18), the left closed-loop eigenvector associated with the finite modes can be computed:

$$v_1^T = [-1.00 \quad 0.00 \quad 0.00 \quad 0.00]$$

$$v_2^T = [0.00 \quad -4.00 \quad 0.00 \quad 0.00]$$

We place the other two eigenvalues of (A-HC) in the left half-plane as far as possible. The directions of w_3^T and w_4^T do not matter because the associated eigenvalues are far away. Figure 7-6 shows that the farther away from the imaginary axis the two infinite eigenvalues of (A-HC) are, the closer $K(s)G_p(s)$ will be to $G(sI_{nn}-A)^{-1}B$. Assuming :

$$\mu_3 = -30, \mu_4 = -36, w_3^T = [1 \ 0], w_4^T = [0 \ 1]$$

and using equation (7.41), the left eigenvectors associated with infinite modes can be computed:

$$v_3^T = [-0.0333 \quad 0.0000 \quad -0.0322 \quad 0.0000]$$

$$v_4^T = [0.0000 \quad -0.0278 \quad 0.0000 \quad -0.1103]$$

Using equation (7.45), H can be computed:

$$H = \begin{bmatrix} 1.0000 & 0.0000 \\ 0.0000 & 0.2500 \\ 30.0000 & 0.0000 \\ 0.0000 & 0.9000 \end{bmatrix}$$

The finite transmission zeros of $G(sI_{nn}-A)^{-1}B$ are located at -4.3270 and -1.3675 . Table 7-1 shows that the transmission zeros of $K(s)$ approach the transmission zeros of $G(sI_{nn}-A)^{-1}B$ as μ_3 and μ_4 move farther into the left half complex plane (corollary 1). Table 7-1 also shows that the farther μ_3 and μ_4 are from the imaginary axis, the closer the eigenvalues of

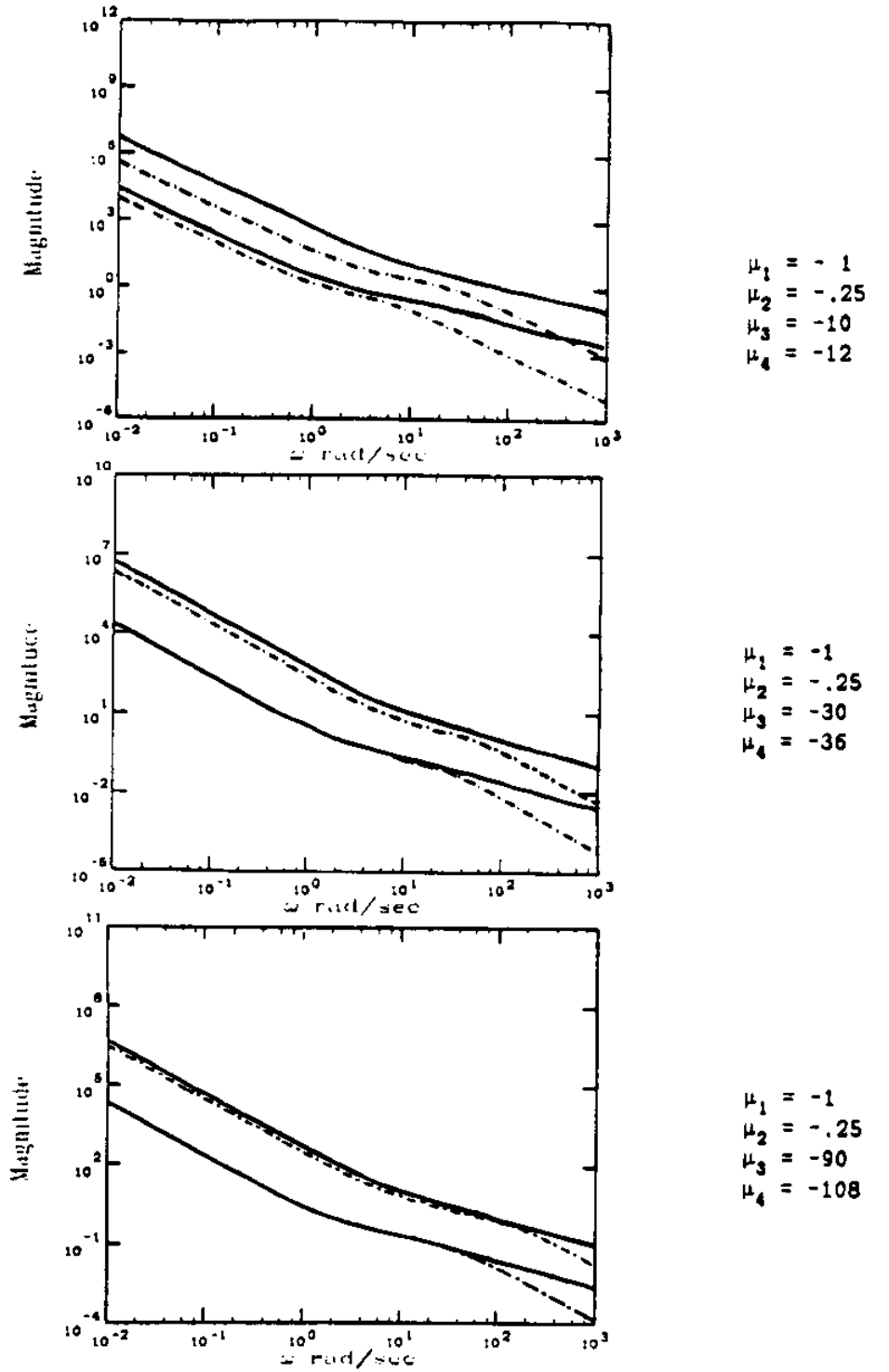


Figure 7-6: Maximum and Minimum Singular
 Values of $K(s)G_p(s)$ -----
 Maximum and Minimum Singular
 Values of $G(sI - A)^{-1}B$ ———

Closed loop eigenvalues	Transmission zeros of K(s)	Eigenvalues of K(s)
$\mu_1 = -1$ $\mu_2 = -.25$ $\mu_3 = -10$ $\mu_4 = -12$	-2.8097 -1.2662 $-\infty$ $-\infty$	-30.5672 -24.2387 -1.0000 -0.2500
$\mu_1 = -1$ $\mu_2 = -.25$ $\mu_3 = -30$ $\mu_4 = -36$	-3.6734 -1.3311 $-\infty$ $-\infty$	-49.4030 + 10.4478i -49.4030 - 10.4478i -1.0000 -0.2500
$\mu_1 = -1$ $\mu_2 = -.25$ $\mu_3 = -90$ $\mu_4 = -108$	-4.0855 -1.3551 $-\infty$ $-\infty$	-115.40 + 20.46i -115.40 - 20.46i -1.0000 -0.25

Table 7-1: Poles and Zeros of K(s)

K(s) will be to the transmission zeros of the plant (corollary 2).

7.7 Conclusion

A key step in the recent work on the synthesis of model-based feedback compensators for multivariable systems is the selection of the observer gain. The observer gain must be selected so that the final loop-transfer function, $K(s)G_p(s)$ in Figure 7-1, is the same as the state-feedback loop transfer function, $G(sI_{nn}-A)^{-1}B$ (shown in Figure 7-2), for some bounded frequency range. In LTR, the eigenvalues of the compensator, $K(s)$, cancel the transmission zeros of the plant. It is also true that the compensator, $K(s)$, will share the same transmission zeros as $G(sI_{nn}-A)^{-1}B$. By exploring the eigenstructure of the model-based compensator when loop transfer recovery takes place, we provide an alternative design procedure which eliminates the need for the Kalman filter mechanism via direct assignment of the eigenvalues and left eigenvectors of the observers. The sufficient condition for LTR and the stability of the closed-loop system is that the plant be minimum-phase. The limitation of this method might arise when the plant has multiple finite transmission zeros, and n left independent closed-loop eigenvector cannot be constructed.

In impedance control theory, the LTR method can be used to approximate $K(s)G_p(s)$ by $G(sI_{nn}-A)^{-1}B$. Since all transmission zeros of the system $[A, B$ and $C]$, given by equation

(4.18) are at infinity [59], the eigenvalues of $(A-HC)$ can be placed in the left half complex plane to recover the loop transfer function. The farther the eigenvalues of $(A-HC)$ are from the origin, the closer $K(s)G_p(s)$ will be to $G(sI_{nn}-A)^{-1}B$.

Chapter 8 Conclusion

We started with conventional controller design specifications concerning the treatment of the interaction forces and torques when the system is not constrained. Generalizing this treatment to include cases when the system is constrained, we stated a set of controller design specifications to assure compliant motion with stability in the presence of bounded uncertainties (Figure 2-1). One of the most important contributions of this thesis is the formulation of the concept of compliant motion in terms of a meaningful set of controller design specifications. This set (shown in Figure 2-1) is a proper definition of the compliant motion. In Chapter 2, we show that Hogan's target impedance [20], given by equation (2.2), can parametrize our set of performance specifications. The following is a summary of the parametrization of the set of performance specifications:

stiffness matrix > K;
 ω_0 > J;
stability > C.

We assume C to be a matrix that always produces a slightly damped or underdamped stable system; therefore, for a given K-matrix, the J-matrix is the parameter that affects ω_0 the most and many J-matrices can parametrize ω_0 . In particular, we show how a wide ω_0 (or a small J-matrix) may cause instability in the presence of high frequency unmodelled dynamics. In Section 5.3.4, we gave some methods for arriving at a proper value for the J-matrix.

The target impedance mandates a closed-loop relationship between the interaction loads and the motion of the system in the global cartesian coordinate frame. In general, the closed-loop behavior of a system cannot be shaped arbitrarily over an arbitrary, bounded frequency range, but we show that this target impedance is mathematically achievable, and in Chapter 5 we offer a geometrical design method to achieve it. This is a fundamental result which is proved in Appendix A. By considering the dynamics of the manipulators and its actuators, continuous feedback and feedforward gains are given in closed form to guarantee the achievement of the target dynamics in the presence of model uncertainties.

If a dynamic system behaves according to equation (A.2), then the dynamic system and its environment taken as a whole will remain stable. Appendix A proves this, and it gives a

sufficient condition for the stability of the target dynamics. The stability of the target impedance and its global stability with the environment result from the appropriate choice of the target dynamics and not the design methodology.

To achieve the target impedance given by equation (2.2), we need to measure the joint angles, joint angle rates, actuator torques and interaction forces of the system. Most direct-drive manipulators are not equipped with fast actuators, and it is necessary to consider their dynamics and to measure the actuator torques (or motor currents) in the design process if a wide frequency range of operation is needed. In Chapter 4 we develop a mathematical model for manipulators and their actuators to represent their dynamic behavior during low-speed, constrained maneuvers. When the actuators are fast (i.e., their bandwidths are much wider than the desired frequency range of operation, ω_0), the dynamics of the actuators can be neglected, which eliminates the need for torque feedback (See Appendix C). If ω_0 is small enough to be parametrized by the target inertia matrix given by equation (5.41), then force measurement can also be eliminated. In other words, if the target inertia is selected to be the inertia of the manipulator in the global coordinate frame (given by equation (5.41)), then it is not necessary to measure the interaction forces. We use force-feedforward only to change the inertia of the system. If the actuators are fast and the frequency range of operation is small enough that the target inertia can be chosen according to equation (5.41), then it is necessary to measure only the joint angles and joint angle rates.

Stability in the presence of model uncertainties is another significant issue in our design method. Large feedback gains produce poor robustness to high-frequency unmodelled dynamics and good robustness to uncertainties within the modelled dynamics. Selecting a wide ω_0 will produce a large feedback gain, which means the system will be less robust to high-frequency unmodelled dynamics and more robust to uncertainties in the modelled dynamics. On the other hand, a narrow ω_0 will result in a small state-feedback gain, which will assure good robustness to high-frequency unmodelled dynamics. Since ω_0 is parametrized by J , we can state that for a given K , a small J -matrix may cause instability in the presence of high-frequency unmodelled dynamics, and a large J -matrix may cause instability if there are uncertainties in the model at low frequencies.

The trade-off between the size of the target inertia and stability robustness relative to high frequency unmodelled dynamics is another contribution of this thesis. Another factor in the size of the state-feedback gain is α , which measures the locations of the closed-loop eigenvalues of the actuators. The farther from the origin the n closed-loop eigenvalues of the actuators are located, the larger the feedback gain matrix, G , will be. In other words, large

closed-loop bandwidths of actuators result in less robustness to high frequency unmodelled dynamics.

As mentioned in Chapter 1, there are two approaches for assuring the compliant motion of a dynamic system, each with its own application. Their fundamental differences are described as follows:

- In hybrid force/position control [43, 46, 55, 38, 61], force is controlled along those directions constrained by the environment, while position is controlled along those directions in which the system is free to move. This method allows the direct, and therefore precise, control of the interaction forces. In impedance control, there is no direct closed loop around the interaction force. In fact, we sometimes do not even measure the interaction force. The interaction force is controlled in an open loop fashion. By controlling the position and orientation of the system and assigning an appropriate impedance, we arrive at a reasonable range for the desired interaction force ($\Delta D(j\omega) = K \Delta Y(j\omega)$).
- Unlike hybrid force/position control, impedance control never forfeits the positioning capability of the system. Consider a maneuver such as approaching a stiff wall; the positioning of the system and a low impedance allow the manipulator to hit the environment with a light contact force. In hybrid force/position control, such a maneuver can be done with two sets of controllers: a pure positioning system to move the system in the free environment, and a hybrid force/position control to move the system after it touches the environment.
- In hybrid force/position control, the structure of the controllers and the global stability of the system depend heavily on the dynamic and geometrical properties of the environment. We arrived at a controller structure which is independent of environment characteristics.

Dynamic/graphic simulations were performed to illustrate differences. Another contribution of this thesis is presented in Chapter 7. A key step in recent work in multivariable synthesis involves selecting an observer gain so the final loop-transfer function is the same as the state-feedback loop transfer function for a bounded frequency range. This is called Loop Transfer Recovery (LTR). This chapter shows how identification of the eigenstructure of the compensators that achieve LTR makes possible a design procedure for observer gain. This procedure is based on eigenstructure assignment of the observers (dual to the impedance control synthesis).

Appendix A Stability

If the J-matrix and K-matrix in equation (2.2) are selected arbitrarily (J is any non-singular matrix) to parametrize the first and second items of the set of performance specifications, a value for the C-matrix that assures the stability of the target dynamics is not guaranteed. But for a non-singular K-matrix, there always exist many J- and C-matrices such that the eigenvalues of the target dynamics are in the left half complex plane (e.g., the J-matrix and C-matrix may be selected to be $\gamma_1 K$ and $\gamma_2 K$, as on page 19).

The selection of J, C and K will be much easier if they are restricted to some class of matrices. Theorem 1 gives a sufficient condition for the stability of the target dynamics, while Theorem 2 considers the stability of both the dynamic system and its environment. Theorem 1, which expresses the essential concept of stability of this class of impedances, is discussed in references [13, 11] and is given here only for continuity of the material.

Theorem 1

If J, C and K are real and symmetric, positive definite matrices, then the system in equation (2.2) is stable, and if C and K are symmetric, non-negative definite matrices, then the system in equation (2.2) will be marginally stable.

Proof:

The eigenvalue problem associated with the target dynamics is expressed by equation (3.5).

$$\begin{aligned} [J \lambda_i^2 + C \lambda_i + K] q_i &= 0_n & i = 1, 2, \dots, 2n & \quad (A.1) \\ q_i &\neq 0_n \end{aligned}$$

Pre-multiplying equation (A.1) by q_i^H results in equation (A.2).

$$q_i^H [J \lambda_i^2 + C \lambda_i + K] q_i = 0 \quad i = 1, 2, \dots, 2n \quad (A.2)$$

Where q_i^H is the complex conjugate transpose of q_i . Since J is a symmetric positive definite matrix, then:

$$j_i = q_i^H J q_i > 0 . \quad (A.3)$$

Since J is a symmetric matrix, equality (A.3) is true for any vector in C^n , including the right latent vector q_i . Similarly, $c_i = q_i^H C q_i > 0$, and $k_i = q_i^H K q_i > 0$.

Equation (A.2) can be simplified to equation (A.4).

$$j_i \lambda_i^2 + c_i \lambda_i + k_i = 0 \quad i = 1, 2, \dots, 2n \quad (A.4)$$

where j_i , k_i and c_i are real, positive scalars. Any complex number λ_i that satisfies equation (A.4) is in the left half complex plane. Equation (A.4) may result in complex roots on the imaginary axis (and consequently a marginally stable solution) if c_i and/or k_i vanish. Absolute stability of the target dynamics results if J , C and K are symmetric, positive definite matrices. The set of the eigenvalues that result from equation (A.4) is self-conjugate. ■

Note that the conditions on J , C and K are sufficient for stability, but not necessary. We might arrive at a set of J , C and K that assures stability without satisfying the theorem condition. As long as matrices J , C and K are symmetric, positive definite, the eigenvalues of the target dynamics given by equation (2.2) are in the left half complex plane.

The stability of the target dynamics is not enough to assure the stability of the overall system of the dynamic system (manipulator) and its environment. In other words, the following question cannot be answered by Theorem 1: *If a manipulator with a stable impedance as expressed by equation (2.2) is in contact with a stable environment, does the system of the manipulator and its environment remain stable?* This is not clear; two stable systems interacting with each other may result in an unstable system. Theorem 2 is needed for the rigorous assurance of the overall stability of the manipulator and its environment; this is given by Theorem 2.

Theorem 2

If the closed-loop dynamic behavior of the dynamic system is given by equation (A.5):

$$J \Delta \ddot{Y}(t) + C \Delta \dot{Y}(t) + K \Delta Y(t) = \Delta D(t) \quad \Delta D(t) \text{ and } \Delta Y(t) \in \mathbb{R}^n \quad (A.5)$$

$$J = J^T > 0 \quad , \quad K = K^T > 0 \quad , \quad C = C^T > 0 ;$$

and if the environment is a system with the dynamic behavior represented by equation (A.6):

$$J_e \Delta \ddot{Y}_e(t) + C_e \Delta \dot{Y}_e(t) + K_e \Delta Y_e(t) = \Delta D_e(t) + \Delta D_e^0(t) \quad (A.6)$$

$\Delta D_e(t)$, $\Delta D_e^0(t)$ and $\Delta Y_e(t) \in \mathbb{R}^m$

$$J_e = J_e^T > 0 \quad , \quad K_e = K_e^T > 0 \quad , \quad C_e = C_e^T > 0 ;$$

where:

$\Delta D_e(t)$ = the load (force and torque) that the manipulator exerts on the environment;

$\Delta D_e^0(t)$ = all other loads on the environment (uncorrelated with manipulator states and environment states); and

$\Delta D(t)$ = the environmental load on the manipulator,

then the overall system (manipulator and environment) is stable.

Proof:

Since the dynamic system is in contact with the environment, vectors $\Delta Y(t)$ and $\Delta Y_e(t)$ might have members in common. Form a p -dimensional vector $\Delta W(t)$ such that equation (A.7) and equation (A.8) are satisfied ($n + m \geq p$). $\Delta W(t)$ is a vector that contains all states of the manipulator and environment. Since the manipulator and environment are in contact with each other, then $\Delta Y_e(t)$ and $\Delta Y(t)$ will have some common members. The first $(p-n)$ members of $\Delta W(t)$ are those states of the environment that are not states of the dynamic system (manipulator). The last $(p-m)$ members of $\Delta W(t)$ are those states of the dynamic system that do not represent the environmental dynamics.

$$\Delta Y_e(t) = T_e \Delta W(t) \tag{A.7}$$

$$\Delta Y(t) = T_y \Delta W(t) \tag{A.8}$$

T_e and T_y are $m \times p$ and $n \times p$ matrices with 0 and 1 as their members. Substituting for $\Delta Y_e(t)$ and $\Delta Y(t)$ in equations (A.5) and (A.6) results in equations (A.9) and (A.10).

$$J T_y \ddot{\Delta W}(t) + C T_y \dot{\Delta W}(t) + K T_y \Delta W(t) = \Delta D(t) \tag{A.9}$$

$$J_e T_e \ddot{\Delta W}(t) + C_e T_e \dot{\Delta W}(t) + K_e T_e \Delta W(t) = \Delta D_e(t) + \Delta D_e^0(t) \tag{A.10}$$

Because of the interaction between the dynamic system and the environment, equation (A.11) is also true.

$$T_y^T \Delta D(t) = - T_e^T \Delta D_e(t) \tag{A.11}$$

Omitting $\Delta D(t)$ and $\Delta D_e(t)$ from equations (A.9) and (A.10) by means of equation

(A.11) results in:

$$\begin{aligned} & (T_y^T J T_y + T_e^T J_e T_e) \Delta \ddot{W}(t) + (T_y^T C T_y + T_e^T C_e T_e) \Delta \dot{W}(t) + \\ & (T_y^T K T_y + T_e^T K_e T_e) \Delta W(t) = T_e^T \Delta D_e^o(t) . \end{aligned} \quad (A.12)$$

It can be verified that :

$$\begin{aligned} T_y^T J T_y + T_e^T J_e T_e &= \text{a symmetric, positive definite matrix;} \\ T_y^T C T_y + T_e^T C_e T_e &= \text{a symmetric, positive definite matrix;} \text{ and} \\ T_y^T K T_y + T_e^T K_e T_e &= \text{a symmetric, positive definite matrix.} \end{aligned}$$

According to Theorem 1, equation (A.12) (which shows the dynamics of the manipulator and the environment) is stable.

According to this theorem, if J, C and K are selected as symmetric, positive definite matrices, the overall system of the manipulator and its environment taken together will yield eigenvalues in the left complex plane. ■

Note that, this theorem guarantees the global stability of the dynamic system and the environment taken as a whole, if the dynamic system behaves according to equation (2.5). The theorem in Chapter 5 shows that the target dynamics can be achieved for a bounded frequency range. The examples in Chapter 6 show this matter. If the controller does not achieve the target impedance exactly, but results in a controlled behavior "approximately" like the target dynamics for a bounded frequency range, then the above theorem does not guarantee the global stability. The importance of the theorem 2 is that it shows that the target impedance has desirable properties.

The block diagram in Figure A-1 shows how the dynamic system and the environment interact with each other in an ideal case when the target impedance is achieved for all $0 < \omega < \infty$. $\Delta Y(s)$ is the imposed motion on the manipulator which consists of the algebraic addition of the commanded incremental motion and environmental motion.

Theorem 2 simply justifies the conditions under which the closed-loop system in Figure A-1 is stable. The theorem in Chapter 5 shows that the target dynamics cannot be achieved for all $0 < \omega < \infty$. The examples in Chapter 6 also show this matter. According to the theorem in Chapter 5, the controllers result in a behavior approximately like the target impedance for a bounded frequency range. The resulting impedance can be shown as:

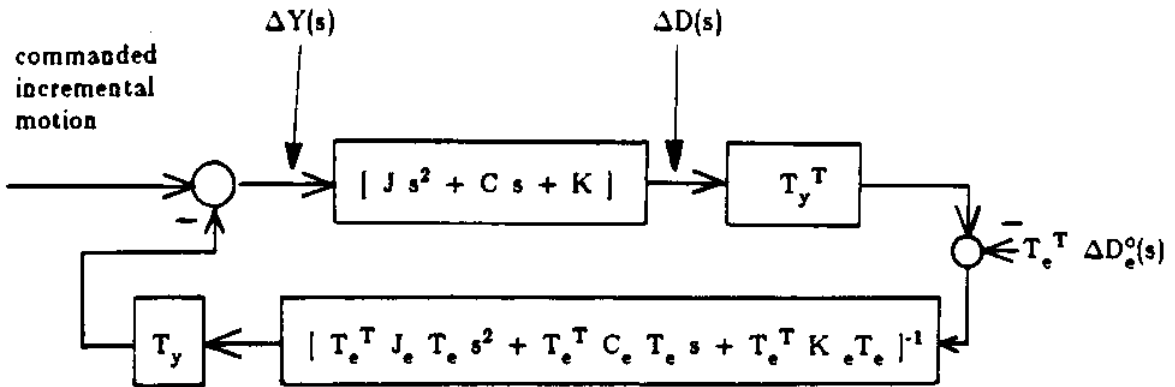


Figure A-1: The interaction of the dynamic system and environment in the ideal case when the target impedance is achieved for all $0 < \omega < \infty$

$$[J s^2 + C s + K] [I_{nn} + E'(s)] \tag{A.13}$$

where $E'(s)$ shows the difference between the achievable target dynamics and the ideal target dynamics. The closed-loop combination of the dynamic system and the environment, considering expression (A.13), is shown in figure A-2.

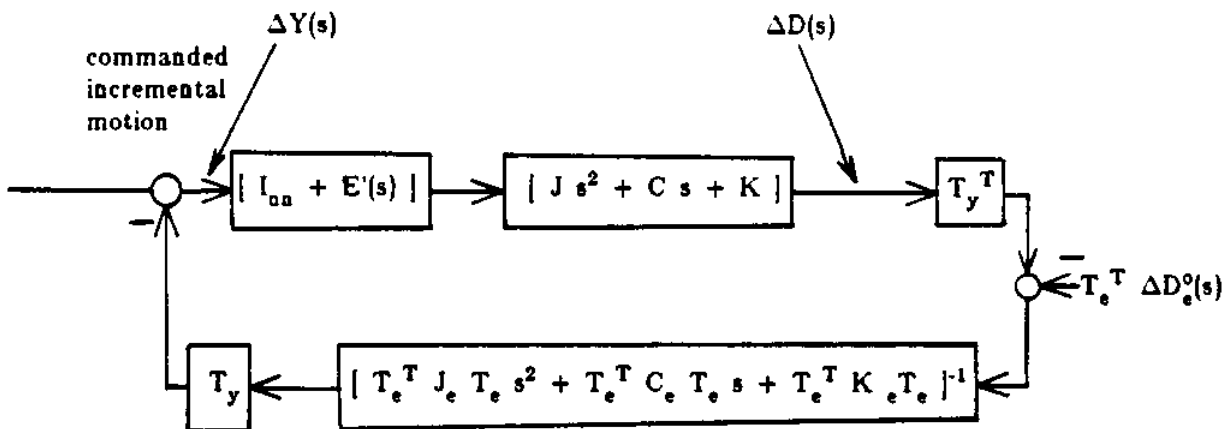


Figure A-2: The interaction of the dynamic system and environment when the target impedance is achieved for some bounded frequency range

The global stability of the system in Figure A-2 is no longer guaranteed by theorem 2. Using the result of Appendix E, the closed-loop system in figure A-2 will be stable if the

following inequality is satisfied for all $0 < \omega < \infty$.

$$\sigma_{\min} \left[I_{nn} + [Js^2 + Cs + K]^{-1} [T_y G_e(s) T_y^T]^{-1} \right] > \sigma_{\max} |E(s)|$$

where : $G_e(s) = [T_e^T J_e T_e s^2 + T_e^T C_e T_e s + T_e^T K_e T_e]^{-1}$

Appendix B Simple Impedances

In this appendix, we consider the properties of a special class of impedances that are called *simple*. Simple impedances guarantee a complete set of right eigenvectors, V , despite the multiplicity of their eigenvalues. Simplicity is a necessary condition for the achievability of the target dynamics, but stability is a desired property (i.e., it is the third item of the set of the performance specifications) and is not necessary for achievability. If we assume the C -matrix is always selected such that it produces a slightly over-damped (or slightly under-damped) stable system, then the J -matrix is the only parameter that parametrizes ω_0 . We are looking for a method to arrive at a C -matrix for a given K - and J - matrix such that the target dynamics in equation (2.2) are always stable and simple. After an analysis of the eigenstructure of the simple impedances, this appendix proceeds to the determination of a bound for matrix C that guarantees the stability and simplicity of the target dynamics, given symmetric, positive definite matrices for J and K .

Definition

Assume that the interaction load, $\Delta D(t)$, and the motion of the dynamic system, $\Delta Y(t)$, satisfy equation (B.1) in the global coordinate system.

$$J \ddot{\Delta Y}(t) + C \dot{\Delta Y}(t) + K \Delta Y(t) = \Delta D(t) \quad \Delta Y(t) \text{ and } \Delta D(t) \in \mathbb{R}^n \quad (\text{B.1})$$

J , C and K are non-singular matrices.

The eigenvalues λ_i and the right latent vectors q_i satisfy equation (B.2).

$$D(\lambda_i) q_i = 0_n \quad i = 1, 2, \dots, 2n \quad (\text{B.2})$$

$$q_i \neq 0_n$$

$$\text{where } : D(\lambda) = J \lambda^2 + C \lambda + K$$

If $D(\lambda)$ has a degeneracy equal to the multiplicity of eigenvalue λ_α in equation (B.2), then $J \lambda^2 + C \lambda + K$ is a simple impedance. In other words, for simplicity of the target dynamics expressed in equation (B.1), the right latent vectors, q_i , associated with the eigenvalues, λ_α , with multiplicity α must be independent. If an impedance is not simple,

then it is called *defective*. It is clear that all impedances with unequal eigenvalues are simple. If J, C and K are symmetric, then the above definition will also be true for the left latent vectors. This is true because equation (B.2) with symmetric J, C and K results in equal left and right latent vectors. The definition of simple impedances is borrowed from the terminology associated with simple matrix polynomials. We are going to use the definition of simple impedances to arrive at a class of impedances that always yield a complete set of right eigenvectors. We prove in Theorem 5 that over-damped and under-damped impedances always have n independent right eigenvectors. Then for a given set of symmetric, positive definite J- and K-matrices, we give a bound for matrix C to generate a stable and slightly over-damped (and consequently simple) impedance. We need the result of theorems 3 and 4 to prove theorem 5. These theorems are proved in references [25, 32, 13, 11] in a leisurely fashion for matrix polynomials of order n. Here we just mention the theorems.

Theorem 3

If the matrix polynomial given by (B.3) is simple:

$$J \lambda^2 + C \lambda + K \tag{B.3}$$

$$J = J^T > 0, \quad C = C^T > 0, \quad K = K^T > 0,$$

then equality (B.4) is true:

$$Q_\alpha^T (2 J \lambda_\alpha + C) Q_\alpha = I_{\alpha\alpha} \tag{B.4}$$

$$\text{where : } Q_\alpha = [q_1 \quad q_2 \quad \dots \quad q_\alpha] . \tag{B.5}$$

The q_i ($i=1, 2, \dots, \alpha$) are the normalized right latent vectors associated with eigenvalue, λ_α , of multiplicity α , all of which satisfy equation (B.6).

$$D(\lambda_\alpha) q_i = 0_n \quad i = 1, 2, \dots, \alpha \tag{B.6}$$

Theorem 4

The impedance $(J s^2 + C s + K)$ is defective if and only if there exists an eigenvalue, λ_α , with the right latent vector, q_i , such that $r_i^T (2 J \lambda_\alpha + C) q_i = 0$ for all left latent vectors, r_i^T , associated with λ_α .

Theorem 5

Consider equation (2.2) when the following inequalities are satisfied:

$$J = J^T > 0, \quad C = C^T > 0, \quad K = K^T > 0 .$$

If equation (2.2) results in over-damped eigenvalues, then $J s^2 + C s + K$ is a simple impedance.

Proof:

By contradiction.

Consider the eigenvalue problem in equation (B.7).

$$\begin{aligned} [J \lambda_i^2 + C \lambda_i + K] q_i &= 0_a \quad i = 1, 2, \dots, 2n & (B.7) \\ J = J^T > 0, \quad C = C^T > 0, \quad K = K^T > 0 \end{aligned}$$

Multiplying equation (B.7) by q_i^H yields equation (B.8).

$$\begin{aligned} q_i^H J q_i \lambda_i^2 + q_i^H C q_i \lambda_i + q_i^H K q_i &= 0 \quad i = 1, 2, \dots, 2n & (B.8) \\ \text{or, equivalently: } j_i \lambda_i^2 + c_i \lambda_i + k_i &= 0 \end{aligned}$$

where:

$$j_i = q_i^H J q_i, \quad c_i = q_i^H C q_i, \quad k_i = q_i^H K q_i,$$

and j_i , c_i and k_i are real non-negative numbers. The roots can be computed from equation (B.9).

$$\lambda_i = \frac{-c_i \pm \sqrt{c_i^2 - 4k_i j_i}}{2 j_i} \quad i = 1, 2, \dots, 2n \quad (B.9)$$

$$\text{or, equivalently: } 2 j_i \lambda_i + c_i = \pm \sqrt{c_i^2 - 4 k_i j_i} \quad i = 1, 2, \dots, 2n \quad (B.10)$$

If the impedance is over-damped, then inequality (B.11) is true.

$$c_i^2 - 4 k_i j_i > 0 \quad i = 1, 2, \dots, 2n \quad (B.11)$$

If the impedance is not simple, according to theorem 4 there must be an eigenvalue, λ_s , with right latent vector, q_s , such that equation (B.12) is true.

$$q_s^H (J \lambda_s + C) q_s = 0 \quad (B.12)$$

$$\text{or, equivalently: } 2 j_s \lambda_s + c_s = 0 \quad (B.13)$$

where:

$$j_s = q_s^H J q_s, \quad c_s = q_s^H C q_s$$

Equations (B.13) and (B.10) result in equation (B.14).

$$c_j^2 - 4 k_j j_j = 0 \quad (B.14)$$

But equation (B.14) contradicts equation (B.11). Therefore, the over-damped impedances are simple and result in a complete set of eigenvectors. The proof fails for critically damped systems. This theorem is also true for under-damped impedances; proof is similar but needs more elaboration. ■

A bound for C to guarantee the simplicity of the target impedance

Matrix C plays a significant role in assuring the simplicity of the target impedance. A "small" C may result in imaginary eigenvalues, and consequently, under-damped target dynamics. A "large" C may result in a slow and ill-conditioned impedance with eigenvalues that are far apart. It is necessary to propose a bound for C in terms of J and K so the triplet (J, C and K) will result in a slightly over-damped (and consequently simple) impedance for the target dynamics. Consider the conservative dynamics of equation (B.15) with real-valued non-singular matrices K and J.

$$J \Delta \ddot{Y}(t) + K \Delta Y(t) = 0 \quad , \quad J = J^T > 0 \quad , \quad K = K^T > 0 \quad (B.15)$$

The eigenvalue problem associated with (B.15) is expressed by equation (B.16).

$$\begin{aligned} [J \omega_i^2 + K] r'_i &= 0_n \quad i = 1, 2, \dots, n \\ r'_i &\neq 0_n \end{aligned} \quad (B.16)$$

Since J is symmetric, positive definite, equation (B.16) can be written as equation (B.17).

$$\begin{aligned} \sqrt{J} [\omega_i^2 I_{nn} + \sqrt{J^{-1}} K \sqrt{J^{-1}}] \sqrt{J} r'_i &= 0_n \quad i = 1, 2, \dots, n \\ \text{where: } J &= \sqrt{J} \sqrt{J} \quad \text{and} \quad J^{-1} = \sqrt{J^{-1}} \sqrt{J^{-1}} \end{aligned} \quad (B.17)$$

$\sqrt{J^{-1}} K \sqrt{J^{-1}}$ is a real symmetric matrix and has n positive eigenvalues, ω_i^2 , and n linearly independent eigenvectors, $\sqrt{J} r'_i$. Since the latent vectors r'_i are obtained from these by a non-singular transformation \sqrt{J} , it follows that the latent vectors r'_i are also linearly independent. Since J is non-singular and all latent vectors r'_i are independent, equations (B.18) and (B.19) are true [11, 32, 12].

$$R^T K R = \text{diag} (\omega_1^2 , \omega_2^2 , \dots , \omega_n^2) = \Omega^2 \quad (B.18)$$

$$R^T J R = I_{nn} \quad (B.19)$$

$$\text{where: } R = [r'_1 \quad r'_2 \quad \dots \quad r'_n]$$

Choose a new coordinate, $\Delta Z(t)$, according to equation (B.20).

$$R \Delta Z(t) = \Delta Y(t) \quad (B.20)$$

Substitute for $\Delta Y(t)$, $\dot{\Delta Y}(t)$ and $\ddot{\Delta Y}(t)$ in equation (2.2).

$$R^T J R \ddot{\Delta Z}(t) + R^T C R \dot{\Delta Z}(t) + R^T K R \Delta Z(t) = 0_n \quad (B.21)$$

Using equations (B.18) and (B.19) we arrive at equation (B.22).

$$\ddot{\Delta Z}(t) + R^T C R \dot{\Delta Z}(t) + \Omega^2 \Delta Z(t) = 0_n \quad (B.22)$$

Suppose C is chosen so that $R^T C R$ is a diagonal matrix with the following structure:

$$R^T C R = \text{diag} (2\xi_1\omega_1, 2\xi_2\omega_2, \dots, 2\xi_n\omega_n) \quad (B.23)$$

$$\text{where: } \xi_i \geq 1 \quad i = 1, 2, \dots, n.$$

Then equation (B.22) results in n uncoupled second-order differential equations. The polynomial matrix associated with equation (B.22) is given by expression (B.24).

$$I_{nn} \lambda^2 + R^T C R \lambda + \Omega^2 \quad (B.24)$$

Using equation (3.6) and expression (B.24), n second-order uncoupled equations can be constructed to arrive at the eigenvalues of the target dynamics. Each equation results in two eigenvalues. Since $\xi_i > 1$ ($i = 1, 2, \dots, n$), all eigenvalues are real. $R^T C R$ and $R^T K R$ are both diagonal, and C can be computed from equality (B.25).

$$R^T C R = 2 \xi \sqrt{(R^T K R)} \quad (B.25)$$

where: $\xi = \text{diag} (\xi_1, \xi_2, \dots, \xi_n)$. Thus, from equation (B.25):

$$C = 2 (R^T)^{-1} \xi \sqrt{(R^T K R)} R^{-1}. \quad (B.26)$$

Example

Suppose the target-inertia matrix and stiffness matrix are given as:

$$J = \begin{bmatrix} .0368 & .0343 \\ .0343 & .0509 \end{bmatrix} \quad K = \begin{bmatrix} 0.06 & 0.0 \\ 0.0 & 0.6 \end{bmatrix}$$

Two independent, right latent vectors form matrix R:

$$R = \begin{bmatrix} 4.7696 & -7.0931 \\ 0.4666 & 7.2500 \end{bmatrix}$$

$R^T K R$ is a diagonal matrix:

$$R^T K R = \begin{bmatrix} 1.4956 & 0.0 \\ 0.0 & 34.5564 \end{bmatrix}$$

Considering ξ as:

$$\xi = \begin{bmatrix} 1.2 & 0.0 \\ 0.0 & 1.2 \end{bmatrix}$$

results in a damping matrix with real eigenvalues for the target dynamics:

$$C = \begin{bmatrix} 0.1096 & 0.0833 \\ 0.0833 & 0.3264 \end{bmatrix}$$

The eigenvalues of the target impedance are located at -10.9535, -6.6563, -2.2787 and -3.1548 .

Appendix C

This appendix arrives at feedback and feedforward gains when the actuators bandwidths are much greater than ω_o . If the bandwidths of the actuators are much larger than the desired frequency range of operation, ω_o , then it is possible to ignore the actuator dynamics from the dynamic equations of the manipulators. Eliminating the actuator dynamics, A, B, C and L in equations (4.19) and (4.20) gives:

$$A = \begin{bmatrix} 0_{nn} & I_{nn} \\ -M^{-1}(\theta_o)GR(\theta_o) & 0_{nn} \end{bmatrix} \quad B = \begin{bmatrix} 0_{nn} \\ M^{-1}(\theta_o)T_s \end{bmatrix} \quad L = \begin{bmatrix} 0_{nn} \\ M^{-1}(\theta_o)J_c^T \end{bmatrix} \quad (C.1)$$

$$C = [I_{nn} \quad 0_{nn}] .$$

After some algebraic manipulation similar to that shown in Section 5.2.1, the achievable, right closed-loop eigenvector is:

$$u_i = \begin{bmatrix} J_c^{-1}q_i \\ \lambda_i J_c^{-1}q_i \end{bmatrix} \quad i = 1, 2, \dots, 2n . \quad (C.2)$$

m_i can be calculated as follows:

$$m_i = T_s^{-1} [GR(\theta_o) + M(\theta_o) \lambda_i^2] J_c^{-1} q_i \quad i = 1, 2, \dots, 2n . \quad (C.3)$$

Since J_c^{-1} exists in both equations (C.2) and (C.3), in forming G, J_c^{-1} can be cancelled out to ease the computations. The state-feedback gain, G, can be computed from equation (C.4).

$$G = [m_1 \quad m_2 \quad \dots \quad m_{2n}] [u_1 \quad u_2 \quad \dots \quad u_{2n}]^{-1} \quad (C.4)$$

Theorem 5.3.1 is also true since the eigenvalues of the actuators can be placed at $-\infty$, which allows G_d to be computed by a method similar to the one in Section 5.3.2.

$$G_d = T_s^{-1} [GR(\theta_o) + T_s G_1] J_c^{-1} K^{-1} - J_c^T \quad (C.5)$$

$$\text{where: } G_d = [G_1 \quad G_2]$$

Since we do not assign any eigenstructure for the dynamics of actuators, the freedom to adjust for the robustness specification does not exist. The only parameter that can be altered to meet the stability robustness specifications at high frequencies is ω_0 . Selection of the J-matrix according to equation (5.41) results in a value of zero for G_d .

Appendix D

Proof of the theorem in Section 5.3.1 on page 55 is given here. This theorem does not prescribe any value for G_d . It justifies the conditions under which limit (5.33) is true for all $0 < \omega < \omega_b$ without regard to stability robustness. According to this theorem, the satisfaction of inequality (5.32) as ρ approaches ∞ , and the selection of G such that V and A are guaranteed, ensures a unique value for G_d that leads to limit (5.33) for all $0 < \omega < \omega_b$.

Proof:

$$\text{If } L_p = L + B G_d, \text{ then:} \quad (D.1)$$

$$L_p = \begin{bmatrix} 0_{nn} \\ M^{-1}(\theta_0) J_c^T \\ B_s G_d \end{bmatrix} \quad (D.2)$$

Assume:

$$G_c(j\omega) = G_1(j\omega) + G_2(j\omega) \quad (D.3)$$

where $G_1(j\omega)$ and $G_2(j\omega)$ represent in diadic form [26] the contribution of the dominant modes (represented by A) and the modes of the actuators of the closed-loop system, given by equations (D.4) and (D.5).

$$G_1(j\omega) = C \left[\sum_{i=1}^{2n} \frac{u_i w_i^T}{j\omega - s_i} \right] L_p \quad (D.4)$$

$$G_2(j\omega) = C \left[\sum_{i=2n+1}^{3n} \frac{u_i w_i^T}{j\omega - s_i} \right] L_p \quad (D.5)$$

u_i and w_i^T are the right and left closed-loop eigenvectors in C^{3n} that satisfy equations (5.7) and (D.6).

$$w_i^T s_i = w_i^T (A - B G) \quad i = 1, 2, \dots, 3n \quad (D.6)$$

As the first step in the proof, limit (D.7) will be shown to be true.

$$\lim_{\rho \rightarrow \infty} G_2(j\omega) = 0_{nn} \quad \text{for all } 0 < \omega < \omega_b \quad (D.7)$$

The right closed-loop eigenvector associated with each actuator is given by equation (D.8). This was already derived in equation (5.24).

$$u_i = \begin{bmatrix} [M(\theta_0) s_i^2 + GR(\theta_0)]^{-1} T_s \\ [M(\theta_0) s_i^2 + GR(\theta_0)]^{-1} T_s s_i \\ I_{nn} \end{bmatrix} \begin{bmatrix} g_i \end{bmatrix} \quad i = 2n+1, 2n+2, \dots, 3n \quad (D.8)$$

If inequality (5.32) is satisfied and ρ approaches ∞ , it can be verified that each of the upper $2n$ members of each right eigenvector, u_i , in equation (D.8) approaches a small number, while the last n members stay constant. This implies that the members of U_{12} of matrix U in equation (5.10) will be much smaller than unity. If W^T is the matrix of left closed-loop eigenvectors, then $W^T = U^{-1}$. With the assumption that the members of U_{12} are much smaller than unity and with some algebraic manipulations, W^T can be represented by approximation (D.9) as ρ approaches a large number.

$$W^T \approx \begin{bmatrix} U_{11}^{-1} & -U_{11}^{-1} U_{12} U_{22}^{-1} \\ -U_{22}^{-1} U_{21} U_{11}^{-1} & U_{22}^{-1} \end{bmatrix} \quad (D.9)$$

The n left closed-loop eigenvectors associated with the actuators form the lower partition of matrix (D.9). In other words:

$$\begin{bmatrix} w_{2n+1}^T \\ w_{2n+2}^T \\ \vdots \\ w_{3n}^T \end{bmatrix} = \begin{bmatrix} -U_{22}^{-1} U_{21} U_{11}^{-1} & U_{22}^{-1} \end{bmatrix} \quad (D.10)$$

Matrices U_{22} , U_{21} and U_{11} are independent of the closed-loop eigenvalues of the actuators. This was observed in equations (5.24) and (5.19). Because of this independence, if the closed-loop eigenvalues of the actuators become very large in magnitude, all members of w_i^T ($i = 2n+1, 2n+2, \dots, 3n$) in equation (D.10) will stay bounded.

Consider the matrix with complex members given by equation (D.11).

$$\left[\frac{u_i w_i^T}{j\omega - s_i} \right] \quad i = 2n+1, 2n+2, \dots, 3n \quad (D.11)$$

If the complex number, s_i , becomes very large in magnitude (with negative real parts for stability), then it is trivial to prove that the complex matrix in equation (D.11) will approach an $n \times n$ complex matrix with very small members. This is true because matrix $u_i w_i^T$ ($i = 2n+1, 2n+2, \dots, 3n$) will always have bounded elements, and because ω is a bounded variable (i.e., $0 < \omega < \omega_b$). The above limit can be formally stated by equation (D.12).

$$\lim_{\rho \rightarrow \infty} \left[\frac{u_i w_i^T}{j\omega - s_i} \right] = 0_{nn} \quad i = 2n+1, 2n+2, \dots, 3n \quad (D.12)$$

$$\rho \rightarrow \infty$$

$$\text{where: } 0 < \omega < \omega_b$$

Since $G_2(j\omega)$ in equation (D.5) consists of a finite summation, the limit in equation (D.13) is also true.

$$\lim_{\rho \rightarrow \infty} G_2(j\omega) = 0_{nn} \quad \text{for all } 0 < \omega < \omega_b \quad (D.13)$$

$$\rho \rightarrow \infty$$

At the second step of the proof, limit (D.14) will be shown to be true.

$$\lim_{\rho \rightarrow \infty} J_c G_1(j\omega) = G_1(j\omega) \quad \text{for all } 0 < \omega < \omega_b \quad (D.14)$$

$$\rho \rightarrow \infty$$

Since G is selected to guarantee the eigenstructure properties of the target dynamics for the manipulator, then equation (D.15) is true.

$$J_c C \begin{bmatrix} u_1 & u_2 & \dots & u_{2n} \end{bmatrix} = C_t \begin{bmatrix} z_1 & z_2 & \dots & z_{2n} \end{bmatrix} \quad (D.15)$$

z_i ($i = 1, 2, \dots, 2n$) is given by equation (3.1). Equation (D.15) is true because the right closed-loop eigenvectors of the target dynamics are achievable. We will use this equality later.

Equation (D.16) is true because both sides are the left eigenvectors of the target impedance.

$$\begin{bmatrix} t_1^T \\ t_2^T \\ \vdots \\ t_{2n}^T \end{bmatrix} = \begin{bmatrix} U_{11}^{-1} \\ \vdots \\ \vdots \end{bmatrix} \begin{bmatrix} J_c^{-1} & 0_{nn} \\ 0_{nn} & J_c^{-1} \end{bmatrix} \quad (D.16)$$

where t_i^T is the left eigenvector of the target dynamics in the global coordinate frame and satisfies the following equation:

$$t_i^T (\lambda_i I_{2n2n} - A_t) = 0_n^T \quad i = 1, 2, \dots, 2n \quad (D.17)$$

Multiplying both sides of equation (D.16) by B_t from equation (2.6) results in equation (D.18).

$$\begin{bmatrix} t_1^T \\ t_2^T \\ \vdots \\ t_{2n}^T \end{bmatrix} B_t = U_{11}^{-1} \begin{bmatrix} 0_{nn} \\ J_c^{-1} J^{-1} \end{bmatrix} \quad (D.18)$$

Equation (D.19) is also true because both sides show the left closed-loop eigenvectors associated with modes selected from A when ρ approaches ∞ .

$$\begin{bmatrix} w_1^T \\ w_2^T \\ \vdots \\ w_{2n}^T \end{bmatrix} = \begin{bmatrix} U_{11}^{-1} & -U_{11}^{-1} U_{12} U_{22}^{-1} \end{bmatrix} \quad (D.19)$$

Multiplying both sides of equation (D.19) by L_p from equation (D.2) results in equation (D.20).

$$\begin{bmatrix} w_1^T \\ w_2^T \\ \vdots \\ w_{2n}^T \end{bmatrix} L_p = \begin{bmatrix} U_{11}^{-1} & -U_{11}^{-1} U_{12} U_{22}^{-1} \end{bmatrix} \begin{bmatrix} 0_{nn} \\ M^{-1}(\Theta_o) J_c^T \\ B_s G_d \end{bmatrix} \quad (D.20)$$

Considering that $U_{22} = I_{nn}$, equation (D.19) can be simplified to equation (D.21).

$$\begin{bmatrix} w_1^T \\ w_2^T \\ \vdots \\ w_{2n}^T \end{bmatrix} L_p = U_{11}^{-1} \begin{bmatrix} 0_{nn} & -U_{12} B_s G_d \\ M^{-1}(\Theta_o) J_c^T & \end{bmatrix} \quad (D.21)$$

U_{12} is a $2n \times n$ matrix. As the closed-loop eigenvalues of the actuators become larger, the upper $n \times n$ partition of U_{12} vanishes faster than the lower partition. The columns of U_{12} are given by the $2n$ upper members of u_i in equation (D.8). So as ρ approaches ∞ , equation (D.21) can be written as approximation (D.22).

$$\begin{bmatrix} w_1^T \\ w_2^T \\ \vdots \\ w_{2n}^T \end{bmatrix} L_p \approx U_{11}^{-1} \begin{bmatrix} 0_{nn} \\ M^{-1}(\Theta_o) J_c^T - U_{12}^l B_s G_d \end{bmatrix} \quad (D.22)$$

where U_{12}^l is the $n \times n$ lower partition of U_{12} . Consider equations (D.22) and (D.18). If the following equality is true:

$$M^{-1}(\Theta_o) J_c^T - U_{12}^l B_s G_d = J_c^{-1} J^{-1} \quad (D.23)$$

then the right-hand sides of equations (D.22) and (D.18) will also be equal. Therefore, the left-hand sides of equations (D.22) and (D.18) will be equal.

$$\begin{bmatrix} w_1^T \\ w_2^T \\ \vdots \\ w_{2n}^T \end{bmatrix} L_p \approx \begin{bmatrix} t_1^T \\ t_2^T \\ \vdots \\ t_{2n}^T \end{bmatrix} B_t \quad (D.24)$$

Approximation (D.24) and equality (D.15) taken together result in limit (D.25).

$$\lim_{\rho \rightarrow \infty} J_c G_1(j\omega) = G_t(j\omega) \quad \text{for all } 0 < \omega < \omega_b \quad (D.25)$$

$\rho \rightarrow \infty$

where:

$$G_1(j\omega) = C \left[\sum_{i=1}^{2n} \frac{u_i w_i^T}{j\omega - s_i} \right] L_p \quad (D.26)$$

$$G_t(j\omega) = C_t \left[\sum_{i=1}^{2n} \frac{z_i t_i^T}{j\omega - s_i} \right] B_t \quad (D.27)$$

Equation (D.23) can be used to compute a unique value for G_d . This is true because the inverse of $U_{12}^t B_s$ always exists.

$$\text{Since } G_{c1}(j\omega) = G_1(j\omega) + G_2(j\omega),$$

$$\lim_{\rho \rightarrow \infty} J_c G_{c1}(j\omega) = G_t(j\omega) \quad \text{for all } 0 < \omega < \omega_b \quad (D.28)$$

$\rho \rightarrow \infty$.

Appendix E Stability Robustness

This appendix gives a summary of multivariable stability-robustness criteria. For more details, refer to references [49, 33].

Fulfillment of the multivariable Nyquist Criterion is a frequency-domain condition for stability. This criterion requires that the encirclement count of the map of $\det[I_{nn} + K(j\omega)G_p(j\omega)]$ evaluated on the standard Nyquist D-contour, must equal the negative number of unstable modes of $K(j\omega)G_p(j\omega)$. $G_p(j\omega)$ is given by equation (4.23).

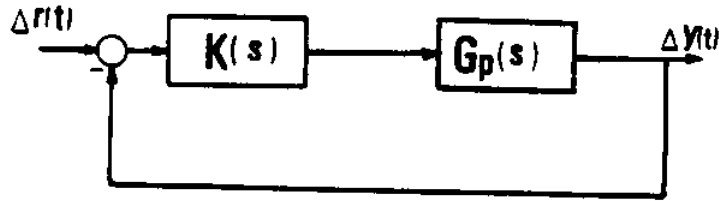


Figure E-1: Closed-Loop System

Similarly, for the stability of the perturbed system, the number of encirclements of the map of $\det[I_{nn} + K(j\omega)G'_p(j\omega)]$ must equal the negative number of unstable modes of $K(j\omega)G'_p(j\omega)$. Under the assumptions governing $G'_p(j\omega)$, this number is the same as for $K(j\omega)G_p(j\omega)$. Therefore, the perturbed system will be stable if and only if the number of encirclements of $\det[I_{nn} + K(j\omega)G'_p(j\omega)]$ remains unchanged for all $G'_p(j\omega)$ permitted by equation (4.23). This is guaranteed if and only if $\det[I_{nn} + K(j\omega)G'_p(j\omega)]$ remains non-zero as $G_p(j\omega)$ continuously approaches $G'_p(j\omega)$, or equivalently, if and only if:

$$\det \left[I_{nn} + K(j\omega)G_p(j\omega) \left[I_{nn} + E(j\omega) \right] \right] \neq 0 \quad \text{for all } 0 < \omega < \infty . \quad (\text{E.1})$$

If $\left[I_{nn} + K(j\omega)G_p(j\omega) \left[I_{nn} + E(j\omega) \right] \right]$ is singular for at least one frequency, such as ω_p ,

then there exists a non-zero vector, $x_n \in \mathbb{C}^n$, such that equation (E.2) is true.

$$\left[I_{nn} + [K(j\omega_s) G_p(j\omega_s)]^{-1} \right] x_n = - E(j\omega_s) x_n \quad x_n \neq 0 \quad (E.2)$$

If inequality (E.3) is satisfied, then equality (E.2) will never happen in all $0 < \omega < \infty$ and $\left[I_{nn} + K(j\omega)G_p(j\omega) [I_{nn} + E(j\omega)] \right]$ will always be non-singular.

$$\sigma_{\min} \left[I_{nn} + [K(j\omega) G_p(j\omega)]^{-1} \right] > \sigma_{\max} [E(j\omega)] \quad \text{for all } 0 < \omega < \infty \quad (E.3)$$

Therefore, the sufficient condition for the closed-loop stability of the system using the perturbed model is given by inequality (E.3). $\sigma_{\max}(\cdot)$ is defined on page 42. Chapter 7 explains how $K(j\omega) G_p(j\omega)$ can be approximated by the state-feedback loop transfer function $G (j\omega I_{nn} - I_{nn})^{-1} B$. In Chapter 7 we prove that $K(j\omega) G_p(j\omega)$ converges pointwise to $G (j\omega I_{nn} - I_{nn})^{-1} B$ if H is selected according to some criterion. Because of this convergence, inequality (E.4) can be satisfied instead of inequality (E.3) to guarantee stability robustness specifications.

$$\sigma_{\min} [G_o(j\omega)] > e(\omega) \quad \text{for all } 0 < \omega < \infty \quad (E.4)$$

$$\text{where: } G_o(j\omega) = I_{nn} + [G(j\omega - I_{nn})^{-1} B]^{-1}$$

$$\text{and } e(\omega) \geq \sigma_{\max} [E(j\omega)]$$

The object is to design G so that inequality (E.4) will be satisfied. Figure 6-6-b shows a case in which inequality (E.4) is satisfied.

References

- [1] Asada, H., Youcef-Toumi, K.
Analysis and Design of a Direct-Drive Arm with a Five-Bar-Link Parallel Drive Mechanism.
ASME Journal of Dynamic Systems, Measurement, and Control 106:225-230, September, 1984.
- [2] Athans, M.
The Role and Use of the Stochastic Linear Quadratic Gaussian Problem in Control System Design.
IEEE Transaction on Automatic Control AC-16(6):529-551, December, 1971.
- [3] Cook, N. H.
Manufacturing Analysis.
Addison-Wesley Publishing Inc., Reading, MA., 1966.
- [4] Crandall, S. H., Karnopp, D. C., Kurtz, E. F., Pridmore-Brown, D. C.
Dynamics of Mechanical and Electromechanical Systems.
McGraw-Hill Book Company, 1968.
- [5] Davison, E. J., Wang, S. H.
Properties and Calculation of Transmission Zeros of Linear Multivariable Systems.
Automatica 10:643-658, 1974.
- [6] Desoer, C. A., Schulman, J. D.
Zeros and Poles of Matrix Transfer Functions and Their Dynamical Interpretation.
IEEE Transaction on Circuits and Systems CAS-21(1):3-8, January, 1974.
- [7] Doyle, J. C., Stein, G.
Multivariable Feedback Design: Concepts for a Classical / Modern Synthesis.
IEEE Transaction on Automatic Control AC-26(1):1-16, February, 1981.
- [8] Doyle, J. C., Stein, G.
Robustness with Observers.
IEEE Transaction on Automatic Control AC-24(4):607-611, August, 1979.
- [9] Fahmy, M. M., O'Reilly, J.
On Eigenstructure Assignment in Linear Multivariable Systems.
IEEE Transaction on Automatic Control AC-27(3):690-693, June, 1982.
- [10] Fahmy, M. M., O'Reilly, J.
Eigenstructure Assignment in Linear Multivariable Systems - A Parametric Solution.
IEEE Transaction on Automatic Control AC-28(10):990-994, October, 1983.
- [11] Frazer, R. A., Duncan, W. J., Collar, A. R.
Elementary Matrices.
The Macmillan Company, New York, N.Y., 1938.

- [12] Gantmacher, F. R.
The Theory of Matrices.
Chelsea Publishing Company, New York, N.Y., 1977.
- [13] Gohberg, I., Lancaster, L., Rodman, L.
Matrix Polynomials.
Academic Press, 1982.
- [14] Goodman, G. C.
The LQG/LTR Method and Discrete-Time Control Systems.
Master's thesis, MIT, Mechanical Engineering Department, June, 1984.
- [15] Gott, R. L.
An Approach to Automated Deburring Using an Industrial Robot.
Master's thesis, MIT, Mechanical Engineering Department, July, 1985.
- [16] Harvey, C. A., Stein, G.
Quadratic Weights for Asymptotic Regulator Properties.
IEEE Transaction on Automatic Control AC-23(3):378-387, June, 1978.
- [17] Hogan, N.
Programmable Impedance Control of Industrial Manipulators.
In *Proceedings of the Conference on CAD/CAM Technology in Mechanical Engineering.*
MIT, Cambridge, MA., March, 1982.
- [18] Hogan, N.
Impedance Control of a Robotic Manipulator.
In *Proceedings of the Winter Annual Meeting.* ASME, Washington D. C., November, 1981.
- [19] Hogan, N. .
Adaptive Control of Mechanical Impedance by Coactivation of Antagonist Muscles.
IEEE Transaction on Automatic Control AC-29(7), July, 1984.
- [20] Hogan, N. .
Impedance Control of Industrial Robots.
Journal of Robotics & Computer Integrated Manufacturing 1(1):97-113, 1984.
- [21] Hogan, N.
Mechanical Impedance Control in Assistive Devices and Manipulators.
In *Proceedings of the Joint Automatic Control Conference.* San Francisco, CA., August, 1980.
- [22] Hogan, N.
Impedance Control: An Approach To Manipulation, Part 1: Theory, Part 2:
Implementation, Part 3: Applications.
To be published in ASME Journal of Dynamic Systems, Measurement, and Control ,
1985.

- [23] Hollerbach, J. M.
A Recursive Lagrangian Formulation of Manipulator Dynamics and a Comparative Study of Dynamics Formulation Complexity.
IEEE Transaction on Systems, Man, and Cybernetics SMC-10(11):730-736, November, 1980.
- [24] Hollerbach, J. M.
Dynamic Scaling of Manipulator Trajectories.
ASME Journal of Dynamic Systems, Measurement, and Control 106:102-106, March, 1984.
- [25] Huseyin, K.
Vibrations and Stability of Multiple Parameter Systems.
Sijthoff and Noordhoff, Netherlands, 1978.
- [26] Kailath, T.
Linear Systems.
Prentice-Hall, Englewood Cliffs, N.J., 1980.
- [27] Klein, G., Moore, B. C.
Eigenvalue-Generalized Eigenvector Assignment with State-feedback.
IEEE Transaction on Automatic Control AC-22(1):140-141, February, 1977.
- [28] Kouvaritakis, B., MacFarlane, A. G. J.
Geometric Approach to Analysis and Synthesis of System Zeros Part 1: Square Systems, Part 2: Non-square Systems.
International Journal of Control 23:149-181, 1976.
- [29] Kouvaritakis, B., Shaked U.
Asymptotic Behaviour of Root-Loci of Linear Multivariable Systems.
International Journal of Control 23:297-340, 1976.
- [30] Kramer, B. M. et al.
Robotic Deburring.
In *Proceedings of the International Conference on the Manufacturing and Technology of the Future.* MIT, Cambridge, MA., October, 1984.
- [31] Kwakernak, H., Sivan, R.
Linear Optimal Control Systems.
Wiley-Interscience, 1972.
- [32] Lancaster, P.
Lambda-Matrices and Vibrating Systems.
Pergamon Press, 1966.
- [33] Lehtomaki, N. A., Sandell, N. R., Athans, M.
Robustness Results in Linear-Quadratic Gaussian Based Multivariable Control Designs.
IEEE Transaction on Automatic Control AC-26(1):75-92, February, 1981.
- [34] Luenberger, D. G.
Observers for Multivariable Systems.
IEEE Transaction on Automatic Control AC-11(2):190-197, April, 1966.

- [35] Luenberger, D. G.
An Introduction to Observers.
IEEE Transaction on Automatic Control AC-16(6):596-602, December, 1971.
- [36] MacFarlane, A. G. J.
A Survey of Some Recent Results in Linear Multivariable Feedback Systems.
Automatica 8:455-492, 1972.
- [37] MacFarlane, A. G. J., Karcaniias, N.
Poles and Zeros of Linear Multivariable Systems: a survey of the algebraic, geometric and complex-variable theory.
International Journal of Control 24(1):33-74, 1976.
- [38] Mason, M.T.
Compliance and Force Control for Computer Controlled Manipulators.
IEEE Transaction on Systems, Man, and Cybernetics SMC-11(6):418-432, June, 1981.
- [39] Moore, B. C.
On the Flexibility Offered by State-Feedback in Multivariable Systems Beyond Closed-loop Eigenvalue Assignment.
IEEE Transaction on Automatic Control AC-21(5):689-692, October, 1976.
- [40] Nobel, B., Daniel, J. W.
Applied Linear Algebra.
Prentice-Hall, Englewood Cliffs, N.J., 1977.
- [41] Ogata, M.
State Space Analysis of Control Systems.
Prentice-Hall, Englewood Cliffs, N.J., 1967.
- [42] Owens, D. H.
Feedback and Multivariable Systems.
Peter Peregrinus LTD., Stevenage, England, 1977.
- [43] Paul, R. P. C., Shimano, B.
Compliance and Control.
In *Proceedings of the Joint Automatic Control Conference*, pages 694-699. San Francisco, 1976.
- [44] Porter, B., D'azzo, J. J.
Closed-loop Eigenstructure Assignment by State-feedback in Multivariable Linear Systems.
International Journal of Control 27(3):487-492, 1978.
- [45] Porter, B., D'azzo, J. J.
Algorithm for Closed-Loop Eigenstructure Assignment by State-feedback in Multivariable Linear Systems.
International Journal of Control 27(6):943-947, 1978.
- [46] Railbert, M. H., Craig, J. J.
Hybrid Position/Force Control of Manipulators.
ASME Journal of Dynamic Systems, Measurement, and Control 102:126-133, June, 1981.

- [47] Rosenbrock, H. H.
Computer-Aided Control System Design.
Academic Press, London, 1974.
- [48] Rosenbrock, H. H.
The Zeros of a System.
International Journal of Control 18:297-299, 1973.
- [49] Safonov M. G., Athans, M.
Gain and Phase Margin for Multiloop LQG Regulators.
IEEE Transaction on Automatic Control AC-22(2):173-179, April, 1977.
- [50] Salisbury, K. J.
Active Stiffness Control of Manipulator in Cartesian Coordinates.
In *Proceedings of the 19th IEEE Conference on Decision and Control*, pages 95-100.
IEEE, Albuquerque, New Mexico, December, 1980.
- [51] Shaked, U., Kouvaritakis, B.
The zeros of linear optimal control systems and their role in high feedback gain stability design.
IEEE Transaction on Automatic Control AC-22(4):547-557, August, 1977.
- [52] Sheridan, T. B., Ferrell, W. R.
Man-Machine Systems: Information, Control and Decision Model of Human Performance.
MIT Press, Cambridge, Massachusetts, 1974.
- [53] Silver, W. M.
On the Equivalence of Lagrangian and Newton-Euler Dynamics for Manipulators.
The International Journal Of Robotics Research, MIT Press 1(2):60-70, 1982.
- [54] Strang, G.
Linear Algebra and Its Applications.
Academic Press, New York, N.Y., 1976.
- [55] Whitney, D. E.
Force-Feedback Control of Manipulator Fine Motions.
ASME Journal of Dynamic Systems, Measurement, and Control :91-97, June, 1977.
- [56] Whitney, D. E.
The Mathematics of Coordinated Control of Prosthetic Arms and Manipulators.
ASME Journal of Dynamic Systems, Measurement, and Control 94-G(4):303-309,
December, 1972.
- [57] Whitney, D. E.
Quasi-static Assembly of Compliantly Supported Rigid Parts.
ASME Journal of Dynamic Systems, Measurement, and Control (104):65-77, March, 1982.
- [58] Wolovich, W. A.
On Determining the Zeros of State-Space Systems.
IEEE Transaction on Automatic Control AC-18(5):542-544, October, 1973.

- [59] Wolovich, W. A.
On the Numerators and Zeros of Rational Transfer Matrices.
IEEE Transaction on Automatic Control AC-18(5):544-546, October, 1973.
- [60] Wolovich, W. A.
On the Cancellation of Multivariable System Zeros by State-feedback.
IEEE Transaction on Automatic Control AC-19(3):276-277, June, 1974.
- [61] Wu, C., Paul, R. P. C.
Manipulator Compliance Based on Joint Torque Control.
In *Proceedings of the Conference on Decision and Control*, pages 88-94. IEEE,
Albuquerque, New Mexico, December, 1980.
- [62] Yuksel, Y. O., Bongiorno, J. J.,
Observer for Linear Multivariable Systems with Applications.
IEEE Transaction on Automatic Control AC-16(6):603-613, December, 1971.